ABSTRACT

Title of Dissertation:	DESIGN OF SELF-ASSEMBLING NANOSTRUCTURES TO PROMOTE IMMUNE TOLERANCE
	Krystina L. Hess, Doctor of Philosophy, 2018
Dissertation directed by:	Dr. Christopher M. Jewell, Associate Professor, Fischell Department of Bioengineering, University of Maryland, College Park

In autoimmune diseases, which affect more than 23 million Americans, the immune system mistakenly attacks healthy tissue. This occurs when the process that normally controls self-reactive inflammatory cells (i.e. tolerance) fails. In multiple sclerosis (MS), the myelin sheath, which insulates nerves, is recognized as a foreign antigen. Demyelination by immune cells results in serious symptoms of neurodegeneration. Current treatments for MS are not curative, but rather manage symptoms by broadly suppressing the immune system, leaving patients unable to fight infection. New therapies that are more specific and effective could greatly improve the quality of life for patients. Biomaterials offer specific advantages for generating antigen-specific tolerance, such as cargo protection, targeted delivery, and controlled release of signals. Additionally, recent reports demonstrate that materials themselves can be intrinsically immunogenic. Two promising biomaterials-based strategies for combating autoimmunity involve: 1) delivery of self-antigen with a regulatory molecule or 2)

delivery of self-antigen alone. Aim 1 of this dissertation focuses on the first strategy, creating a novel delivery system for myelin peptide and GpG, an immunomodulatory oligonucleotide. This approach involves electrostatic self-assembly of the two immune signals, eliminating the need for a carrier that could exacerbate inflammation, while still offering attractive features of biomaterials, such as co-delivery. The goal is for immune cells to encounter both signals simultaneously, biasing the response towards tolerance. This work represents the first studies using self-assembled materials to target toll-like receptor signaling, recently shown to be implicated in many autoimmune diseases. Aim 2 of this dissertation is based on the second strategy above, which relies on evidence that changing the trafficking and processing of a self-antigen can impact the development of inflammation or tolerance. Quantum dots, NPs that are intrinsically fluorescent and rapidly drain to lymph nodes, can be decorated with a large and controllable number of myelin peptides. These key features of QDs were exploited to reveal that parameters of self-antigen display (i.e. dose, density) impact biodistribution and immune cell uptake, and are directly correlated to the level of tolerance induced. Together, the described nanotechnologies offer opportunities to probe important questions towards the design of antigen-specific therapies.

DESIGN OF SELF-ASSEMBLING NANOSTRUCTURES TO PROMOTE IMMUNOMODULATION

by

Krystina L. Hess

Dissertation submitted to the Faculty of the Graduate School of the
University of Maryland, College Park, in partial fulfillment
of the requirements for the degree of
Doctor of Philosophy
2018

Advisory Committee:
Professor Christopher M Jewell, Associate Professor, Fischell Department of Bioengineering, University of Maryland, College Park, **Committee Chair**
Professor Steven M Jay, Assistant Professor, Fischell Department of Bioengineering, University of Maryland, College Park
Professor Jeff Klauda, Assistant Professor, Department of Chemistry and Biochemistry, University of Maryland, College Park, **Dean's Representative**
Dr. Igor L. Medintz, Research Biologist IV, Center for Bio/Molecular Science and Engineering, U.S. Naval Research Laboratory
Professor Silvia Muro, Associate Professor, Fischell Department of Bioengineering, University of Maryland, College Park

Acknowledgements

Thank you to Chris for always supporting and encouraging me. Thank you to the members of the Jewell Lab for all of your help along the way. Thank you to my collaborators at the NRL for the time and expertise you have shared with me. Thank you to my family for endlessly supporting me throughout this process.

Table of Contents

List of Tables

List of Figures

List of Abbreviations

Antigen-presenting cell	APC
Gold nanoparticle	AuNP
Central nervous system	CNS
Carbon nanotube	CNT
Cytotoxic T lymphocyte	CTL
Dendritic cell	DC
Dynamic light scattering	DLS
Experimental autoimmune encephalomyelitis	EAE
Enzyme-linked immunosorbent assay	ELISA
Helper T cell	T_H
Immune polyelectrolyte multilayer	iPEM
Intraperitoneal	*i.p.*
Lymph node	LN
Lipopolysaccharide	LPS
Major histocompatibility complex	MHC
Myelin oligodendrocyte glycoprotein	MOG
Microparticle	MP
Multiple sclerosis	MS
Nanomaterial	NM
Nanoparticle	NP
Ovalbumin	OVA
Pathogen-associated molecular pattern	PAMP

Polydispersity	PDI
Poly(lactic-co-glycolic acid)	PLGA
Poly(inosinic:cytidylic acid)	polyIC
Post injection	*p.i.*
Quantum dot	QD
Regulatory T cell	T_{REG}
Rheumatoid arthritis	RA
Secondary lymphoid organ	SLO
Subcutaneous	*s.c.*
Type 1 diabetes	T1D
Toll-like receptor	TLR

Chapter 1: Introduction

During autoimmune diseases like type 1 diabetes (T1D) or multiple sclerosis (MS), the immune system mistakenly recognizes and attacks healthy tissues in the body. In MS, myelin, which surrounds and protects the axons of neurons, is attacked by inflammatory cells leading to neurodegeneration. The current standard of care for MS patients is regular injection (i.e., daily or weekly) of immunosuppressive drugs. A major issue with these treatment strategies is that they suppress immune function, leaving patients immunocompromised and open to opportunistic infection. These treatments are also not curative, meaning that disease often still progresses. Researchers are currently aiming to address these limitations by creating vaccine-like therapies that reprogram the response to myelin but leave a functioning immune system intact to fight infection.

Many new investigations are focused on creating immunotherapies that promote myelin-specific tolerance. Two distinct strategies have emerged in this field. One involves the delivery of self-antigen along with a regulatory signal aimed to polarize the response away from inflammation and towards tolerance. The second strategy is to alter the form in which self-antigen is delivered as recent reports also reveal that the development of inflammation or tolerance against certain molecules is influenced by the concentration and form of self-antigen presented to immune cells. Biomaterials provide unique properties for immune signal delivery including tunable cargo loading, targeted delivery, and controlled release. Additionally, biomaterials themselves can be

intrinsically immunogenic, promoting the induction of an inflammatory or tolerogenic response. Materials-based strategies are among the most promising in the immunotherapy field, yet the immunogenicity of even the most commonly used biomaterials has yet to be fully characterized. This creates an opportunity to determine specific design rules for inducing tolerance or inflammation by materials-based delivery of immune signals.

Recognizing this need, my dissertation work combined techniques from the fields of materials science, engineering, and immunology to design biomaterials-based strategies to study autoimmune disease. Engineering techniques were used to design and synthesize two novel nanotechnologies: self-assembling immune complexes and self-assembling peptide-coated nanoparticles (NPs). Characterization of the technologies was carried out using materials science tools such as dynamic light scattering (DLS), zeta potential measurement, and spectrophotometry. These were paired with biological and immunological techniques including cell culture, flow cytometry, enzyme-linked immunosorbent assay (ELISA), immunofluorescent staining, and important animal models of disease. The combination of tools were used to complete two aims:

1) Design of carrier-free complexes composed entirely of immune signals to reprogram the immune system for autoimmune disease treatment.

2) Exploit quantum dots (QDs) as well-defined a NP tool to understand parameters for materials-based tolerance induction in autoimmunity.

The objectives outlined above explore novel therapeutic strategies for combatting autoimmune disease. Polyplexes are typically formed by condensing a nucleic acid with a polymer and are often used in vaccination and gene therapy. The first aim describes the synthesis of "polyplex-like" structures by instead condensing a nucleic acid with a cationic peptide. This platform does not require a polymer carrier and allows the isolation of the effects of immune signals. The QDs, by comparison, allow tunable conjugation of biomolecules, enabling new knowledge about threshold densities and doses of self-antigen to drive tolerance. Additionally, both described platforms are modular and therefore can be applied to a number of disease models. New insight gained from this work could inform the rational design of materials-based immunotherapies.

The work completed in the above aims addresses the broad goal of bringing fundamental insight and materials design rules to the area of autoimmune disease treatment. **Chapter 2** provides a detailed overview of the immune system and discusses key classes of biomaterials that have been used in immunological applications, including materials that are intrinsically immunogenic. **Chapter 3** described inorganic nanomaterials (NMs) in this context. The materials may be have inflammatory or regulatory properties and can be applied to vaccination against infectious disease or to immunotherapies aimed at treatment of cancer or autoimmunity. **Chapter 4** describes a strategy that has the advantages of biomaterials, but eliminates the potentially inflammatory material. The "carrier-free" polyplexes are formed by condensing an immunomodulatory DNA sequence with a self-antigen peptide. The tolerizing effect

of these complexes was studied *in vitro* and in an animal model of progressive MS. **Chapter 5** investigates a particular example of an inorganic material delivering an immune signal, in which QDs are decorated with self-antigen as a strategy to combat autoimmunity. This nanotechnology is tested in a mouse model of MS, and is used to probe the effects of self-antigen dose and peptide ligand density on tolerance. In **Chapter 6**, the QDs are used as a tool to determine design rules for induction of tolerance by biomaterials-based strategies. The unique features of the particles are exploited to elucidate how the number and density of self-antigen impacts development of tolerance, and the underlying trafficking and processing of self-antigen, changes in APC function, LN remodeling, and T cell polarization. **Chapter 7** provides an outlook on the work discussed in the preceding chapters and details ongoing and future studies. The *in vitro* mechanism of immune polyplexes described in Aim 1 will be investigated and the QDs described in Aim 2 will be used to define particle parameters for inducing tolerance **Chapter 8** discusses scientific contributions of this work, including the design of two novel nanotechnologies for combatting autoimmunity, and my contributions to the field such as dissemination of knowledge in peer-reviewed journals and serving communities underrepresented in science. Finally, there is an appendix listing my publications and intellectual property filings and a library of references.

Chapter 2: Biomaterials-based strategies to promote immunological tolerance

2.1 Immunological processes and the development of autoimmune disease

2.1.1 Antigen recognition initiates the adaptive immune response

Innate immunity provides the first line of defense to foreign pathogens through physical and chemical barriers such as the epithelia, phagocytic and natural killer cells, blood proteins, and cytokines.[1] Adaptive immunity develops in the days to weeks following infection and has extreme specificity for distinct molecules, called antigens, and the capacity to create a memory response. These antigen-specific responses are generated in highly organized secondary lymphoid organs (SLOs) such as the spleen and lymph nodes (LNs).[2, 3] Antigens must reach SLOs either by passive drainage through lymphatic vessels or through phagocytosis by antigen-presenting cells (APCs) such as a dendritic cells (DCs) that carry antigens to SLOs.[4-6] APCs process and present antigen to naïve T and B cells in LNs, leading to the generation of cell-mediated and antibody-mediated immunity, respectively. These responses can create $CD8^+$ cytotoxic T cells (CTLs) that destroy infected host cells or antibodies that are secreted by B cells and bind to and neutralize antigens.[7, 8] Antibody-mediated immunity requires interaction with $CD4^+$ helper T cells (T_H) including T_H1, T_H2, and T_H17 cells. The activation of both $CD4^+$ and $CD8^+$ T cells requires recognition of antigen presented in major histocompatibility complexes (MHCs) and binding of costimulatory factors such as CD40, CD80, and CD86 (**Figure 2.1**).[7]

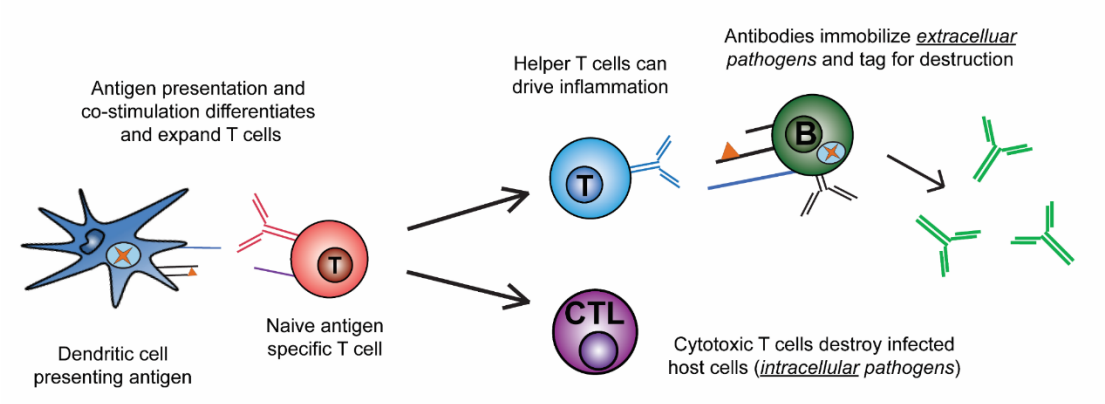

Figure 2.1: The immune response begins by antigen recognition. DCs engulf and process antigen before presenting it along with costimulatory factors to naïve T cells. T cells then polarize towards CTLs that can directly kill infected cells or T_H cells that assist in the production of antibodies by B cells.

2.1.2 Tolerance prevents inflammatory responses to self-antigens

Immune cells regularly develop with receptors specific for self-antigens (e.g. host proteins) rather than foreign antigens, but a normal functioning immune system controls these autoreactive cells with two processes known as tolerance.[9] Central tolerance occurs as lymphocytes mature in generative lymphoid organs, such as bone marrow or the thymus, and can lead to apoptosis, changing of self-antigen receptors, or differentiation into regulatory T cells (T_{REGs}). T_{REGs} can migrate to the periphery and inhibit activation and effector functions of inflammatory T cells upon recognition of self-antigen. Not every self-antigen that a cell may encounter is expressed in the thymus, meaning that central tolerance alone is insufficient. Peripheral tolerance maintains unresponsiveness to self in peripheral tissues by ensuring that mature lymphocytes become incapable of responding to antigen (anergy), die by apoptosis (deletion), or are suppressed by T_{REGs}. When tolerance fails and an inflammatory response is mounted against self-antigens, autoimmune disease develops. There are

more than 80 such diseases, including rheumatoid arthritis (RA), allergies, and MS, affecting more than 23 million people in the United States.[10]

2.1.3 Myelin antigens are recognized and attacked in multiple sclerosis

MS is an autoimmune disease affecting more than 2 million people worldwide in which myelin, which insulates and protects the axons of neurons in the central nervous system (CNS), is recognized as a foreign antigen.[11, 12] Myelin membranes feature a protein-lipid-protein-lipid-protein structure and are part of Schwann cells in the peripheral nervous system, and oligodendroglial cells in the CNS. Oligodendrocytes produce myelin which spreads as a sheet around axons and provides nutritional support and accelerates neural conduction.[13, 14] Myelin protein-derived antigens are thought to be the targets of auto-reactive cells in MS.[15] For example, $CD4^+$ T cells have been found to recognize myelin basic protein (MBP), proteolipid protein (PLP), and myelin oligodendrocyte glycoprotein (MOG) (**Figure 2.2**).[16] Beyond just $CD4^+$ T cells, the attack on myelin is carried out more broadly and also involves innate immune cells, myelin-reactive $CD8^+$ T cells, and even myelin-specific antibodies secreted by B cells.[17, 18] These cells first develop in LNs where signals are presented, and then migrate to the CNS where they demyelinate neurons and secrete inflammatory cytokines that recruit more immune cells to the site.[17, 19-21] Inflammatory lymphocytes cross the blood brain barrier (BBB) through interactions with adhesion molecules, chemokines, and matrix metalloproteinases. At disease onset, monocyte-derived macrophages initiate and mediate demyelination by the production of toxic factors such as nitric oxide.[15]

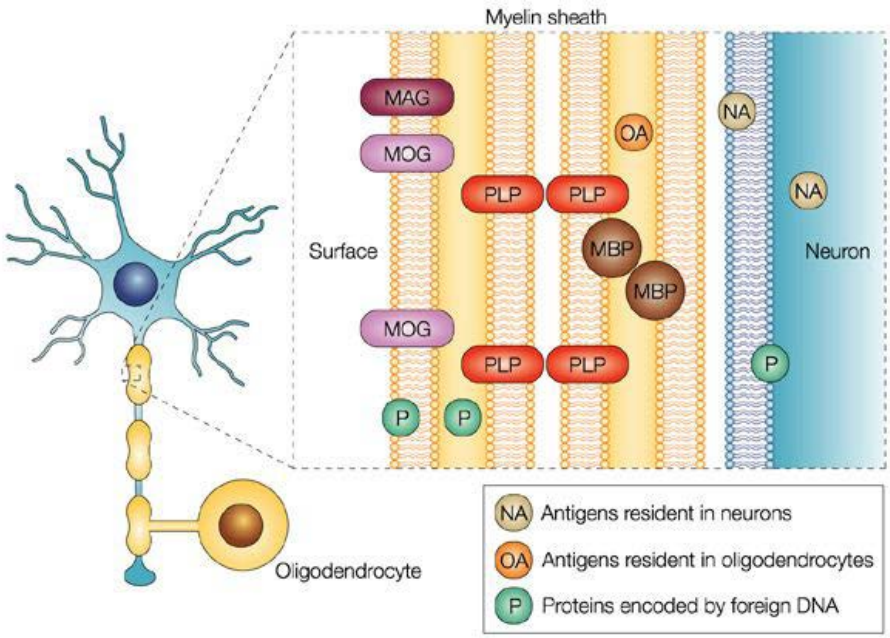

Figure 2.2: Myelin antigens are the targets of auto-reactive cells in MS. Oligodendrocytes produce myelin which surround and protects the axons of neurons. Myelin contains multiple potential self-antigens such as MOG, MBP, and PLP. Reprinted with permission from [16].

A hallmark of MS is the presence of areas of focal demyelination throughout the CNS known as plaques or lesions that vary in early and late stages of disease.[22] The neurodegeneration characteristic of MS leads to serious symptoms such as loss of motor skills, vision problems, and seizures. The four clinical types of MS are relapsing-remitting (RR), primary progressive (PP), secondary progressive (SP), and progressive relapsing (PR).[17] RRMS is the most common and while it has many clinically approved treatments, none of these treatments are curative. Existing therapies involve regular injection of immunosuppressive drugs or molecules that are non-specific and therefore can leave patients severely immunocompromised.[23] For example, one form of treatment involves subcutaneous (*s.c.*) injection of the cytokine interferon beta, which blocks the number of inflammatory cells that cross the BBB but can lead to an overall reduction in immune cells capable of fighting infection. Monoclonal antibody

therapy is an improvement over small molecule drugs, but still targets both healthy and dyfunctional cells. Additionally, the described treatments only manage symptoms and are not curative. Thus, current treatments are limited by i) off-target effects that immunocompromise patients, ii) lack of efficacy in progressive MS, and iii) life-long dosing. These hurdles have driven great interest in vaccine-like therapies that promote myelin-specific tolerance.

2.2 Biomaterials offer advantageous features for immunological applications

2.2.1 Biomaterials have become ubiquitous in the field of medical research

Biomaterials are being investigated to improve the delivery and efficacy of immune signals, drugs, and other molecules. The term "biomaterial" refers to vast library of materials including polymers, engineered cells, inorganic materials such as carbon nanotubes (CNTs) or QDs, and self-assembled structures.[24] These materials can be used to synthesize particles that deliver cargo[25], be formulated to build hydrogels or scaffolds[26], or to build devices and biosensors[27]. One commonly referenced advantage of biomaterials is encapsulation of multiple cargos (e.g., small molecule drugs) in a particle, ensuring that the cells or tissues of interest receive all intended signals. The biodegradation of these particles can be tuned to release cargo on different time scales including a classing burst release or a sustained release profile, depending on the desired application.[28] polymeric particle. Release of cargo at a desired area can be improved by adding targeting moieties onto the particle surface. The combination of these features is useful for protecting cargo from degradation and for reducing systemic effects.

The above advantages, as well as the ability of biomaterials to promote trafficking to SLOs, and the capacity of APCs to engulf particulates, are specifically attractive for the delivery of immune signals [29] An area of increasing research focus in recent years has been the use of delivery vehicles to engineer a response towards immunity or tolerance.[7, 30] For example, some researchers design materials that enhance antigen uptake by APCs through targeting the DC endocytic receptor DEC205 with antibodies[31] or by the use of particles that degrade to form a gradient of DC chemoattractants.[32] Biomaterials can also target therapies intracellularly exploiting the pH change[33, 34] and reduction-oxidation state[35, 36] in lysosomal compartments. Size of particles encapsulating immune signals can also be tuned to promote trafficking to LNs either by passive drainage[4] or phagocytosis by APCs.[6, 37]

2.2.2 Biomaterials can be intrinsically immunogenic

While biomaterials offer many attractive features for immunotherapy delivery, several recent reports have shown that biomaterials themselves can properties that can promote inflammation or tolerance.[7, 28, 38-41] Widely used biomaterials including poly(lactic-co-glycolic acid) PLGA and polystyrene have been shown to activate a general inflammation pathway known as the inflammasome through induction of IL-1β secretion.[38, 39] The intrinsic immunogenicity of many common biomaterials has been linked to their physicochemical properties such as molecular weight, particle size and shape, surface chemistry, and hydrophobicity.[40, 41] For example, it was recently

reported that a class of polymers frequently used in vaccination induce DC activation *in vitro* and *in vivo*.[28] When in particle form, poly(beta-amino esters) induced inflammation without the addition of antigen or an immunostimulator used to enhance vaccination response (adjuvant) (**Figure 2.3A**). Interestingly, the level of activation was dependent on the extent of particle degradation. These studies reveal that carriers commonly used for delivery of immune signals can elicit inflammation, which may be desirable when designing vaccines. Intrinsically immunogenicity of materials can be detrimental, however, when developing therapies for autoimmune disease, as the inflammation resulting from a delivery vehicle could exacerbate disease. Other studies have demonstrated that certain materials can have a tolerizing effect rather than an inflammatory one.[42, 43] For example, a recent report demonstrated that graphene QDs can promote the secretion of regulatory cytokines and suppress inflammatory cytokines in human immune cells.[44] Peripheral blood mononuclear cells (PBMCs) were stimulated with phytohemagglutinin and incubated with graphene QDs, which led to a dose-dependent decrease in IL-6 and increase in IL-10, compared to the stimulated controls (**Figure 2.3B**). Until the effects of biomaterials on the promotion of inflammation or tolerance are fully characterized, platforms that are “carrier-free” but still offer features of biomaterials such as codelivery and cargo protection, may be of interest.

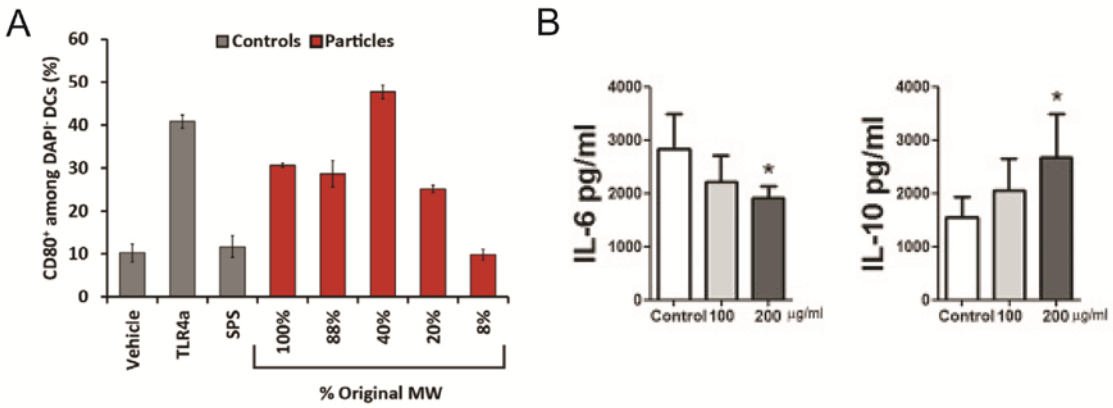

Figure 2.3: Biomaterials exhibit properties that can promote inflammation or tolerance without additional signals. A) PBAEs activate DCs in a manner that is dependent on molecular weight. **B**) Graphene QDs reduce inflammatory IL-6 secretion in stimulated PBMCs but enhance secretion of regulatory IL-10. Reprinted with permission from [28] and [44].

2.2.3 Two promising materials-based strategies to combat autoimmunity

As introduced above, existing therapies for MS are non-specific and therefore cause broad suppression. This can leave patients immunocompromised and increasingly susceptible to opportunistic infection.[45] Therefore, treatments that can inhibit the inflammatory response to myelin without non-specific suppression are of great interest. Biomaterials-based strategies for the delivery of immune signals have been heavily researched for this application and two general platforms have emerged. One approach involves the co-delivery of a self-antigen that is attacked in a particular autoimmune disease alone with a regulatory or suppressive immune cue.[25, 46-48] In autoimmune disease, the T cell population is skewed towards inflammatory effector T cells (T_H1, T_H17). Treatments that polarize self-antigen specific T cells towards regulatory populations could control disease.[9] For example, one recent report describes PLGA NPs that coadminister the model antigen ovalbumin (OVA) and rapamycin, an inhibitor of the mTOR pathway, that promotes a tolerogenic DC phenotype capable of polarizing

T_{REGs}. The particles were capable of inducing antigen-specific tolerance in models of allergy and adoptive transfer (**Figure 2.4A**).[47] This strategy has also been applied to a mouse model of MS, EAE, with PLGA particles encapsulating MOG and rapamycin.[25] Another group synthesized particles through layer-by-layer deposition of MOG and GpG, an antagonist to an inflammatory pathway implicated in MS, creating a carrier-free codelivery system.[49] This system resulted in the development of antigen-specific T_{REGs} and eliminated disease in a mouse model of MS.

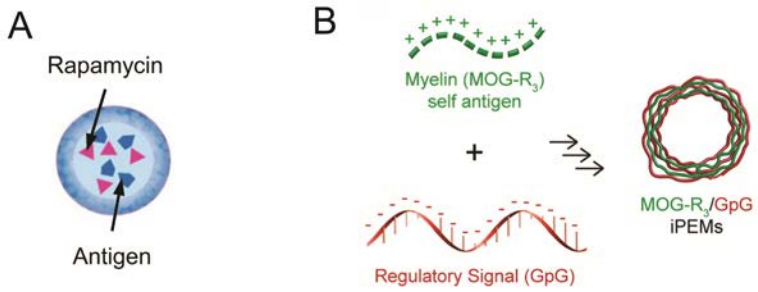

Figure 2.4: A promising strategy to induce tolerance involves delivery of self-antigen and a regulatory signal. A) PLGA NPs delivering OVA and rapamycin induced T_{REGs}. **B**) Capsules composed entirely of MOG and GpG induced tolerance in EAE. Reprinted with permission from [47] and [49].

The second strategy towards developing antigen-specific tolerance focuses on changing how self-antigens are encountered in SLOs (i.e., by particle delivery), without the addition of a regulatory signal.[50-52] Display of self-antigen on particulate materials can promote trafficking to microdomains within LNs that are associated with tolerance. In one example, polystyrene beads (PSB) that had been coated with MOG and drained to LNs and colocalized with MARCO, a receptor found on macrophages (**Figure 2.5A**).[53] These cells are involved in the clearing of apoptotic cell debris, but do not initiate an inflammatory immune response to the debris, indicating a tolerogenic

capacity. It is thought that antigen derived from apoptotic debris drive tolerance through T cell anergy or depletion. One report described a self-antigen from a T1D model bound to the surface of red blood cells (RBCs), a cell type known to be quickly recycled.[54] This platform protected mice from diabetes onset in an aggressive model that results in severe disease in a matter of days (**Figure 2.5B**).

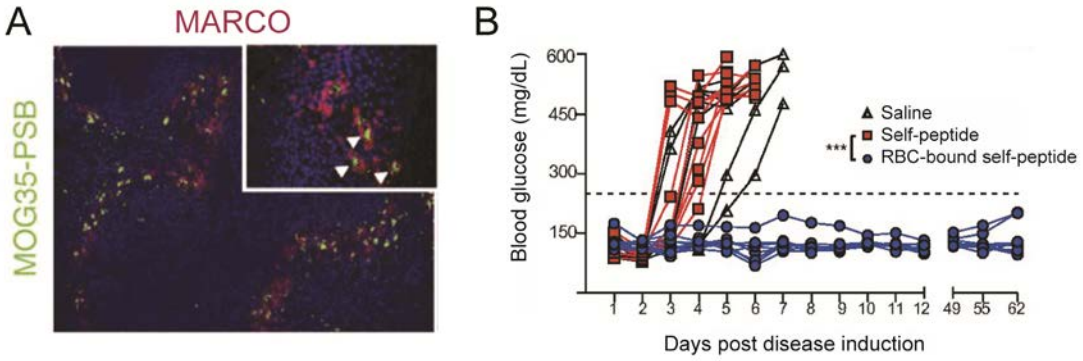

Figure 2.5: Delivery of self-antigen in particulate form, without a regulatory signal, can induce tolerance. A) PSBs coated with MOG localize in tolerogenic MARCO domains of LNs. **B**) A T1D self-peptide bound to RBCs protects mice from the development of disease. Adapted with permission from [53] and [54].

This chapter briefly discussed intrinsic immunogenicity of biomaterials. Current research is focused on harnessing the immunostimulatory or immunomodulatory properties of these materials. **Chapter 3** describes the application of inorganic materials (i.e. gold nanoparticles (AuNPs), QDs, CNTs) to immunotherapy with specific focus on to infectious disease, cancer, and autoimmunity. This sets up **Chapters 5** and **6**, which detail Aim 2: self-antigen coated QDs as a strategy to induce tolerance and establish design parameters for particle-based immunotherapies.

Chapter 3: Developing inorganic nanomaterials for immunological applications[1]

3.1 Introduction

Materials-based approaches to tune immunity have received increasing interest in recent years due to advantages such as co-delivery of immune signals, cargo protection, and specific targeting capabilities.[55-57] Notably, many materials themselves exhibit immunomodulatory properties, leading to direct stimulation or regulation of immune pathways.[28, 38, 39, 58-60] One realization from this discovery is that material properties are critically important in determining the effectiveness of candidate vaccines or immunotherapies because these carriers impact the response to the active immune components. From another perspective, these same studies highlight the potential impact of gaining greater control over the interactions of vaccines and immunotherapies with target immune cells and tissues. Inorganic materials differ from materials (e.g., polymers, lipids) that have been widely reviewed in the immune engineering field [7, 61-64] because they are derived almost entirely from non-natural materials. This characteristic creates unique structural, optical, electric, and magnetic properties that can be exploited for immunological applications through targeting of multiple immune signals, enhanced stability, and delivery otherwise insoluble cargo. Here we discuss this topic across four areas, including i) the immunomodulatory properties of inorganic materials, and the application of this material class to ii)

[1]Adapted from **KL Hess**, IL Medintz, CM Jewell; "Developing inorganic nanomaterials for immunological applications" (*invited review in preparation*)

infectious disease, iii) cancer immunotherapy, and iv) autoimmune disease. While a vast library of inorganic NMs is currently developing, we illustrate key themes using categories such as AuNPs, QDs, CNTs, and silicon or iron oxide nanoparticulates. We first provide some key immunological background and material considerations.

3.1.1 The immune cascade is triggered by antigen recognition

The immune system functions across interconnected types of responses: innate and adaptive. The innate immune system is the body's first line of defense and includes cells such as macrophages that engulf pathogens and natural killer cells that induce cell death ("apoptosis") in infected host cells. This arm of the immune response relies on the ability of pattern recognition receptors to respond to molecular patterns associated with viruses and bacteria, or other types of danger (e.g., heat, toxins). In the adaptive immune system, pathogens travel to the LNs either by passive drainage through lymphatic vessels or are phagocytosed by APCs and actively trafficked to the node. APCs such as DCs then process and present the antigen in MHCs, along with costimulatory molecules, to T cells with specific receptors. T cells can then become CTLs with antigen-specific direct killing cell capabilities or T_H cells that can be further characterized based on the types of inflammatory signaling molecules, or cytokines, they produce.

The processes just outlined are not carried out unchecked, but instead, are part of a constant balance between immune activation (e.g., against a pathogen) and immune

regulation that conserves resources and protects self-tissue from inadvertent attack by the immune system. These latter processes – termed immune tolerance – are particularly important, as some T and B cells naturally develop receptors with reactivity with for molecules found in the body. Inflammation and other detrimental outcomes are avoided through functional tolerance by receptor editing, deletion of these self-reactive cells, or suppression by T_{REGs}. During autoimmune diseases such as MS and T1D, aspects of tolerance fail, leading to inflammation and attack of host tissue.

3.1.2 Vaccination and immunotherapy have revolutionized disease treatment and prevention

Over the past century, prophylactic vaccination has become a standard practice, resulting in the eradication of diseases such as polio and small pox. This strategy relies on the host immune system's ability to respond to antigen exposure and create "memory." Most existing vaccines drive B cells to produce antibodies that can, even years later, protect against subsequent antigen exposure. A typical vaccine consists of an antigen and an immunostimulatory molecule, termed an adjuvant. The mechanism of the most commonly used adjuvants, aluminum salts, is still not understood. For this reason, a strategy being heavily investigated for vaccination is to include agonists that stimulate specific immune warning pathways, promoting a more predictable molecular response. One such pathway involves TLRs, which recognize mainly bacterial and viral products and can induce a high level of inflammation in response. Agonists of these

receptors have been investigated in hundreds of clinical trials for conditions ranging from cancer to allergies.[65]

The immune engineering field is rapidly developing, with exciting ideas emerging to improve prophylactic vaccines against infectious agents, as well as new therapeutic vaccines or immunotherapies targeting cancer and autoimmunity. For example, the tumor microenvironment fosters growth and metastasis in part due to immunosuppression, which deactivates immune cells seeking to destroy the tumor. These and other challenges have driven interest in strategies to generate potent, tumor-specific T cells that can overcome this immunosuppressive environment.[24] As alluded to above, immunotherapy also has potential to turn off or correct defects during autoimmune disease, where the immune system recognizes and attacks healthy cells. These are both examples of therapeutic vaccines.[62] Materials, including natural and inorganic, are increasingly investigated in the field of immunotherapy as delivery vehicles for immune signals, for their intrinsic immunogenicity, or even as imaging agents.

3.2 Considerations for designing inorganic materials

There is no universally accepted definition for what constitutes a NM, but one of the more accepted definitions is a material derived by an engineered process that has at least one of its dimensions at a scale of <100 nm. [66, 67] This engineered derivation is meant to define the material as man-made and not naturally occurring, while use of

the word “material” distinguishes NM from synthetic chemicals. NMs come in two generalized categories, hard NMs and soft NMs. Hard NMs are typically synthesized from metals or semiconductors while, soft NMs include polymers, dendrimers, liposomes, and biological derivatives such as DNA origami and recombinantly-modified viral protein scaffolds.[66, 67] The number of available NMs continues to grow with each passing year and now include subclasses such as NPs, nanorods, nanotubes, nanocapsules, nanosheets, and others.

There are many considerations to account for in designing NMs for a given biological application – with many yet to be discovered, but several of are particular relevance to immunology, including physicochemical properties, how NMs are modified for a given purpose or made biocompatible, and the available characterization tools for a specific application. Key considerations across these areas are described below.

3.2.1 Physicochemical Properties

In addition to unique quantum confined properties, NMs differ from molecules like drugs or proteins in significant ways, even though these classes may be in the same size range. The molecules that make up a drug or a monoclonal antibody formulation are often all considered identical, particularly for approved therapeutics. This is not true for a NM formulation which is an ensemble containing many distinct, but closely related, species. Using AuNPs as an example, a given sample is typically polydisperse with a distribution of sizes exhibiting a Gaussian profile centered on the average

diameter. This means the number of atoms constituting such NPs are also variable. Given the nanoscale size, NMs have incredibly high surface-to-volume ratios, but the surfaces are not uniform and may display vertices, defects, lattices, and edges amongst other facets. Many NPs, such as semiconductor QDs, have multilayer structures with a core and shell, or multiple layers of shells. The coatings used to make NMs biocompatible and any biological moiety attached at the surface can be considered further layers in this structure. The net charge of a NM is dictated by the groups present and displayed around its surface at the bulk solution interface. Moreover, in solution, NPs commonly exhibit a Debye-Hückel charge counter layer surrounding the particle, making prediction of the charge character complicated.[68] Lastly, NMs can diffuse in solution, albeit at a slower rate than a similarly-sized biomolecule, and display complex hydrodynamic diameters that are hard to predict given they consist of a hard, insoluble material surrounded by dissolved components.

3.2.2 Colloidal Stabilization

Aside from certain small metallic oxides, most hard NP materials have no intrinsic solubility of their own, thus requiring surface modification with what are termed "surface ligands" to enable dissolution or stabilization. Some NPs such as AuNPs are synthesized directly in buffer using nucleating/stabilizing surface ligands that provide colloidal stability through either intrinsic charge (e.g., cetyltrimethylammonium bromide - CTAB) or the presence of appended poly(ethylene glycol) (PEG) groups.[69, 70] Other NPs, such as QDs, are frequently synthesized at high temperature in organic

phase and require either encapsulation or a complete surface “cap” exchange for phase transfer to aqueous.[71] Large molecular weight amphiphilic polymers provide a set of hydrophobic groups that interdigitate with the organic molecules already present on the NP’s surface while their hydrophilic surfaces mediate colloidal stability. This approach tends to add significantly to the NP’s hydrodynamic diameter but helps maintain good quantum yield by protecting the core/shell structure from water and charge interactions. Smaller, more discrete modular ligands are used for cap-exchange. In these cases, a terminal thiol, for example, provides direct surface coordination, while charged, zwitterionic, or PEG groups mediate colloidal stability. If the charged groups are exclusively amines or carboxyls, this composition will limit stability to a pH regime dictated by that group’s pKa. These groups are also often used for further bioconjugation. Monothiolated ligands suffer a strong dynamic off rate which can be ameliorated using multidentate thiol groups.[66, 71] The choice of which NP surface chemistry to utilize is primarily application driven since each approach is defined by both benefits and liabilities that must be carefully balanced. Carbon allotropes such as CNTs and graphene have similar requirements although colloidal stability is usually provided by direct chemical or plasma modification of the surface to display hydroxyl and carboxyl groups.[72]

3.2.3 Bioconjugation

For most biological applications, NPs are further modified with some type of biomolecule; these span proteins, peptides, nucleic acids, carbohydrates, drugs, and

lipids.[66] The biomolecules are meant to provide wide-reaching features, such as cell/tissue targeting, improved cellular uptake, or antigen presentation. These capabilities are accomplished through either heterogeneous or homogeneous bioconjugation chemistry, with the latter being the most desirable. In-depth discussion can be found in other reviews.[66, 73, 74] Heterogeneous chemistry such as a carbodiimide (EDC) linkage targets the ubiquitous groups on proteins such as amines or carboxyls, for example, and will result in a NP-bioconjugate where the proteins have different orientations, mixed avidity, and different ratios per NP. Homogeneous chemistry provides far more control over pertinent variables such as ratio of biomolecule per NP, their relative orientation, the attachment strength, and linkage or separation distance, and reproducibility.[75] These characteristics can all be critical for immunological applications, where the combination and density of antigens or stimulatory cues determine the nature of immune response. Bioorthogonal chemistries are undergoing concerted development to accomplish the latter with minimal perturbation to either the biomolecule or the NP through the use of non-natural chemical functional groups such as azides and alkynes.[76] Attaching a single biomolecule or similarly low densities to a NP may result in conjugates actually displaying a Poisson distribution centered around the average value. In contrast, attempting to add very large numbers may perturb the NP's colloidal stability.

3.2.4 Nanoparticle Interfacial Phenomena

NP physicochemical properties rarely conform exactly to predictions from models or simulations.[68] In seminal work, Zobel and colleagues confirmed that NPs structure

their surrounding environment regardless of whether the environment is organic or aqueous, and that this structure can extend to almost twice the NPs diameter.[77] Such structuring is believed to give cause and strongly influence complex phenomena at the NP-bulk interface including pH, pKa, and ionic gradients, charge layers, changes in localized density, and creation of boundary zones. Understanding these phenomena may help clarify some of the unexplained interactions between NPs and their bioconjugates. Prominent amongst these are the observation that activity of an enzyme can be enhanced when attached to a NP. Examples includes enzymes acting on NPs displaying a substrate or NPs displaying the enzymes themselves. Preliminary mechanistic studies suggest these enhancements result from high, localized avidity for enzyme acting on NP-substrate along with alleviation of rate-limiting steps for NPs displaying enzymes: the latter presumably arises from the many changes that occur in the structured environment.[78, 79]

Corona formation is another critically important phenomena that arises once a NP-bioconjugate is transferred to a biological environment or is introduced in vivo. This process is characterized by the rapid binding of proteins and other biomolecules to the NP surface with a continuous dynamic process whereby lower concentration species with higher affinity replace higher concentration species with lower affinity.[80, 81] The corona is influenced by the type and character of the NP materials themselves and will obscure molecules on the NP surface, thus directly affecting in vivo function, along with altering distribution, excretion, long-term fate, and toxicity profiles. Our poor

understanding of the protein corona phenomenon and how it alters downstream immunological effects severely limits NP translation attempts.

3.2.5 Characterization

To allow for proper control over experimental formats and subsequent data analysis, it would be ideal to have a full physicochemical characterization of a NP-bioconjugate including NP polydispersity (PDI), size, hydrodynamic diameter, stability, average number of biomolecules attached, their orientation, and their effective binding constants. The primary issue here is that very few analytical techniques exist that can provide such detailed information, and those that do exist only provide either indirect data or data averaged over the ensemble, like DLS.[82] Thus, characterization is usually an amalgam of several indirect techniques along with interpretation of functional results. Along with characterization come many concerns about NP toxicity in vivo. These concerns arise from the presence of materials such as Cd, in the case of QDs, along with a lack of understanding of how nanoscale size and architecture influences biological interactions and can make a material previously considered inert, such as gold or silicon, potentially problematic.[83-85]

Of course, the above overview is a simplification of all the considerations that go into the use of a NM or NP for a given biological application. What it does reflect, however, is that use of NMs within the context of biology, let alone an immunological focus, is not a plug-and-play process; concerted thought is required in both designing

experiments and analyzing data. It is not always a given that what worked in one model system can be readily transferred to another system. Pertinent issues surround the choice of NM, its size, how it is colloidally stabilized, what its surface chemistry is, its potential toxicity, what is attached to it, confirming that the conjugate is actually that desired, and ultimately how it is applied.

3.3 Biophysical parameters of inorganic materials impact intrinsic immunomodulatory properties

As the previous section demonstrates, the physicochemical properties of inorganic materials play an important role in the interaction with biological molecules. This is true to an even greater extent for vaccines and immunotherapies because studies in the last decade reveal that many inorganic materials can actually induce inflammatory or tolerizing immunological effects. Not surprisingly then, a new focus is elucidating the mechanisms behind intrinsic immunomodulatory properties of inorganic materials such as AuNPs, QDs, silver NPs[86], iron oxide nanomaterials[87, 88], titanium dioxide NPs[42, 86], and others. These materials and the effects of factors such as size, shape, charge, and surface functionalization relating to their roles in promoting or inhibiting inflammation will be discussed below and are summarized in **Table 4.1**.

Setting	Inorganic material	Effect	Ref.
Intrinsic immunogenicity	AuNPs	Block IL-1β-induced activation	140
		Increased hydrophobicity correlates with increased gene expression of pro-inflammatory cytokines	143
	QDs	Modulate NF-κB inflammatory pathway	148
	MWCNTs	Mimic response due to TLR agonists	43
		Induce macrophage activation by a calcium-dependent signaling cascade	151
		Increase antigen-specific killing ability	153
	Graphene QDs	Induce apoptosis by NF-κB pathway and autophagy by p38MAPK pathway	154
		Polarize T cells towards T_H2 phenotype	44
	Silica NPs	Particle size, charge, and hydrophobicity impact immunogenicity	156
		Induce antigen-specific T cell and antibody responses	157
		Particle size and charge impact uptake and inflammatory cytokine secretion	160

Table 3.1: Inorganic materials can promote inflammation or tolerance in the absence of other immune signals.

3.3.1 Gold Nanomaterials

Gold has been used in modern medicine since the 1920's when it became a common treatment for tuberculosis.[89] Its use in autoimmunity began shortly after when it was thought that tuberculosis led to RA. More recently, gold has been used in other applications such as cancer and as an antimicrobial agent. AuNPs can range in size from 1 nm to 100 nm and have strong optical absorption and light scattering due to localized surface plasmon resonance (LSPR).[73] This optical phenomena occurs when light interacts with conductive NPs that have a diameter smaller than the incident wavelength. Resonance can be tuned by altering the aspect ratio of gold NMs. These features make AuNPs desirable for imaging applications and photothermal therapy. Additionally, they can be conjugated with a wide variety of biomolecules such as immune signals.

Despite its long-term use, the mechanism of gold's ability to modulate immune responses is still widely unknown. One study probed the effectiveness of gold in treating inflammatory diseases that are dependent on IL-1β, a pro-inflammatory cytokine associated with inflammation, pain, and autoimmunity. [90] Citrate-stabilized AuNPs measuring 5, 15, 20, and 35 nm in diameter were incubated with THP-1 human myeloid leukemia cells because they express numerous IL-1β receptors per cell. Interestingly, treatment with 5 nm particles specifically blocked activation induced by IL-1β. Since larger particles did not have the same result on activation, size effects were further probed by normalizing overall surface area of the AuNPs, irrespective of the diameter of the particles used to treat. Interestingly, this approach revealed that activation decreased with decreasing particle size, suggesting that the anti-inflammatory activity is related to the ability of AuNPs to interact with extracellular IL-1β (**Figure 3.1**). AuNP size has also been implicated in other important immunological steps: particle size was shown to impact the mechanism by which they are internalized [91] and the ability to blunt inflammatory TLR9 signaling [92] in macrophages.

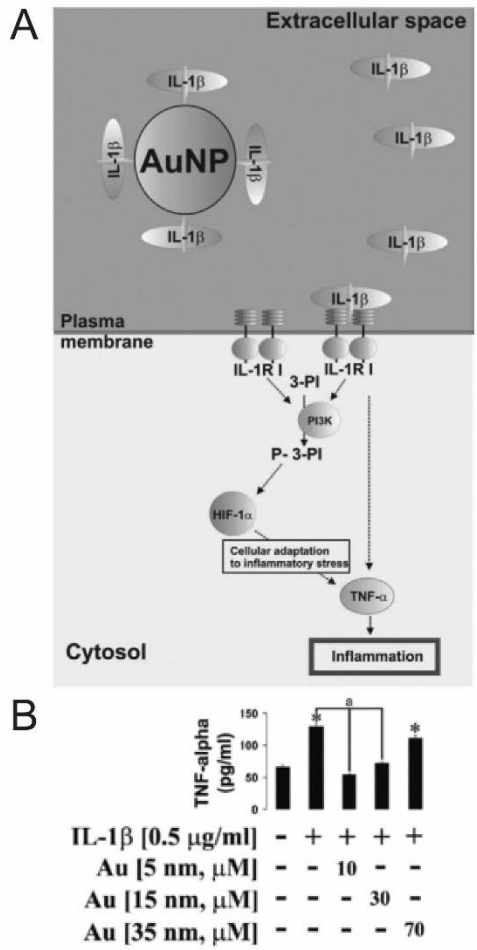

Figure 3.1: The ability of AuNPs to block IL-1β-induced cell activation is dependent on particle size. A) AuNPs interact with extracellular IL-1β, blocking interactions with receptors. **B)** The effect of AuNPs on pro-inflammatory cytokine expression is dependent on size. Adapted with permission from [90].

Using a systematic approach, the effect of hydrophobicity on immune response was analyzed by developing AuNPs functionalized with different surface groups.[93] Importantly, a spacer was employed to remove background effects and specifically isolate the effects of the increasingly hydrophobic groups. The immune response to eight different functionalized particles, with a core size of 2 nm, was investigated by treating splenocytes isolated from mice and quantifying mRNA expression by QT-PCR

(**Figure 3.2A**). Remarkably, an essentially linear correlation was found between increasing hydrophobicity and increased expression of a number of pro-inflammatory genes including TNF-α, IL-6, and IFN-γ (**Figure 3.2B**). This work reveals important information about activation of the innate immune response, as hydrophobicity is essentially a danger-associated molecular pattern because hydrophobic regions of the cell membrane are exposed during necrosis or protein denaturation.

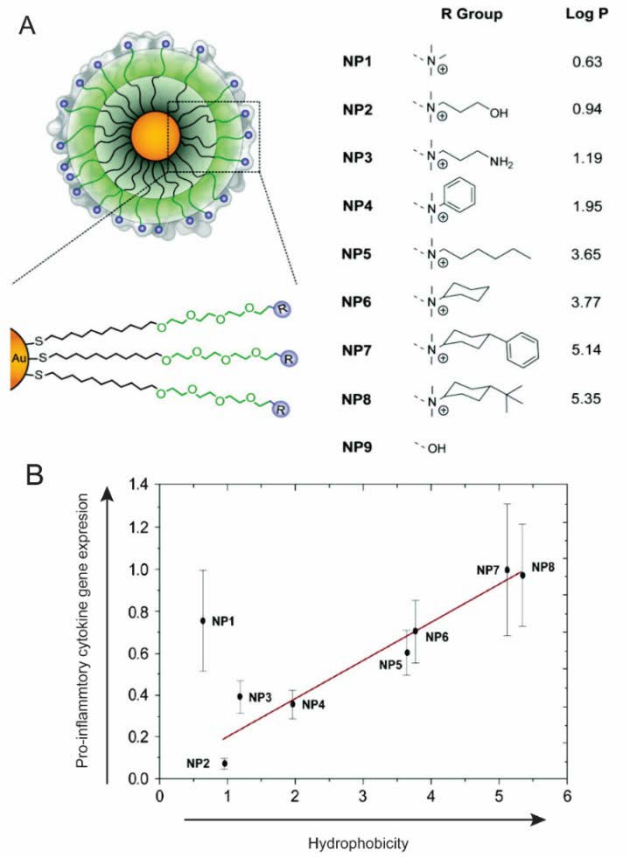

Figure 3.2: Pro-inflammatory cytokine expression is dependent on AuNP surface charge. **A**) AuNP surfaces were modified with surface groups of increasing hydrophobicity. **B**) Increased hydrophobicity resulted in increased gene expression of three pro-inflammatory cytokines. Adapted with permission from [93].

3.3.2 Quantum Dots

Luminescent QDs are nanocrystals consisting of binary combinations of II-IV or II-V semiconductors with radii that are usually found in the 2-10 nm range. Their nanoscale size gives rise to discrete energy bandgaps that allow tuning of their photoluminescence as a function of their diameter from the visible to the near infrared. This tunable photoluminescence, high multiphoton action cross section, photostability, and strong resistance to degradation suggest them as unique fluorescent probes for direct use or in multiplexed analysis, participants in energy transfer, and deep-tissue imaging agents. In addition, their non-trivial surface area allows QD to serve as a nanoscaffold and undergo conjugation with multiple different biomolecules. Their preparation, bioconjugation, and utility for biological applications are described in more detail in several reviews.[74, 94-96]

The properties of QDs mentioned above, including ultra-small size and intrinsic fluorescence, were exploited to develop a real-time imaging modality to track the flow through lymphatics and into LNs.[97] This is important information to gather, as it is the primary route that antigens travel through to reach LNs, the tissues where immune responses develop. CdSe/ZnS core/shell QDs were tracked by fluorescence microscopy and allowed rapid visualization of flow through the cervical lymphatics into the cervical LNs (**Figure 4.3A**). This approach provided impressive spatial information, revealing that within LNs, the QDs flowed first around the edges of the node through the subcapsular sinuses, then flowed through the intermediate sinus into the medullary sinus (**Figure 3.3B**). This work could be especially important for determining which

regions of LNs antigens or immunotherapies may gather in first, which could help predict the development of an inflammatory or tolerogenic response.

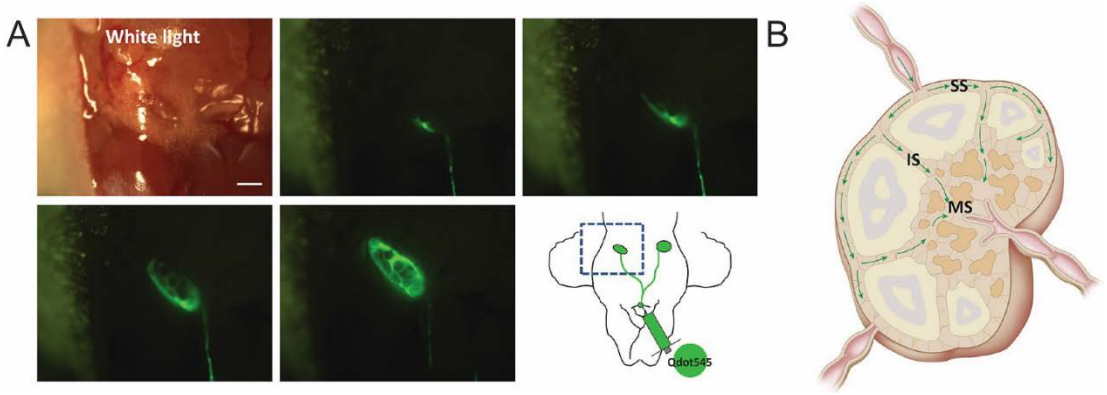

Figure 3.3: QDs serve as a tool to visualize lymph flow. A) Interstitial injection of QDs at the chin allowed rapid visualization of lymph flow through cervical lymphatics into cervical LNs. **B**) QDs flowed first through the subcapsular sinuses, then the intermediate sinus and into the medullary sinus. Adapted with permission from [97].

Another study investigated the immunological impact of QDs on human epidermal keratinocytes (HEK) and human dermal fibroblasts (HDF).[98] Skin cells are considered one of the first lines of defense in the immune system and one possible route of exposure to QDs. Fluorescence microscopy revealed that internalization of the 15 nm CdSe/ZnS-COOH QD nanocrystals by either cell line increased with concentration and exposure time. Analysis of 84 genes associated with the innate and adaptive immune systems revealed that many of the genes impacted by QD treatment were linked to the NF-κB pathway, which plays an important role in inflammation. A decrease in nuclear NF-κB over time was also seen, indicating that QDs may alter pathways associated with oxidative stress, inflammation, or apoptosis.

3.3.3 Carbon Nanomaterials

Numerous NMs, such as CNTs, can be derived from carbon allotropes.[73] For example, single-walled CNTs (SWCNTs) are a single sheet of rolled up graphene and multi-walled CNTs (MWCNTs) are composed of multiple sheets of graphene rolled concentrically. Additionally, these materials can be metallic or semiconducting, as in the case of graphene QDs. The electronic and optical properties, as well as the large surface-to-volume ratio of CNTs make them attractive for biological applications. Important to note is that CNTs are hydrophobic, meaning that functionalization is typically required before use in these applications. Carbon NMs offer specific advantages for immunotherapy such as flexible surface chemistry and enhanced internalization by cells.[99] As they are increasingly used in research, it is important to understand both desirable and undesirable effects they may have on the immune system.[100] These effects can, in part, be attributed to material characteristics of CNTs. Below we will discuss factors including length, charge, and surface functionalization.

Whole genome expression was utilized in an attempt to better understand the complex interactions between CNTs and the immune system.[43] Multi-walled CNTs (MWCNTs) of two different sizes (20 – 30 nm diameter or 9.5 nm diameter) were either oxidized or oxidized and modified with ammonium. Treatment of T cells or monocytes with any of the four types of CNTs led to changes in genes associated with a wide range of pathways, including those related to DC maturation, NF-κB signaling, and T_H1 chemokine secretion. Interestingly, each treatment had a different effect on gene

expression, with no single gene being affected by all four types of CNTs studied. MWCNTs that were modified with ammonium had very little effect on gene expression in T cells compared to those that were unmodified. When analyzing cytokine secretion, however, it was seen that the surface-modified CNTs led to a much larger increase in the secretion of IL-6, IL-1β, and TNF-α. Further, this effect was enhanced with the ammonium-modified CNTs that had a smaller diameter. The changes in gene expression and cytokine secretion seen with CNT treatment mimic those induced by pathogen interaction with TLR, meaning they may produce responses similar to infection or vaccination.

Other studies have continued probing what immunological pathways surface-functionalized CNTs activate to gain understanding of the intrinsic immunogenic features of these materials. For example, one study assessed the stimulation and migration of macrophages following treatment with carboxylated MWCNTs. [101] While quiescent RAW264.7 macrophages showed little capacity for migration *in vitro*, incubating the cells with CNTs led to a high level of migration, indicating that they can act as a chemokine. Analysis of cells that had migrated towards the MWCNTs revealed a high level of internalization, and further led to activation. Due to recent revelations that calcium mobilization initiates immune cell activation, the impact of calcium transport inhibitors on CNT-induced activation and migration was also studied.[102] It was discovered that inhibitors significantly blunted migration, leading to the conclusion that carboxylated MWCNTs lead to macrophage activation through a

calcium signaling cascade (**Figure 3.4**). These studies may shed light on specific mechanisms of the effects CNTs have on a cellular level.

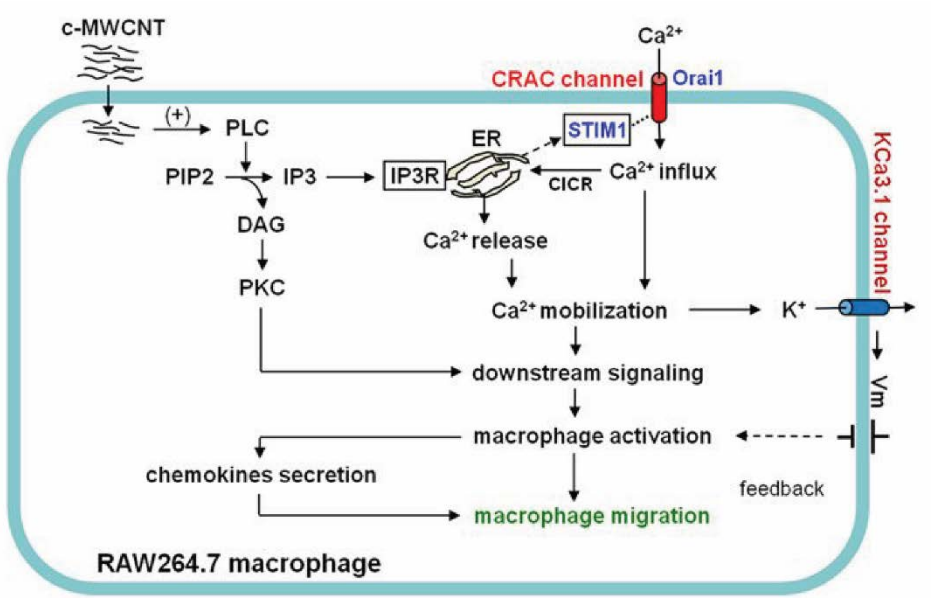

Figure 3.4: Carboxylated MWCNTs induce macrophage activation and migration through a calcium-dependent signaling cascade. Reprinted with permission from [101].

As previously mentioned, many factors are thought to influence the immunogenicity of inorganic materials. For this reason, the impact of size and surface charge of MWCNTs on immune response is also of interest. Short (~122 nm) and long (~386 nm) CNTs that were positively or negatively charged were tested in bone marrow DCs (BMDCs). [103] Interestingly, short MWCNTs with a negative charge (-23.4 mV) were much more readily internalized by BMDCs than long, positively charged (+5.8 mV) CNTs. The tubes were also conjugated with a model antigen, OVA, to test the impact on T cells. T cells were isolated from transgenic mice expressing a T cell receptor that recognizes OVA. When BMDCs treated with OVA-MWCNTs were co-cultured with

T cells, those that were short and negatively charged increased proliferation and IFN-γ secretion, which correlates with uptake in BMDCs (**Figure 4.5**). Additionally, mice that were injected with short, negatively charged CNTs had an increased antigen-specific killing ability. This fundamental information could improve the rational design of CNT-based immunotherapies which specific emphasis on how to enhance internalization by immune cells.

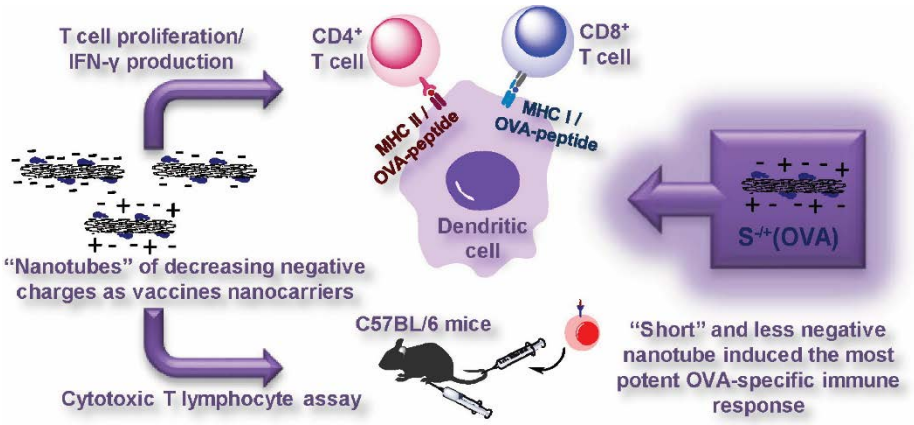

Figure 3.5: Cellular uptake of CNTs and subsequent T cell response is dependent on both size and charge. Reprinted with permission from [103].

The interaction of graphene QDs with macrophages was studied by focusing on two important inflammatory pathways.[104] It was first determined that increasing doses of QDs (~3 nm) induced increasing levels of apoptosis and autophagy in cells. QD incubation increased the activity of p38 MAPK, which responds to stress factors and inflammatory cytokines, and NF-κB, which regulates the level of pro-inflammatory cytokines. Inhibitors of each pathway were used to further probe the mechanisms of immunotoxicity, and revealed that QD-induced apoptosis was regulated by the NF-κB pathway and autophagy was regulated via the p38MAPK pathway. Understanding the

cellular pathways at play in intrinsic immunogenicity of materials is a key aspect to the design of immunotherapies.

While the previous example investigated graphene QDs in a macrophage cell line, it is important to probe interactions of materials with human cells. In stimulated human PBMCs, non-toxic doses of QDs inhibited proliferation. [44] The oval-shaped QDs were 2 nm high and 23.6 ± 7.0 nm long with a surface charge of -9.4 ± 0.8 mV. The treated cells also produced less inflammatory and T_H1 associated cytokines, such as IL-6 and IFN-γ, respectively. Interestingly, QD treatment induced enhanced secretion of anti-inflammatory and T_H2 associated cytokines. Additionally, while QD treatment had little effect on immature DCs, stimulated DCs produced less T_H1 and T_H17 associated cytokines. When these stimulated and treated DCs were incubated with T cells, less proliferation was seen compared to control co-cultures. Intracellular cytokine staining also confirmed a polarization towards the T_H2 phenotype, away from the T_H1 and T_H17 phenotypes. This polarization away from inflammatory phenotypes demonstrates a tolerizing effect from graphene QDs.

3.3.4 Silica Nanomaterials

Silica NPs, which can range in size from tens to hundreds of nanometers, are biocompatible and relatively low cost. These materials have been investigated as delivery vehicles for vaccine components because the size, surface chemistry, and morphology can be tuned during synthesis. Through silane chemistry, a silica particle

can be modified to include a variety of functional groups such as carboxyl, amine, or thiol.[105] Functionalization ability and large surface area are desirable for conjugation of biomolecules. Additionally, silica NPs can be formed with pores of tunable size by manipulating reaction conditions. Mesoporous NPs are specifically useful for cargo transport and release.

The surface characteristics of monodisperse silica NPs can be controlled by coating them with numerous poly(amino acid)s (PAAs).[106] To study the impact of surface character on immune response, *N*-hydroxysuccinimide (NHS)-coated particles were decorated by either polymerization of amino acids or conjugation of an amino acid to the particle surface. Cytokine production was measured in response to the synergistic immunostimulatory effect of silica NPs and one of two TLR ligands. The secretion of IL-1β by mouse BMDCs was found to be correlated with both NP size and hydrophobicity. Highly hydrophobic particles coated with poly(histidine) were found to be the most immunogenic and were used to compare particles of different sizes (**Figure 3.6A**). Interestingly, the smallest particles (300 nm) induced the highest IL-1β levels compared to 1 μm or 10 μm particles. Surface charge, which was controlled by amino acid conjugation, had no effect on immunogenicity in BMDCs. This varied greatly when IFN-γ production levels were measured in T cells activated by treated BMDCs. In this case, cytokine secretion was enhanced as surface charge of the NPs became more cationic (**Figure 3.6B**). Like in BMDCs, more hydrophobic particles were found to be more immunogenic. Experiments that systematically control

biophysical parameters of particles provide essential information for understanding interactions with the immune system.

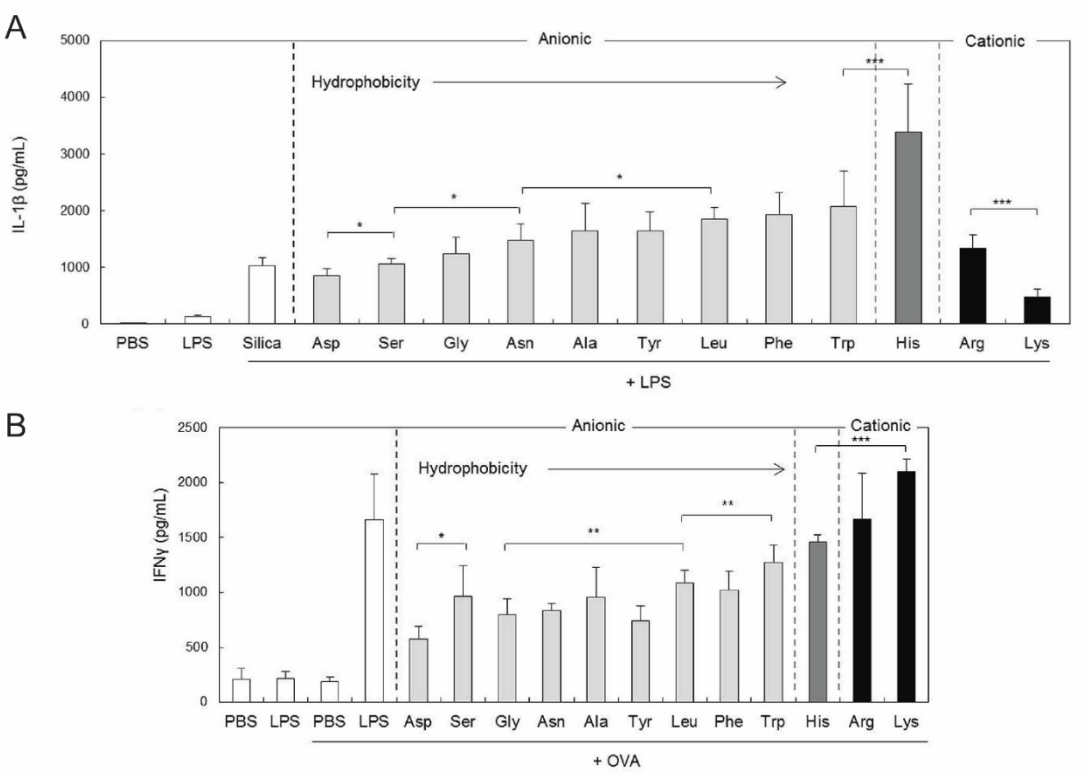

Figure 3.6: Immunogenicity of silica NPs is dependent on size, charge, and hydrophobicity. A) Secretion of IL-1β by BMDCs increases with increasing hydrophobicity of amino acid groups added to the particle surface. **B**) IFN-γ secretion by T cells increases with increasing hydrophobicity and charge of NP surface. Adapted with permission from [106].

Rather than testing particles in conjunction with TLR agonists, one study investigated the self-adjuvanting abilities of mesoporous silica NPs delivering OVA in mice.[107] The 91 nm NPs were formed with 3.6 nm pores. Interestingly, when particles were amino-functionalized by co-condensation, they were able to adsorb OVA with 2.5-fold greater efficiency than non-functionalized NPs. Mice receiving either a low dose or a high dose of OVA bound to NPs showed a strong antibody response. Interestingly,

however, a much stronger antigen-specific T cell-mediated response was seen when mice were treated with the higher dose. Interestingly, other studies have found that the inflammatory effects of silica NPs can be inhibited by functionalizing the particle surface with carboxyl, phosphate, or amino groups. [108, 109]

In an investigation probing size effects on immunogenicity, silica-titania core-shell hollow NPs were synthesized with distinct sizes: 25, 50, 75, 100, and 125 nm.[110] Silica NPs were prepared and titanium tetraisopropoxide was added to create the titania-coated layer. Silane treatment was then used to modify these particles with cationic (amine), anionic (carboxylate), or neutral (methyl) surface groups. Cellular uptake, toxicity, and immunogenicity were measured in mouse alveolar macrophages and human breast cancer cells. A correlation was found between increasing cell uptake and decreasing NP diameter. There was also a trend associated with surface charge, where cationic NPs were taken up more efficiently than neutral or anionic particles. The impact of size and charge on the innate immune response was then tested by measuring the expression of IL-1, IL-6, and TNF-α by macrophages. The 50 nm particles, which were internalized most efficiently, induced the highest secretion levels of each cytokine in macrophages. Size-dependent effects on inflammatory cytokine secretion were also observed in the THP-1 macrophage cell line.[111]

3.4 Inorganic materials can improve vaccination strategies targeted at infectious diseases

The goal of vaccination against infectious diseases is to produce a robust, antigen-specific response that protects against future exposure. While there has been great success with existing vaccine strategies, challenges still exist such as the need for controlled release, targeting to specific tissues, and the delivery of insoluble molecules. Inorganic materials offer unique properties in this regard. Researchers have studied a wide array of materials such as gold NMs, QDs, silica NPs, CNTs,[112-114] and iron oxide NPs[115] as delivery platforms for immune signals and/or as self-adjuvants in infectious disease vaccination. Some examples are summarized in **Table 4.2** and discussed in detail below.

Setting	Inorganic material	Effect	Ref.
Infectious disease	AuNPs	Delivering antigen and adjuvant reduces viral load in liver infection model	171
		Adjuvant delivery results in 100% survival in a glanders lethal challenge model	174 176 177
	Au NMs	Surface area is correlated to cytokine and antibody production against West Nile virus envelope protein	178
	Silica NPs	Delivery of a DNA vaccine results in 100% protection from Newcastle disease virus challenge	182
		Antigen delivery results in strong, long-lasting antibody and cell-mediated responses	183 184 185
	QDs	Inhibit replication of herpes simplex virus-1	186

Table 3.2: Efficacy of vaccines can be enhanced by inorganic materials.

3.4.1 Gold Nanomaterials

Gold NMs have been investigated in immunotherapeutic applications to infectious diseases such as HIV[116, 117], listeria[118], and malaria[119] with successful results seen in mice and rabbits. As demonstrated above, material characteristics can play a crucial role in the inflammatory response generated by NMs. AuNP size can be easily and precisely controlled over a large range from a few to several hundred nanometers. Additionally, they can be decorated with a large amount of antigen or adjuvant by simple chemistry.

Several groups have systematically tested the effect of AuNP size on response to viral proteins. For example, it was found that the antibody response to a foot-and-mouth disease-related peptide was dependent on particle size.[120] In a study of AuNP size effects in a codelivery system, particles ranging from 15 to 80 nm were screened for optimal delivery of OVA and an oligonucleotide that interacts with TLR9, CpG. [121] The antigen and adjuvant were directly conjugated to the particle surface through Au-S bonds. 60 nm OVA-NPs led to the highest level of antigen presentation by DCs and 80 nm CpG-NPs induced the highest expression of activation markers. Both antigen presentation and activation of DCs is necessary to induce a T-cell mediated and/or antibody-mediated response. For this reason, DCs were pulsed with a cocktail of 60 nm OVA-NPs and 80 nm CpG-NPs and injected into mice. After 48 hours, the pulsed DCs largely accumulated in the spleen and in two liver-draining LNs (**Figure 3.7**). When a robust antigen-specific T cell response to OVA was seen, the approach was next employed to test protection against viral infection. Mice were immunized with DCs 5

days prior to injection of OVA gene-containing adenoviral vectors that lead to liver infection. Mice immunized with AuNP cocktail-pulsed DCs had a significantly reduced viral load compared to control mice or mice receiving DCs that had been pulsed with free CpG and OVA. In a similar strategy, AuNPs were decorated with the matrix 2 protein from influenza A and delivered along with soluble CpG.[122, 123] This vaccination strategy led to complete protection from a lethal influenza challenge, further demonstrating the utility of AuNPs as delivery vehicles for antigen and/or adjuvants.

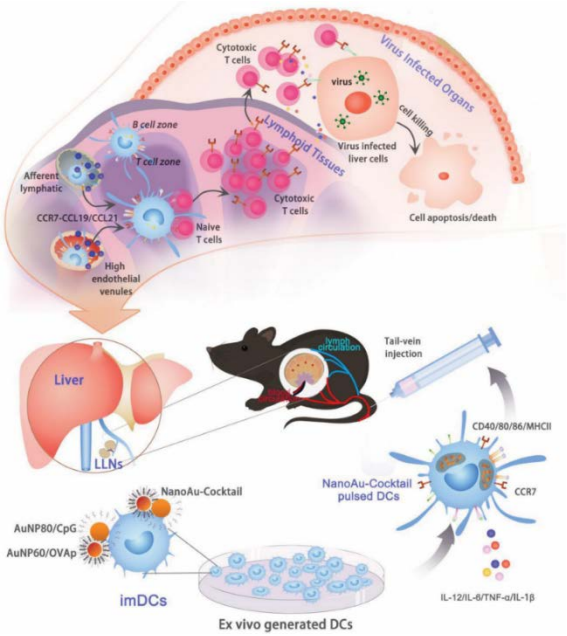

Figure 3.7: A cocktail of AuNPs found to induce APC activation and presentation accumulates in liver-draining LNs and reduces viral load in a mouse model of liver infection. Reprinted with permission from [121].

In another disease model, AuNPs were used as an immunization strategy to protect against glanders, which primarily affects horses and results in death in just a few days. [124] The bacterium responsible for glanders leads to a high mortality rate that is

partially due to its expression of lipopolysaccharide (LPS), an agonist to TLR4. Limited success has been seen with immunization with LPS alone, leading only to partial protection, likely owing to LPS's T cell-independent nature.[125] In an attempt to improve this effort, LPS was conjugated to a protein carrier and covalently coupled to the surface of 15 nm AuNPs.[124] Immunized mice produced significantly enhanced IgG and IgM responses compared to control groups. Nano-glycoconjugates synthesized with one of three protein carriers (TetHc, Hcp1, or FliC) all improved survival in a mouse challenge model of glanders compared to LPS treatments alone. In a Rhesus macaque model, slightly increased protection was seen in vaccinated animals, but the difference in overall survival was not significant. [126] For this reason, the vaccine was resynthesized by first screening an array of antigens *in silico*.[127] Impressively, when two proteins identified by this method (hemagglutinin and FlgL) were incorporated into the nano-glycoconjugate vaccine, 100% survival was observed in Rhesus macaques following a lethal challenge of glanders. This series of studies underscores the importance of rational design in vaccine applications.

While both studies above demonstrated the conjugation of an adjuvant to AuNPs, it has been shown that metallic NMs can, themselves, serve as the adjuvant in vaccination strategies.[128] One study tested gold NMs as a self-adjuvanting delivery system and vaccine. As previously discussed, biophysical parameters impact the degree to which inorganic materials stimulate the immune system, leading the researchers to also test the impact of size and shape on the immune response to a viral protein.[129] Spherical, rod, and cubic NMs were developed and coated with West Nile virus envelope

(WNVE) protein. Interestingly, each shape induced a different level of antibody production against WNVE in mice, with 40nm spherical NMs causing the most significant response (**Figure 3.8**). This did not correlate with uptake of the materials by RAW264.7 macrophages where gold nanorods were internalized most efficiently and led to the production of IL-1β and IL-18, indicating inflammasome activation. In contrast, only the cubes and 40 nm spheres induced the secretion of other inflammatory cytokines such as TNF-α, IL-6, IL-12, and GM-CSF. After analyzing a number of material properties, surface area, which is related to both size and shape, was clearly the most highly correlated parameter with cytokine and antibody production. This study and the work previously described using silica NPs,[106] demonstrate that it is necessary to systematically control multiple particle parameters to gain a more complete understanding of the intrinsic immunogenicity of inorganic materials.

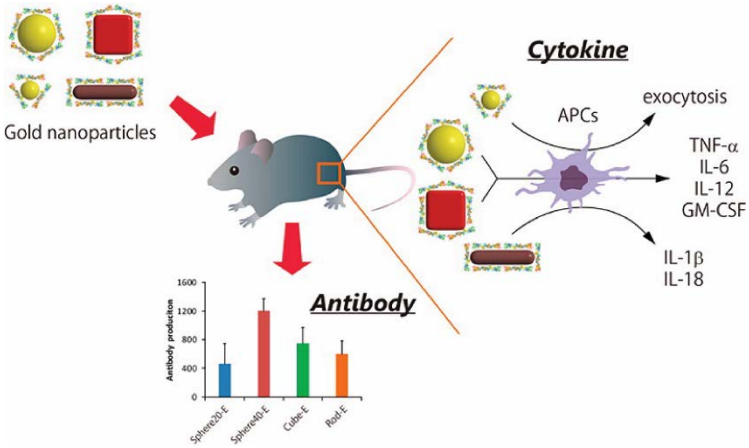

Figure 3.8: Innate and adaptive immune responses induced by gold NMs are dependent on surface area, which relates to both size and shape. Reprinted with permission from [129].

3.4.2 Silica Nanomaterials

Silica NPs have also recently gained the attention of researchers as a self-adjuvanting delivery system for prophylactic vaccine applications.[130, 131] For example, layered

double hydroxide SiO_2 NPs have been synthesized to deliver a DNA vaccine aimed against Newcastle disease virus (NDV), which mainly affects avian species but can be transmissible to humans.[132] These 90 nm particles feature a core-shell structure, protect plasmid DNA from enzymatic degradation, and promote controlled release over 288 hours. Importantly, plasmid-containing NPs could induce a similar level of expression in HEK cells compared to plasmid delivered with a commercial transfection agent. Serum antibody levels against NDV peaked 5 weeks post immunization in chickens. Demonstrating the impact of the NPs as an adjuvant, titers remained significantly higher through 8 weeks in mice that received the NP vaccine compared to those that received naked DNA. Additionally, at weeks 4 through 6, this group also produced the highest level of lymphocyte proliferation. Immunization of chickens with the NP vaccine resulted in 100% protection from disease challenge with no clinical signs observed, compared to 60% death with naked plasmid delivery, exemplifying the unique advantages inorganic materials offer for improving vaccinations against viruses.

Following a previous study that demonstrated the self-adjuvanting abilities of mesoporous silica NPs delivering OVA in mice[107], similar nanovesicles were tested as an immunization strategy for Bovine Viral Diarrhoea Virus (BVDV).[133-135] The NPs, which feature a 50 nm diameter, 6 nm wall thickness, and 16 nm pores, adsorb the viral E2 protein, which is a major immunogenic determinant of BVDV. Mice immunized with the nanovaccine elicited a 10-fold stronger antibody response compared to mice receiving the E2 protein with a strong adjuvant.[134] Importantly, the NPs also led to a strong cell-mediated response that was significantly higher than

the traditional vaccine control. In an attempt to address the cold chain challenge of vaccine storage and delivery, the group also investigated the ability of the nanovaccine to produce long-term immune responses in mice and sheep once freeze-dried.[133, 135] Shortly after vaccination, animals treated with the freeze-dried NPs showed a robust antibody and cell-mediated response. Importantly, both responses were still detectable after 6 months. These studies took the important step of comparing a nanotechnology-based approach to a more traditional vaccine design including only an antigen and adjuvant, which demonstrated a considerable advantage.

3.4.3 Quantum Dots

As discussed in the previous section, various types of QDs have been shown to affect the NF-κB pathway.[98, 104] The mechanism behind NF-κB signaling inhibition was further probed with aqueous synthesized QDs with emissions of 515 nm and 545 nm and corresponding sizes of 2.2 nm and 2.7 nm.[136] Pretreatment of cells with either QD type significantly reduced NF-κB activation induced by TNF-α or TLR agonists. The NF-κB pathway is critical in regulating the expression of viral genes and is implicated in cancer because it negatively regulates apoptosis. Accordingly, QD treatment was shown to significantly inhibit herpes simplex virsus-1 induced activation of NF-κB in cells, which suppressed viral replication. Additionally, QD treatment promoted apoptosis in a human pancreatic cancer cell line, as evidenced by both a down regulation of anti-apoptotic genes and the cleavage of proteins in the apoptotic pathway. Interestingly though, the QDs had no effect on two other important signaling

pathways that have implications in cancer. Unlike other studies discussed in this section, this work analyzed QDs alone, rather than as a delivery vehicle for antigen and/or adjuvant, and found significant effects in pathways related to but viruses and cancer.

3.5 Cancer immunotherapies can produce more robust responses when delivered by inorganic materials

A major challenge in cancer is the immunosuppressive environment that surrounds tumors and limits the immune system's ability to recognize and attack cancer cells. The current treatment methods of chemotherapy and radiation are non-specific and highly toxic to healthy tissues. The goals of cancer immunotherapy are similar to those of infectious disease vaccination in that the desired outcome is a strong, antigen-specific response. Of specific importance to cancer treatment and prevention is the development of a robust T cell response.[137, 138] Recent developments in this field have included checkpoint blockades that prevent T_{REGs} from suppressing CTLs and chimeric antigen receptor (CAR) T cells that are developed *ex vivo* to be specific for an individual patient's tumor before being implanted back into the patient.[24] Despite these advances, many challenges still face the field of cancer immunotherapy. Inorganic materials present an interesting opportunity to face some of these challenges because they can co-deliver multiple signals, target immune cell populations, and even serve as an imaging modality. **Table 3.3** lists examples that are detailed in this section.

Setting	Inorganic material	Effect	Ref.
Cancer	QDs	Promote apoptosis in human pancreatic cancer cell line	186
	AuNPs	Antigen-decoration delays, reduces, or inhibits tumor growth in B16F10, B16-OVA and 4T1 cancer models. Efficacy in EG7-OVA model was dependent on NP size.	194 195 196
		Efficacy in B16-OVA cancer model is dependent on adjuvant choice for immune signal coating	199
	SWCNTs	Antibody-coating targeted intratumor but not peripheral T_{REGs}	200
		Taken up by monocytes, enter tumor interstitium, and extravasate blood vessel walls.	201
		Ablation results in strong local and systemic anti-tumor response with memory	208
	Iron oxide NPs	Magnetic targeting of IFN-γ coated NPs destroys tumors	210
		DCs containing tumor lysates and heat shock protein-coated NPs increase survival in glioma model	212
	Iron oxide-zinc oxide NPs	DCs containing antigen-coated NPs increase survival in CEA cancer model	214

Table 3.3: Inorganic materials promote strong anti-tumor responses.

3.5.1 Gold Nanomaterials

AuNPs have been heavily researched in cancer applications because they can deliver cancer antigens[139] and adjuvants[140], can be imaged *in vivo*[141], and through thermal application, can ablate tumors.[142] In a model antigen study, AuNPs were coated with red fluorescent protein (RFP) and CpG as a cancer vaccination strategy (**Figure 3.9A**).[141] RFP was attached through an Au-S bond and thiol-modified CpG with a ten adenine spacer was attached to form 20 nm particles. Interestingly, RFP-coated AuNPs were able to elicit antigen-specific antibody (**Figure 3.9B**) and T cell (**Figure 3.9C**) responses regardless of the inclusion of CpG, indicating a self-

adjuvanting ability of the particles. This translated to a delay in the growth of RFP-expressing B16F10 tumors in mice for up to 4 weeks for both groups. Another study reported similar results when co-delivering OVA-AuNPs and CpG-AuNPs.[143] OVA-coated particles alone were sufficient in inhibiting B16-OVA tumor growth and the addition of CpG-AuNPs did not enhance this effect. Researchers that tested the delivery of OVA and CpG on poly(propylene sulfide) NPs, however, reported that the CpG coated particles were necessary to delay EG7-OVA tumor growth.[144] This difference in these results further underscores the importance of understanding the reaction of an inorganic material delivery system with the immune system when developing cancer immunotherapy strategies.

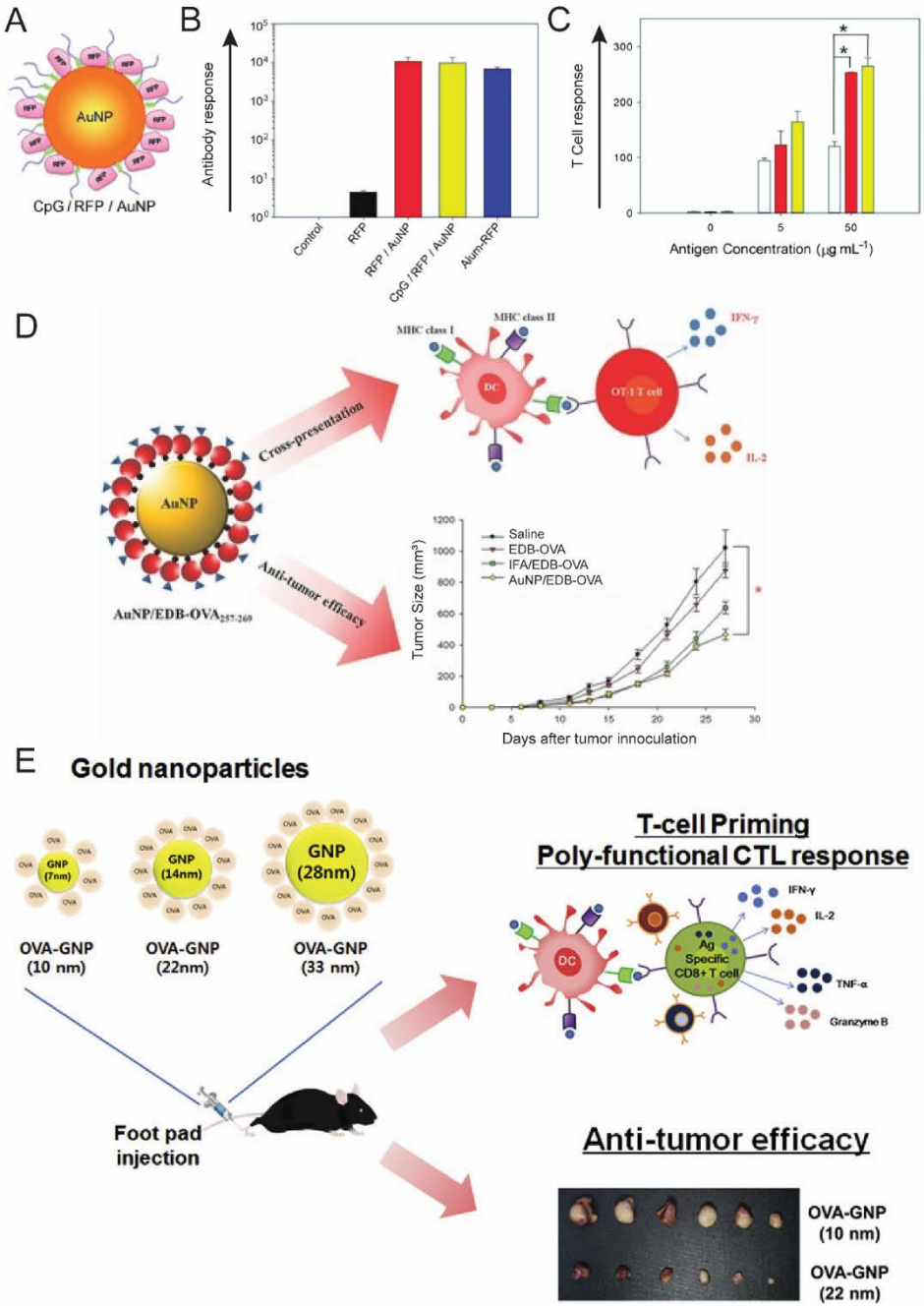

Figure 3.9: AuNPs can serve as a self-adjuvanting delivery system for antigens in multiple cancer models. A) AuNPs coated with model antigen RFP induce a robust antigen-specific antibody (**B**) and T cell (**C**) response without the inclusion of adjuvant. **D**) Conjugation of a cancer antigen to OVA on AuNPs promotes cross presentation and results in a reduction in tumor growth. **E**) CTL response and subsequent efficacy in cancer models depends on AuNP size. Adapted with permission from [141], [145], and [146].

The AuNP platform was next evaluated in the more relevant, 4T1 breast cancer model that highly expresses extra domain B (EDB) of fibronectin.[145] Previous work demonstrated a robust antibody response following an EDB-targeted vaccination, but did not show a cell-mediated response.[147] It was hypothesized that the self-adjuvanting ability of AuNPs could promote a T cell response, thought to be necessary for cancer treatment, to the tumor-associated antigen. By adding OVA to the C-terminus of EDB and two cysteine residues to the N-terminus, the protein could bind to AuNP surfaces (**Figure 3.9D**). The inclusion of OVA promoted cross presentation, a process where antigen is displayed on MHCI to $CD8^+$ T cells – a necessary step in the immune cascade for the development of antigen-specific CTLs. In addition, NP treatment of mice with established 4T1 tumors significantly reduced growth. Therapeutic studies are critical to determining translation potential of cancer immunotherapies due to the unlikeliness of patients receiving prophylactic tumor vaccinations.

Further studies aimed to elucidate the effect of AuNP size on delivery to LNs, where a response against cancer antigens can develop, and the subsequent T cell response (**Figure 3.9E**).[146] *In vitro*, there was a trend associated with increasing size of OVA coated NPs and increases in DC uptake, DC activation, and inflammatory cytokine secretion by T cells, all important steps in the development of robust anti-tumor immunogenicity. Following injection in mice, greater uptake was seen in popliteal LN-resident DCs for 22 nm and 33 nm particles compared to the smallest 10 nm NPs. This uptake was directly correlated with an enhanced $CD8^+$ T cell response, an important

consideration in cancer therapeutics. Next, prophylactic OVA-AuNP injection was tested as a strategy to slow or prevent the growth of tumors in the EG7-OVA cancer model. The effect of size on immunogenicity translated to this model where the larger particles significantly slowed tumor growth, but the smaller particles had no significant effect. This series of studies showed the efficacy of an AuNP delivery system in multiple models of cancer, but underlines the importance of understanding parameters such as particle size in initial steps of the immunological cascade and the ultimate therapeutic outcome.

Another AuNP immunization strategy involves coating them with polyelectrolyte multilayers composed entirely of immune signals (iPEMs).[148] The positively charged antigen (OVA peptide) and negatively charged adjuvant (TLR3 agonist) can be alternatingly deposited onto the particle surface as a method of codelivery (**Figure 3.10A**). Each bilayer added approximately 10 nm to the particle diameter to a final size of 43.5 nm after four bilayers. iPEM-coated AuNPs treatment induced both activation and antigen presentation in DCs. Additionally, injection of the NPs in mice produced a strong antigen-specific T cell response. Understanding the need for more insight into the mechanism of inorganic materials, the impact of injection route, immune signal dose, and adjuvant choice on the T cell response was assessed.[149] Interestingly, intradermal injection produced the most robust response, followed by *s.c.* and intramuscular injections (**Figure 3.10B**). This result could be important for clinical translation of particle-based therapies as intramuscular is the most commonly used injection route in vaccination, but in these studies this route produced the weakest

response. In a B16-OVA murine melanoma model, the adjuvanting abilities of TLR3 agonist poly(inosinic:cytidylic acid) (polyIC) and TLR9 agonist CpG were compared. While iPEMs consisting of OVA peptide and polyIC delayed tumor growth, those containing CpG had a more robust effect resulting in 50% survival, compared to 0% in untreated mice. The rational design of future cancer immunotherapies will require answering such fundamental questions as what the best route is for injection and what the most effective adjuvant is.

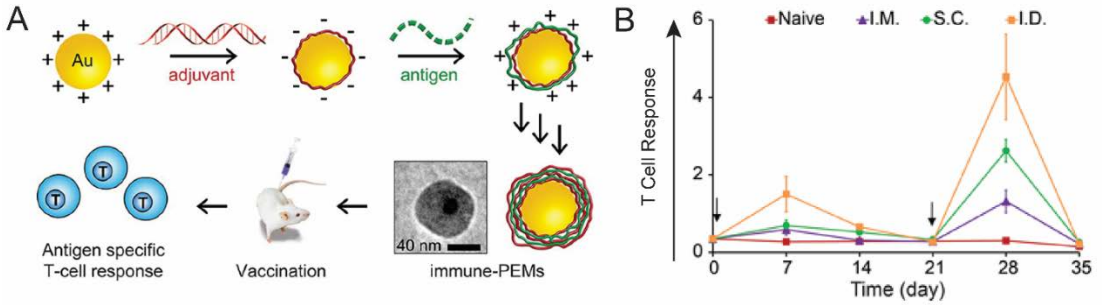

Figure 3.10: Immune signal-coated particles produce robust an immune response. A) AuNPs coated with alternatingly deposited antigen and adjuvant induce an antigen-specific T cell response in mice. **B**) The intradermal injection route produced the most robust response over intramuscular and *s.c*. Adapted with permission from [148] and [149].

3.5.2 Carbon Nanomaterials

T_{REGs} have been increasingly implicated in cancer because they can blunt immune responses directed at the tumor. NMs offer an opportunity to target and potentially destroy this cell population. One group aimed to target intratumor T_{REGs}, but not peripheral T_{REGs} with delivery of SWCNTs (**Figure 3.11**).[150] The first experiment assessed the expression of a number of markers on T_{REGs} and effector T cells. Because glucocorticoid-induced TNFR-related receptor (GITR) displayed the highest

expression on intratumor T_{REGs}, an anti-GITR mAb was chosen as the targeting agent. A systematic analysis of the effects of antibody number per tube, SWCNT concentration, and incubation time on T_{REG} targeting efficiency *in vitro* was performed. Five antibodies per 101 nm-length tube was found to be optimal and maximum internalization occurred after a short incubation time. Relatively low doses (~5 μg) of SWCNTs were most efficiently delivered to T_{REGs} in the spleens of naïve mice. Additionally, in B16 tumor-bearing mice, the GITR-decorated tubes were targeted to T_{REGs} in the tumor with 3-fold higher efficiency than to splenic T_{REGs}, indicating the strategy's specificity.

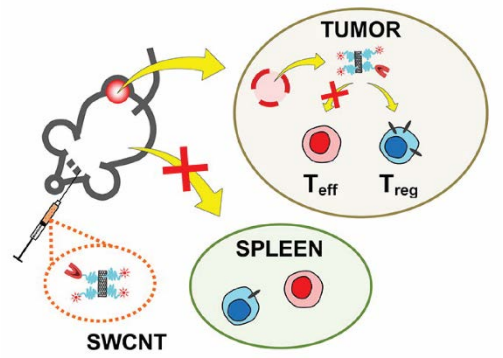

Figure 3.11: GITR-decorated CNTs specifically target intratumor T_{REGs}, implicated in blocking immune responses against cancer. Reprinted with permission from [150].

Studies show that SWCNTs are one of the most efficiently delivered NMs in tumor applications, but little focus has been put on understanding the method of tumor targeting.[151] Following an initial publication demonstrating that SWCNTs can accumulate in the tumor via both active and passive targeting mechanisms, additional factors were assessed.[152] Mice were first injected with tumor cells, followed 10 days later by *i.v.* injection of SWCNTs with a diameter around 1 nm and lengths between

100 and 300 nm. The tubes were mixed with Cy5.5-NHS and sulphosuccinimidyl 4-N-maleimidomethyl cyclohexane-1-carboxylate to enable imaging and were found to be taken up by circulating blood cells, specifically Ly-6C^{hi} monocytes. The monocytes then entered the tumor interstitium and appeared to extravasate blood vessel walls. Interestingly, when the tubes were reacted with a thiolated peptide sequence (RGD) known to target angiogenic tumor blood vessels or an irrelevant peptide (RAD), no differences were seen in tumor accumulation for up to 7 days. After this time, RGD-SWCNTs were retained while RAD-SWCNTs were more readily cleared, suggesting that targeting moieties can be more or less effective depending on the time point when uptake is analyzed. Overall, a better understanding of how inorganic materials can successfully target tumors could lead to overcoming challenges such as systemic toxicity of traditional chemotherapy.

Not only can SWCNTs target tumors [151, 152] and serve as a delivery vehicle for cancer antigens [153, 154] and adjuvants [155], they can also be irradiated *in vivo*. Irradiation can destroy a tumor locally, but recent reports have also demonstrated a systemic immune response following irradiation capable of attacking cancer cells elsewhere in the body.[156, 157] In one approach, 0.8 nm diameter tubes were synthesized with glycated chitosan (GC) as the surfactant.[158] GC serves as a PAMP and when SWCNTs are irradiated, they induce cellular stress leading to secretion of danger-associated molecular patterns (DAMPs). Each of these signals are involved in the activation of innate immunity, and the combination can produce a strong immune response. It was therefore hypothesized that the immunogenicity of tumors could be

enhanced by treatment with GC-SWCNTs. In a mammary tumor model, mice were monitored until they developed 8000 mm^3 tumors. GC-SWCNTs were then injected and the tumor was irradiated by a 980 nm laser after 2 hours, which led to 89.2% apoptosis in local tumor cells. In addition, treatment led to complete tumor regression for all mice in the breast cancer model and for 60% of mice in a hepatoma tumor model. When mice were immunocompromised, however, these effects were substantially inhibited, indicating that efficacy is dependent on a significant immune response rather than just a function of physical destruction of the tumor. Impressively, when immunocompetent mice were rechallenged with mammary tumor cells, the mice that received GC-SWCNTs demonstrated complete protection, indicating a strong memory response. Comparatively, 80% of mice that had originally been treated with PEG-SWCNTs succumbed to rechallenge. A memory response capable of attacking future tumor cells is important as recurrence rates are high for some types of breast cancer. In another experiment, when two tumors were injected on opposite sides of the mouse, treatment in the left tumor significantly inhibited growth of the right tumor, indicating a systemic response. Certain types of cancer, including lung and colon, rapidly metastasize to other tissue types, demonstrating the need for a systemic response following local tumor treatment. This approach can be compared to a similar strategy using NPs formed from degradable polymers that encapsulate a photothermal agent that allows ablation and a TLR7 agonist that serves as the adjuvant.[159] Tumors in the 4T1 breast cancer model or the CT26 colorectal cancer model could be completely ablated by this treatment strategy and combined with checkpoint blockage therapy, the growth of secondary tumors could be completely inhibited. These studies are expressly

interesting because combination strategies are now considered a cornerstone of cancer therapy.

3.5.3 Iron Oxide Nanomaterials

Iron oxide NPs provide an opportunity to target immune signals directly to an area of interest due to intrinsic superparamagnetic nature.[160] Particles can overcome biological barriers and release a payload to a certain area by the application of a magnet. Additionally, these particles can be visualized at to the single-cell level using high-contrast MRI.[161] Recent attention has been put on attaching biomolecules to iron oxide particle surfaces for cancer therapy. The combination of magnetism, imaging, and/or immune signal delivery provides great promise for immunotherapy applications.

One approach involved adsorbing the anti-tumorigenic cytokine IFN-γ to dimercaptosuccinic acid (DMSA)-coated magnetic NPs for use in tumor models.[160] DMSA provides free ligand groups for biomolecule conjugation on the particles, which have a final size of ~400 nm. While IFN-γ can increase the immunogenicity of tumor cells and inhibit tumor angiogenesis, off-target delivery can induce toxicity in other tissues. Magnetic NPs are therefore desirable to deliver the cytokine directly to a specific area. Uncoated NPs were rapidly taken up by Pan02 tumor cells, but IFN-γ-coated NPs exhibited a lower level of uptake which the authors posited could allow longer time for IFN-γ release and localization with receptors located on the cell surface. Following induction of Pan02 tumors in mice, *i.v.* injection of the IFN-γ-coated NPs

led to a 58% reduction in tumor volume compared to PBS-injected mice. When an external magnet was applied to the treated mice, localizing the particles to the tumor site, average tumor volume was reduced by a remarkable 96%. Analysis of the tumor tissue confirmed that mice from this treatment group had the highest level of NP accumulation, which was more specific to the desired site than treatment without the magnetic field. Particle accumulation resulted in higher levels of intra-tumor IFN-γ, and infiltration of cells crucial to an antitumor response including macrophages, T cells, and NK cells. The highest level of anti-angiogenesis and apoptosis in tumors was also seen in mice treated with the IFN-γ-coated NPs and a magnetic field. Inhibition of blood vessel growth within the tumor and promotion of cancer cell death are critical for tumor destruction. Similarly efficacious results were seen in a cancer model that is chemically-induced and more closely mimics human tumor development. This treatment strategy could be applied to the delivery of other toxic molecules that are potent in cancer treatment such as methotrexate or paclitaxel.

Another study on the use of magnetic NPs for cancer treatment involved the delivery of heat shock protein 70 (HSP70) (**Figure 3.12**).[162] A recent study showed that direct injection of HSP70 into tumors resulted in significant inhibition of tumor growth.[163] HSPs are advantageous for immunotherapy applications because they can chaperone antigenic peptides to APCs and promote an adaptive immune response. In an attempt to improve its antigen presenting abilities, HSP70 was coated onto magnetic NPs. Interestingly, HSP70-coated NPs with an average size of 44.3 nm were taken up by DCs more efficiently than uncoated NPs, and accumulated in endosomes and then

lysosomes, suggesting a pathway for endocytosis. When DCs were co-incubated with HSP70-NPs and a FITC-labeled peptide, peptide uptake was significantly enhanced compared to uptake of peptide with uncoated particles. After 24 hours, the peptide was detectable on the surface of DCs, indicating it could be presented to T cells. To confirm this, DCs were first incubated with HSP70-NPs and tumor lysates prior to coculture with $CD8^+$ CTLs. In response, the CTLs produced a high level of IFN-γ and exerted cytotoxicity against four different tumor cell lines. In a glioma model, mice receiving DCs that had been pulsed with HSP70 NPs and tumor lysate showed a significant delay in tumor growth and increased survival rate. These results may have been due to higher infiltration of immune cells into the tumor and an increased killing capacity of CTLs in the peripheral blood. The delivery of HSP-coated inorganic materials provides a unique opportunity to increase the immunogenicity of tumor antigens and promote the development of a robust anticancer immune response.

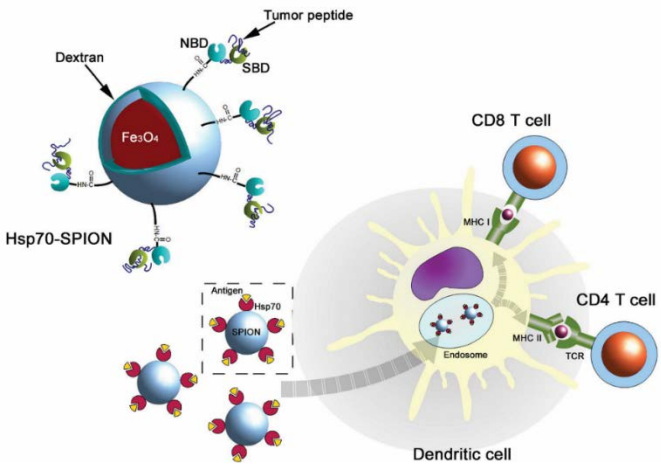

Figure 3.12: Magnetic NPs coated with a heat shock protein enhance cancer antigen uptake and presentation, resulting in a highly cytotoxic T cell response. Reprinted with permission from [162].

A similar NM investigated for cancer immunotherapy applications was iron oxide–zinc oxide core–shell NPs that target DCs.[164] These 15.7 nm particles, capable of serving as an imaging agent, were formed by first synthesizing an Fe_3O_4 core followed by coating with the ZnO shell (**Figure 3.13A**). A novel ZnO-binding peptide was developed to facilitate particle conjugation of carcinoembryonic antigen (CEA), a set of glycoproteins used as a clinical marker of cancer. The DC-targeting ability of these particles was confirmed by microscopy and flow cytometry, which revealed that 95% of cells took up particles within an hour where they localized with endosomes and lysosomes. *In vivo*, NP-containing DCs injected into mouse footpads could be visualized by MRI and produced an antigen-specific $CD8^+$ T cell response. Additionally, NP-DC vaccination significantly reduced tumor growth and prolonged survival in a mouse model with CEA-expressing cancer cells (**Figure 3.13B**). Impressively, tumor growth was also suppressed in transgenic mice spontaneously expressing human CEA, indicating possible translational potential (**Figure 3.13C**).

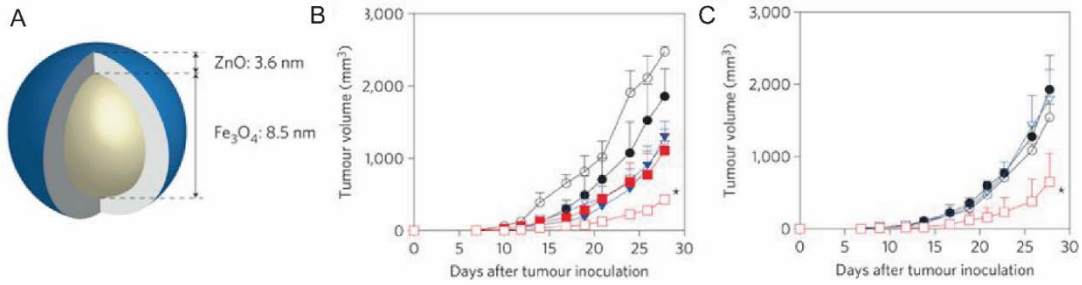

Figure 3.13: A novel core-shell NP design targets DCs for uptake and results in efficacy in cancer models. A) NPs consisting of an iron-oxide core and a zinc-oxide shell can be coated with the cancer antigen CEA. The NPs reduce tumor growth in a mouse model with CEA-expressing cancer cells (**B**) and in mice that spontaneously express human CEA (**C**). Adapted with permission from [164].

3.6 Inorganic materials provide unique opportunities for controlling inflammation in autoimmunity

This review so far has focused on generation of strong immune responses to fight cancer or future infection, but this section will describe the use of inorganic materials to inhibit immune responses. As referenced in the introduction, autoreactive inflammatory immune cells are normally controlled through a process called tolerance. When tolerance is not maintained, autoimmune diseases such as MS, T1D, lupus, and RA can develop. These diseases are characterized by an attack on healthy tissue that leads to chronic inflammation and even death. There are currently no cures available, leaving patients to rely on immunosuppressive drugs or antibodies that can be immunocompromising.[23] The goals of immunotherapy in this context are to restore tolerance to the molecule being attacked, termed a self-antigen. Inorganic NMs offer unique opportunities such as the antioxidant properties of cerium oxide NPs[165] or the innate ability of MWCNTs to inhibit the development of T_H17 cells[166]. Additionally, these materials can deliver immune signals directly to relevant immune cells and tissues to inhibit unwanted inflammation in an antigen-specific manner.[167, 168] Examples of such materials are described below and summarized in **Table 3.4**.

Setting	Inorganic material	Effect	Ref.
Autoimmunity	AuNPs	Antigen and adjuvant delivery induce tolerance is models of MS and T1D	225 230
		Peptide coating reduces disease severity in inflammatory bowel disease model	237
	Iron oxide NPs	Display of self-antigen in MHCs induces tolerance in models of T1D, MS, and arthritis. T_{REG} expansion depends on dose and ligand density.	238 239 240
		Reduce immune cell infiltration in a delayed-type hypersensitivity model	243
	QDs	Efficacy in a model of MS is dependent on self-antigen ligand dose and density	249

Table 3.4: Tolerance can be induced with inorganic materials.

3.6.1 Gold Nanomaterials

One strategy being investigated to restore tolerance in autoimmune disease is delivery of a self-antigen attacked in disease along with a regulatory signal to reprogram the response away from inflammation, towards tolerance.[47, 48, 53, 169, 170] One example of this approach is the synthesis of AuNPs decorated with a self-antigen characteristic of MS, MOG, and a small molecule, ITE, shown to expand T_{REGs} (**Figure 3.14A**).[46] The 60 nm particles were formed by adding MOG and/or ITE dropwise to the mixing gold colloid solution followed by dropwise addition of methoxy-PEG-SH to stabilize against aggregation. The ITE-decorated and co-loaded NPs specifically activated AhR, a pathway stimulated by ITE, while MOG-decorated particles did not. Activation of this pathway has been shown to induce tolerogenic DCs that polarize T cells towards the regulatory phenotype (T_{REGs}).[171-173] It was demonstrated that particle treatment significantly reduced LPS-induced DC activation and maturation *in*

vitro, which led to generation of T_{REGs} in a coculture study. Next, the strategy was tested in a mouse model of primary progressive MS, EAE, which is characterized by increasing paralysis over a 2 – 3 week period. Weekly administration of the co-loaded particles significantly inhibited the development of disease and suppressed the T_H1 and T_H17 cell responses that are characteristic of EAE (**Figure 3.14B**). Additionally, when T cells from mice treated with co-loaded NPs were transferred into naïve mice, they were protected from the development of EAE, pointing towards the development of a strong T_{REG} response. This nanovaccine strategy was also tested as a therapeutic in a relapsing-remitting model of EAE (RR-EAE) which is induced by immunization with amino acids 139 to 151 of PLP and characterized by spreading of the T-cell response to amino acids 178 to 191. Weekly administration of NPs decorated with ITE and $PLP_{139-151}$ and NPs decorated with ITE and $PLP_{178-191}$ resulted in a reduction in severity of paralysis and the number of relapses (**Figure 3.14C**). Efficacy in both disease models is key to translatability as relapsing-remitting MS affects the highest percentage of patients and primary progressive MS is the only type that has no FDA-approved treatments. In a related study that did not feature inorganic materials, degradable PLGA MPs were synthesized to encapsulate and deliver MOG and rapamycin, another small molecule shown to induce T_{REGs}.[25] This strategy achieved reversal of paralysis in

mice with established EAE, further demonstrating the potential of particle-based delivery systems.

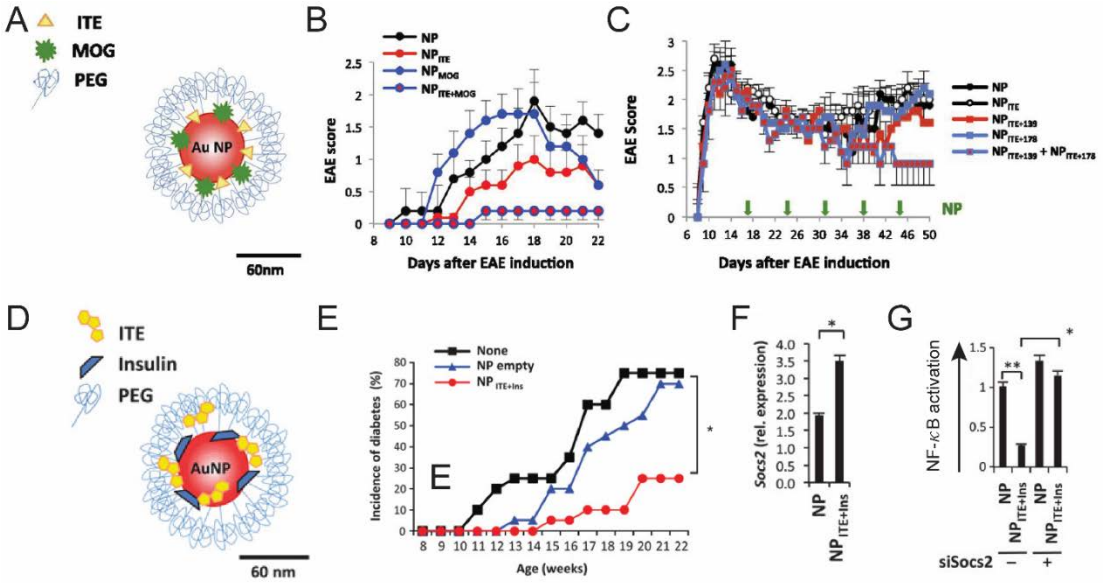

Figure 3.14: AuNPs can codeliver self-antigen and a T_{REG}-promoting small molecule to resolve autoimmune reactions in multiple disease models. A) MOG self-antigen and immunomodulatory molecule, ITE can be coated onto AuNPs. **B**) Particles that deliver both signals significantly inhibited EAE development, while NPs delivering only one signal had a muted effect. **C**) AuNPs delivering self-antigens $PLP_{139-151}$ and $PLP_{178-191}$ reduced relapses in RR-EAE. **D**) AuNPs could also be applied to T1D by delivering ITE and proinsulin, resulting in a reduction of disease incidence in a T1D model. These particles increase the expression of SOCS2 (**F**), and silencing the factor mitigated AuNP suppression of NF-κB expression. Adapted with permission from [46] and [174].

This immune signal-decorated AuNP vaccination strategy was next expanded to T1D, a disease in which T cells attack insulin-producing β cells in the pancreas.[174] Decreased insulin levels leave the body unable to move sugar from the blood stream into cells, resulting in high blood sugar levels which can lead to cardiovascular problems and serious damage to other tissues. In this study, AuNPs were decorated with ITE and a β cell–related antigen, proinsulin, or with ITE and a peptide that activates a diabetogenic T cell clone (**Figure 3.14D**). The particle formulation was

tested in a non-obese diabetic (NOD) model where mice spontaneously develop T1D, and it was found that weekly treatment significantly inhibited disease development (**Figure 3.14E**). Treated mice had decreased levels of inflammatory T_H1 and T_H17 cell-related genes in the pancreatic LNs, but increased expression of a T_{REG}-associated gene. T_H1 and T_H17 cells can both induce diabetes in NOD mice and T_{REGs} are protective against disease development, suggesting a method for tolerance induction by AuNP treatment. When NOD mice received DCs that had been loaded with NPs *ex vivo*, only 10% developed T1D by 22 weeks of age. Further investigation into the mechanism of tolerance revealed that NP treatment in DCs enhanced expression of *Socs2*, a factor associated with suppression of NF-κB activation (**Figure 3.14F**). When *Socs2* was knocked down, the effects of NP administration on NF-κB activation and inflammatory T cell polarization were reverted, suggesting the importance of this factor in the induction of tolerogenic DCs (**Figure 3.14G**). This work provided novel information into the role of NP treatment-induced tolerogenic DCs in T1D development and treatment.

Overactive TLR signaling has been implicated in the pathogenesis of many inflammatory and autoimmune diseases.[175-179] Antagonists of TLRs and downstream pathways are therefore an attractive area of exploration for therapeutics.[65] The recent phase 3 clinical trial failure of a TLR4 inhibitor for sepsis treatment demonstrates the complicated interactions at play and a possible need for therapeutics that can simultaneously block multiple TLRs.[180] To address this need, peptide-AuNP hybrids were developed to inhibit TLR activity and ultimately treat

inflammatory diseases.[181] Peptides were coated onto the 13 nm NPs by simple mixing and were used both to alter the surface chemistry and influence immunomodulatory activity. Screening a library of hybrids identified a specific peptide sequence (CLPFFD) with potent anti-inflammatory activity, designated P12, suppressing the upregulation of 40% of genes in human PBMCs that are typically upregulated by LPS treatment. Further, when particles were taken up by monocytes and macrophages, they localized into endosomal compartments where they blocked acidification (**Figure 3.15**). A control peptide sequence, CPLAAD (P13), did not have the same effect on endosome pH. Modulation of endosomal pH plays an important role in endosomal TLR signaling and more specifically, was linked to reduction in TLR3 and TLR4 signaling. Particle treatment was evaluated in a mouse model of inflammatory bowel disease in which a number of the inflammatory pathways specifically targeted by these NPs have been implicated. Treatment resulted in a reduction in disease severity as measured by body weight loss and colon inflammation, among other factors. These results suggest a new platform to target overactive TLR signaling that may overcome the pitfalls TLR inhibitors have seen thus far in clinical trials.

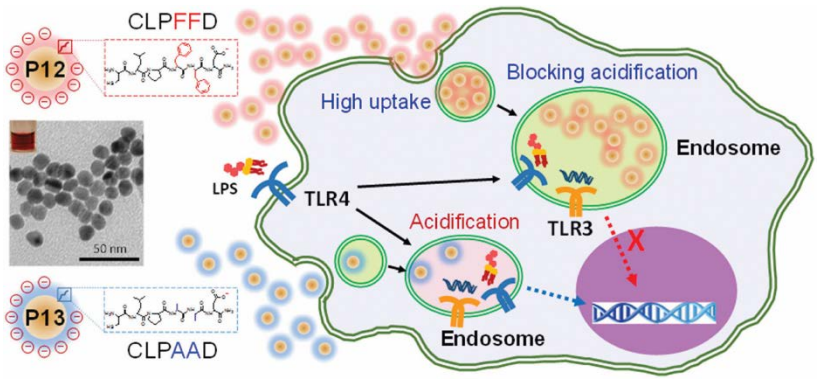

Figure 3.15: AuNPs coated with an immunomodulatory peptide sequence blocked endosomal acidification, resulting in reduced TLR signaling. Reprinted with permission from [181].

3.6.2 Iron Oxide Nanomaterials

As discussed in the introduction, T cells become activated when they interact with a DC presenting both antigen in a MHC and costimulatory factors. When T cells recognize antigen without these factors, however, they will not respond in an inflammatory manner and this can induce tolerance. In T1D, $CD8^+$ T cells recognize multiple epitopes expressed by pancreatic islet cells, resulting in a need for therapies that eliminate autoreactive T cells with different specificities.[57] To this end, iron oxide NPs coated with multiple disease-relevant self-peptides loaded in MHCI (pMHCs) were developed.[182] Oxidized egg white avidin was added to dextran-coated NPs that had been cross-linked with epichlorohydrin, and treated with ammonia.[161] Biotinylated pMHCs were then added at a controlled molar ratio resulting in particles with an average size of 114.1 nm. These NMs are unique in that they can directly interact with T cells, eliminating the need for uptake and processing by APCs. NOD mice treated with a mixture of six different pMHC-NPs, targeting the most prevalent pools of $CD8^+$ cells, were 100% protected from development of

spontaneous T1D. Surprisingly though, treatment with monospecific NPs, targeting self-antigens NRP-V7 or $IGRP_{206-214}$, was also highly effective because they induced expansion of an existing memory population of regulatory $CD8^+$ T cells (**Figure 3.16A**). T_{REGs} have the ability to suppress autoimmune reactions against multiple self-antigens by direct killing of APCs presenting these antigens. This research demonstrates that treatments targeting one self-antigen can be effective in controlling a disease that has many characteristic autoantigens.

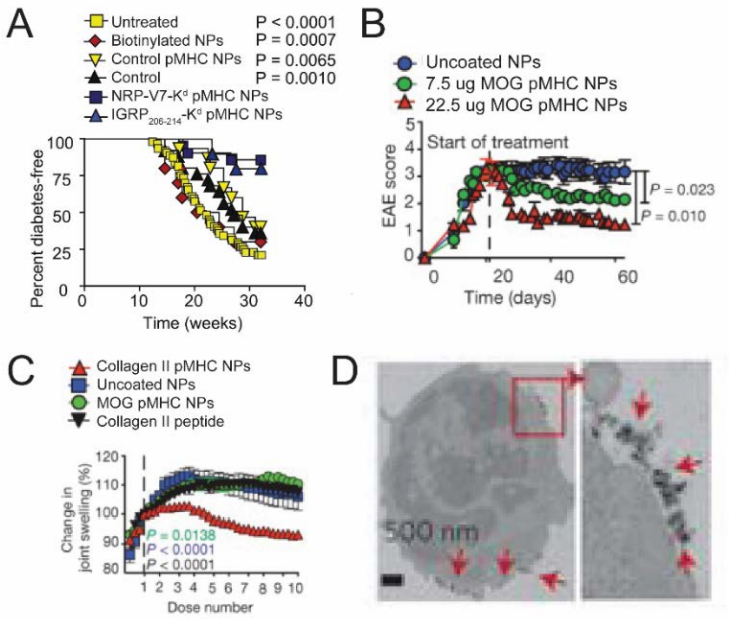

Figure 3.16: APC-like iron oxide NPs deliver self-antigen directly to T cells and control autoimmunity regardless of disease model. A) pMHC NPs can control disease in a T1D model by delivering only one attacked epitope. Disease severity and incidence is also reduced when mice are treated with relevant self-antigen-loaded MHC-coated NPs in models of MS (**B**) and arthritis (**C**). **D**) pMHC coated NPs bind to T cells as "microclusters". Adapted with permission from [182], [183], and [184].

While the initial work focused on controlling autoreactive $CD8^+$ T cells, the next particles developed were coated with autoimmune-disease-relevant peptides loaded in MHCII, which interacts with $CD4^+$ T cells.[183] This subset of T cells is important in

many autoimmune diseases including T1D, MS, and arthritis. Particle treatment was shown to expand antigen-specific regulatory $CD4^+$ T cells capable of suppressing APCs presenting self-antigen and of differentiating regulatory B cells. Remarkably, the therapy was effective in a number of disease models, restoring normoglycemia in NOD mice, reversing paralysis in EAE mice (**Figure 3.16B**), and resolving joint swelling in arthritic mice (**Figure 3.16C**). These results were not reliant on a specific genetic background and could be replicated with ten different pMHC NPs, demonstrating the versatility of the platform.

Following success with iron oxide NP treatment in a number of autoimmune disease models, the researchers recognized the importance of characterizing design rules for inducing specific tolerance.[184] Optimal conditions for synthesis and optimal dose and ligand density for T_{REG} expansion were investigated. Measurement of IFN-γ secretion by T cells revealed an optimal valency for pMHC coating on NPs that changes with particle size. T_{REG} expansion was found to be dependent on both dose and ligand density of pMHCs. Analyzing these parameters is critical not only to determining translation potential, but to reveal fundamental information about the rational design of materials-based immunotherapies. It was also determined that the NPs bind to T cells as clusters and that the formation and size of these microclusters is dependent on pMHC density (**Figure 3.16D**). Examining the interaction of these "APC-like" particles with T cells is necessary to understanding their mechanism of immunomodulation.

Several reports demonstrate that iron oxide NPs that are not coated with immune signals can directly modulate macrophage and T cell functionality.[185-188] Specifically, treatment of OVA-primed splenocytes with carboxydextran-coated iron oxide NPs between 45 nm and 60 nm inhibited T_H1 cytokine expression.[187] The effect of these NPs on a mouse model of delayed type hypersensitivity (DTH), a T_H1-mediated response to antigen, was therefore investigated.[189] One measure of DTH is footpad swelling of OVA-sensitized mice that are re-challenged with OVA. Iron oxide NP treatment significantly reduced this swelling and immunohistochemical staining revealed diminished infiltration of T cells and macrophages and reduced expression of inflammatory cytokines. In agreement with these results, splenocytes isolated from NP-treated, OVA-sensitized mice produced less IFN-γ in response to OVA-restimulation. These results demonstrate the innate tolerizing effect of an inorganic material in halting autoimmune reactions.

3.6.3 Quantum Dots

In immunological applications, QDs have mainly been used as an imaging modality such as for labelling mesenchymal stem cells for T1D therapy.[190, 191] QDs have not, however, been readily investigated as delivery vehicles for immune signals. Several groups have shown that delivery of MOG via a particle, without additional immunomodulatory signals, can induce tolerance in the EAE model of MS.[53, 54, 192] QDs present a unique opportunity in this application by allowing for tunable conjugation of a high number of molecules such as peptides or DNA. In one example

of this approach, 625 nm emitting CdSe/ZnS core/shell QDs were decorated with disease-relevant peptides and used as a tool to probe the relationship between peptide dose and density and efficacy in treating autoimmune diseases (**Figure 3.17**).[52] QDs were able to accommodate up to 100 peptides per particle and were readily taken up by DCs that could process and present MOG to T cells. One specific advantage of QDs, their ultrasmall size (<20 nm), was demonstrated as they rapidly drained to inguinal LNs of mice following *s.c.* injection at the tailbase. The intrinsic fluorescence of QDs allowed for easy imaging of the tissues. While MOG-QDs showed efficacy in EAE, injection of an equivalent dose of free MOG had no effect, demonstrating the need for a materials-based system when delivering self-antigen. The level of tolerance could be tuned by increasing the amount of self-antigen, with a higher dose of MOG showing greater efficacy in the disease model. The most interesting result was that when delivering the same dose of MOG, spreading the ligands over many QDs was more effective for inducing tolerance than packing more peptide onto fewer particles. This work proves QDs to be a useful tool for understanding fundamental questions about tolerance induced by particle delivery systems. The strategy of delivering a self-antigen to treat autoimmunity recently made it to clinical trials with the delivery of autologous PBMCs chemically coupled with seven different myelin peptides.[193] The cells are pulsed with the peptides in the presence of a chemical cross-linker 1-ethyl-3-(3-dimethylaminopropyl)-carbodiimide (EDC) and have demonstrated success in inducing tolerance in EAE models.[194, 195] The therapy proved safe and well

tolerated in humans, and even resulted in a decrease in antigen-specific T cell responses.

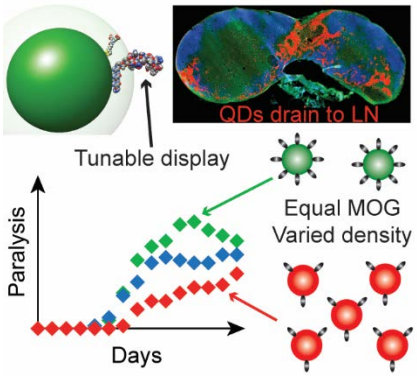

Figure 3.17: Self-antigen-decorated QDs rapidly drain to LNs. The level of tolerance in EAE induced by QD treatment is dependent on self antigen peptide ligand density. Reprinted with permission from [52].

3.7 Conclusions

Biomaterials offer advantages in immunotherapy applications such as targeted and co-delivery of immune signals and cargo protection. Specifically, inorganic materials promote long term stability and can offer unique features such as magnetism or direct imaging capabilities. Despite the possibilities that they offer, NMS still face many challenges. Unlike some other material types, inorganic materials are typically non-biodegradable and non-porous, presenting difficulties for clearance and for release of immune signals. Many of the materials discussed above are still in early stages of clinical development and are there are still debates over toxicity.[196] There are also concerns about the production of NMs with consistently reproducible properties that are desirable for the downstream application.[197] An important goal for the next

stages of materials research for immunotherapy applications is to focus on rational design with specific efforts towards biocompatibility and reproducibility.

Chapter 4, below, details a strategy co-delivering self-antigen and a regulatory molecule. As discussed in this chapter, materials that are commonly used for the delivery of these signals can exhibit immunostimulatory or immunomodulatory properties, but these properties have yet to be fully characterized. The platform studied in the next chapter features advantages of biomaterials but relies on self-assembly to deliver immune signals alone with no potentially immunogenic carrier.

Chapter 4: Polyplexes assembled from self-peptides and regulatory nucleic acids blunt toll-like receptor signaling to combat autoimmunity[2]

4.1 Introduction

Failure to mount an immune response to an antigen is known as immunological tolerance.[9] When tolerance to self-antigens (e.g. host proteins) is not maintained, inflammation and autoimmune disease can develop. Autoimmune diseases such a MS, T1D, lupus, and RA, affect over 20 million Americans.[198, 199] In MS, the myelin sheath that insulates and protects the axons of neurons is recognized as a foreign antigen.[11, 12] Myelin derived antigens are now strongly implicated as the targets of malfunctioning self-reactive cells in MS,[15] inflammatory populations that infiltrate the CNS. In the CNS, the attack by these cells drives demyelination of neurons, while secretion of inflammatory cytokines recruits additional immune cells to the site.[17]

Cures for autoimmune diseases do not exist and treatment options are limited. Typical therapies rely on regular doses of immunosuppressive drugs or antibodies that are non-specific and can leave patients immunocompromised.[23] Thus, great interest has developed in new treatments that can durably block inflammatory responses against self-antigen without non-specific suppression. One exciting new strategy is co-delivery of an antigen, such as myelin, along with immunomodulatory molecules to redirect responses against self-antigen. Biomaterials offer very attractive features in this

[2]Adapted from **KL Hess**, JI Andorko, LH Tostanoski, CM Jewell; "Polyplexes assembled from self-peptides and regulatory nucleic acids blunt toll-like receptor signaling to combat autoimmunity", *Biomaterials* **2017**, 118: 51-62.

context, and, in addition to co-delivery, provide routes for efficiently targeting APCs and for controlled release.[7, 200] In particular, synthetic polymers have been used to co-deliver antigen with regulatory signals—small molecules, cytokines, and proteins—to polarize differentiating T cells away from inflammatory cells and toward T_{REGs}.[25, 46, 47, 53, 62, 169, 170, 201] These populations can control self-reactive effector cells (e.g., T_H1, T_H17) that drive autoimmune disease while limiting broad suppression.[9] Expansion and biasing of T cells toward regulatory response also reduces the absolute number of inflammatory cells and offers the potential for more durable treatments.[182, 183]

TLRs are a collection of signaling pathways that recognize pathogen-associated molecular patterns (PAMPs), resulting in secretion of inflammatory cytokines and activation of the immune cells needed to fight infection.[202] Interestingly, a developing body of new literature demonstrates that many TLRs are overexpressed in MS and other autoimmune diseases, as well as in animal models.[175, 176, 178, 179, 203] For example, in experimental autoimmune encephalomyelitis (EAE), a pre-clinical mouse model of MS, disease is significantly reduced in TLR9 knock-out mice.[179] This example highlights the importance of TLR9 signaling in driving disease. TLR9 typically activates innate immunity following recognition of a characteristic bacterial DNA sequence called CpG.[204] CpG DNA is an agonist for TLR9, ultimately driving inflammation through the MyD88 pathway that leads to activation of DCs, macrophages, monocytes, and B cells, along with secretion of inflammatory cytokines.[205, 206] For this reason, CpG has been intensively studies

as a vaccine adjuvant.[205] In contrast to this common role of TLR9 as an adjuvant, one group has explored TLR9 antagonists to promote tolerance using GpG, an analog of CpG exhibiting a substitution of guanine for cytosine.[207, 208] Like CpG, GpG is unmethylated, single-stranded DNA with a phosphorothioate backbone that can bind TLR9. During cell studies, treatment with GpG suppressed proliferation of inflammatory T_H1 cells. In mice, repeated regular treatment with GpG attenuated EAE—a T_H1-mediated MS model— and further, enhanced induction of tolerance when GpG was mixed just prior to injection with plasmid DNA encoding myelin self-antigens. Thus, we reasoned juxtaposing GpG and self-antigen in polyplex-like NPs might alter the inflammatory signaling associated with recognition of self-antigen, biasing differentiating T cells away from inflammatory phenotypes to help combat autoimmune disease.

One simple class of biomaterials particularly well-suited for the co-delivery strategy above is polyplexes, nano-structured complexes that spontaneously assemble due to electrostatic condensation when nucleic acid is mixed with a cationic polymer.[209-211] Polyplexes condense cargo to a high density that is easily internalized by cells and offer protection from enzymatic degradation. These and other advantages have been exploited in a variety of applications ranging from transfection to vaccination. For the former, great effort has been invested to develop cationic polymers that are non-toxic and offer features (e.g., proton-sponge capacity) that overcome specific barriers to DNA and RNA delivery such as endosomal escape. In the vaccine area—both prophylactic and therapeutic—the particulate nature of polyplexes promotes uptake by

APCs, and further, polyplexes allow simple tuning of vaccine specificity by simply replacing a particular DNA plasmid or RNA molecule with different sequences. Despite these useful properties, only a handful of reports, all in the past 3-4 years, have explored polyplexes to modulate immune function or promote immunological tolerance. In one example, receptors involved in the development of diabetes were targeted in mice by condensing plasmid encoding a soluble ligand for this receptor.[212] In a second example, mice were treated during diabetes with polyplexes formed using chitosan to condense plasmids encoding interleukin 4 (IL-4) and interleukin 10 (IL-10), regulatory cytokines that suppress inflammatory cytokines.[213] The Mellor group has studied a system using poly(ethylenimine) (PEI) to condense plasmid DNA that is free of PAMPs, limiting activation of common inflammatory pathways and cytokines that are also often active during autoimmune diseases.[214-216] Although none of these approaches incorporate self-antigen, we hypothesized polyplexes including such components might allow induction of antigen-specific tolerance. Further, a number of reports demonstrate that commonly used biomaterials, such as chitosan, PLGA, and polystyrene, exhibit intrinsic immunogenicity that drives inflammation.[7, 28, 38, 39, 58, 59] This characteristic could be detrimental when developing therapies for autoimmune disease, as intrinsic inflammation from a delivery vehicle could exacerbate disease. Thus, therapeutics that eliminate carrier components but still offers features of biomaterials such as co-delivery and cargo protection, could offer simpler and lower-risk treatments.

To realize the possibilities discussed above, we designed polyplex-like structures assembled from GpG and MOG, a peptide antigen of myelin, modified with cationic arginine residues. This strategy is unique in four ways. First, these NPs consist entirely of immune signals, and are free of all carriers or supports. The polyplexes thus mimic attractive features of traditional biomaterials, while eliminating the intrinsic immunogenicity described above. This is highly relevant for autoimmune and inflammatory conditions where such traits might worsen disease. Second, we are targeting suppression of TLR signaling to promote tolerance, a new idea arising in immunology research, and that is untapped in the biomaterials field. This is particularly important for autoimmune therapies owing to the intriguing recent studies revealing TLR signaling is overactive in human autoimmune diseases such as MS, T1D, lupus, and RA. Third, because the polyplexes are built entirely from immune signals, they juxtapose both the self-antigen and the regulatory signal at very high densities. This feature provides highly efficient loading (i.e., 100%) relative to polymers or matrices used to load and deliver cargo, as well as the co-delivery needed to polarize T cells away from inflammatory phenotypes. Last, these immune polyplexes are novel because they include self-antigen for specificity, but do not rely on expression of any plasmid component; the nucleic acid cargo is an antagonistic TLR ligand that directly interacts with these receptors. Using this platform, below we show that MOG-GpG polyplexes are readily internalized by APCs, decrease TLR9 signaling, and are non-toxic. Treatment of DCs reduces activation and inflammatory cytokines, biasing myelin-specific T cell function away from inflammatory phenotypes during co-culture studies.

In a mouse model of MS (EAE), polyplex treatment significantly reduces both the severity and incidence of disease.

4.2 Materials and Methods

4.2.1 Materials

GpG DNA (5'-TGA CTG TGA AGG TTA GAG ATG A-3'), CpG DNA (5'-TCC ATG ACG TTC CTG ACG TT-3') and a control oligonucleotide (5'-TCC TGA GCT TGA AGT-3') were purchased from IDT (Coralville, IA). MOG_{35-55} (MEVGWYRSPFSRVVHLYRNGK) was synthesized by Genscript (Piscataway, NJ) with a FITC tag on the N-terminus and either one or two arginine (R) residues on the C-terminus ($MOGR_1$, $MOGR_2$). TE buffer and ethidium bromide were purchased from Amresco (Solon, OH). DNase I kits with 10X reaction buffer were purchased from New England Biolabs (Ipswich, MA). RPMI-1640 media and Molecular Biology Grade Water were purchased from Lonza (Allendale, NJ) and fetal bovine serum (FBS) was supplied by Corning (Tewksbury, MA). β-mercaptoethanol, ethylenediaminetetraacetic acid (EDTA) and bovine serum albumin (BSA) were purchased from Sigma Aldrich (St. Louis, MO). 20X PBS, HEPES, and non-essential amino acids were purchased from VWR (Radnor, PA). L-glutamine, penicillin-streptomycin, and DAPI were purchased from Thermo Fisher Scientific (Grand Island, NY). Spleen Dissociation Medium and CD4 negative selection kits were from STEMCELL Technologies (Vancouver, BC). CD11c microbeads were purchased from Miltenyi Biotec (Cambridge, MA). Cy5 nucleic acid labelling kits were from Mirus

(Madison, WI). HEK-Blue^{TM} TLR9 report cells, detection media, and antibiotics were supplied by Invivogen (San Diego, CA). Fluorescent antibody conjugates and ELISA reagents were purchased from BD (San Jose, CA). Cell Proliferation Dye eFluor® 670 was from affymetrix eBioscience (San Diego, CA). Hooke Kits™ for EAE Induction were supplied by Hooke Laboratories (Lawrence, MA).

4.2.2 Cells and animals

All primary cells were harvested from female C57BL/6 mice (4-12 weeks, stock #000664) and male C57BL/6-Tg(Tcra2D2,Tcrb2D2)1Kuch/J (2D2) mice (10-16 weeks, stock #006912) purchased from Jackson Laboratories (Bar Harbor, ME). 2D2 mice have transgenic $CD4^+$ T cell receptors specific for MOG. Female C57BL/6 mice (10-12 weeks, stock #000664) were used for EAE studies. All animals were cared for in compliance with federal, state, and local guidelines, and using protocols reviewed and approved by the University of Maryland's Institutional Animal Care and Use Committee (IACUC).

4.2.3 Complex formation

Complexes were formed by mixing aqueous solutions of GpG and MOG with $MOGR_x$ (x=1 or 2). The components were mixed at defined mass ratios ranging from 1:20 to 40:1 $MOGR_x$:GpG. In these studies, the total mass of GpG was fixed at 25 µg while the mass of $MOGR_x$ was varied to control the charge ratio. Prior to use in cell and animal studies, complexes were centrifuged for 90 minutes at 5,000 g in a Microfuge

22R (Beckman Coulter, Brea, CA). Supernatants were removed and the pellets were resuspended in water to remove any excess $MOGR_x$ or GpG that was not complexed. Loading studies to determine the amount of complexed $MOGR_x$ and GpG were carried out by measuring the fluorescence levels of FITC-$MOGR_x$ and Cy5-GpG in the supernatant of the centrifuged complexes. Cy5 labeling was carried out using the manufacturer's protocols.

4.2.4 Characterization of complex size and charge

Hydrodynamic diameter and zeta potential of complexes were measured in triplicate using samples prepared in molecular biology grade water and analyzed on a Zetasizer Nano ZS90 (Malvern Instruments Ltd, Westborough, MA). Stability analysis was completed by incubating $MOGR_x$-GpG in media with serum and measuring the hydrodynamic diameter at the indicated intervals.

4.2.5 Ethidium bromide exclusion assay

Ethidium bromide (EtBr) was added to GpG at a 1:5 mass ratio and allowed to equilibrate for one hour. $MOGR_1$ and $MOGR_2$ were then added at GpG:$MOGR_x$ mass ratios ranging from 1:5 to 10:1. Fluorescence was measured using an excitation wavelength of 540 nm and an emission wavelength of 570 nm. The fluorescence of EtBr alone was subtracted from all samples and an intensity ratio was calculated by comparing of the fluorescence of the complex with EtBr to the fluorescence of DNA and EtBr alone.

4.2.6 Enzymatic degradation assay

Complexes were made from Cy5-GpG and $MOGR_x$ and centrifuged as described above, then resuspended in 100 µL 1X DNA I reaction buffer. The fluorescence from the Cy5-GpG was then measured using an excitation wavelength of 640 nm and an emission wavelength of 670 nm. 2 units of DNase I were added to each sample after complex formation, then mixed and incubated for 30 minutes at 37°C. After incubation, 1 µL of 0.5M EDTA was added and the enzyme was heat inactivated at 75°C for 10 minutes per the manufacturer's instructions. The fluorescence of the Cy5-GpG was then measured again to determine the extent of degradation compared to free Cy-5 GpG. Fluorescent measurement was chosen to quantify GpG amount over spectrophotometry because the absorbance of $MOGR_x$ (peak at 280nm) overlaps the absorbance of GpG (peak at 260 nm).[217, 218]

4.2.7 TLR9 reporter cell study

HEK-Blue™ mTLR9 cells are co-transfected with the murine TLR9 gene and an inducible secreted embryonic alkaline phosphatase (SEAP) reporter gene. Stimulation of the cells with an unmethylated CpG-ODN sequence (TLR-9 agonist) activates NF-κB and AP-1, which leads to the production of SEAP to allow colorimetric detection. Cells were first treated with CpG and then either complexes or free controls. After a 16 hour incubation period, the level of SEAP was measured by spectrophotometry at 650 nm.

4.2.8 Dendritic cell isolation and flow cytometry

CD11c+ DCs were isolated from the spleens of female C57BL/6 mice through positive selection with spleen dissociation media and CD11c Microbeads. DCs were plated in a 96 well plate at 100,000 cells per well and cultured in RPMI 1640 media supplemented with 10% FBS, 2 mM L-glutamine, 1X non-essential amino acids, 10 mM HEPES buffer, 1X penicillin and streptomycin, and 55 μM β-mercaptoethanol at 37°C and 5% CO2. DCs were activated by adding CpG (TLR9 agonist) at a concentration of 5 μg/mL and treated with the each complex formulation, vehicle (water) only, or free controls of $MOGR_x$ alone or GpG alone. For activation studies, cells were stained after 24 hours for viability (DAPI-) and for classic surface activation markers (CD80+, CD86+, CD40+) using fluorescent antibody conjugates. For uptake studies, complexes were made with FITC tagged $MOGR_1$ or $MOGR_2$ and Cy5 labelled GpG. Cells were incubated with complexes for two hours prior to collection and staining for viability (DAPI-). For both sets of studies, cells were measured by flow cytometry (BD Cantoll, San Jose, CA) and data were analyzed with FlowJo v.10 (TreeStar, Ashland, OR).

4.2.9 Enzyme-linked immunosorbent assay

Supernatants from DCs treated for activation studies were collected. Cytokine secretion levels were analyzed via ELISA using mouse interferon gamma (IFN-γ) reagents. Briefly, 96-well plates were coated with an IFN-γ capture antibody and after an overnight incubation, the supernatant samples were added. An IFN-γ detection

antibody and streptavidin-horseradish peroxidase conjugate mixture was then added to the wells for 1 hour. A tetramethylbenzidine and hydrogen peroxide mixture was added to each well for 30 minutes and the reaction was stopped by the addition of 1M phosphoric acid before reading the absorbance of each sample at 450 nm. IFN-γ concentrations were calculated from absorbance by comparing to a standard curve.

4,2.10 DC/T cell co-culture and flow cytometry

Isolated DCs were treated with CpG and the same complex formulations or controls described above for DC activation studies, then cultured for 24 hours. CD4+ T cells were next isolated from the spleens of 2D2 mice via a negative selection kit. For phenotypic studies, 300,000 T cells were added to the wells containing the treated DCs. After 48 hours, cells were stained for a T cell surface marker (CD4+) and transcription factors (Tbet+, RORγ+) indicative of TH1 and TH17 cells, respectively. For T cell proliferation studies, cells were labelled with eFlour 670 proliferation dye prior to incubation with DCs. After 48 hours, cells were collected and stained for viability (DAPI-) and for a T cell surface marker (CD4+). Cells were examined for transcription factor expression or proliferation dye dilution with flow cytometry and data were analyzed with FlowJo v.10.

4.2.11 EAE studies in mice

10 week old, C57BL/6 female mice were induced with EAE using a standard induction protocol provide by the reagent vendor (Hooke Laboratories). Briefly, mice were

injected *s.c.* with 50 µL of an emulsion of MOG35-55 and complete Freund's adjuvant (CFA) at the upper and lower back on day 0. Injection of MOG/CFA emulsion primes inflammatory T cells specific for MOG. 100 µL of pertussis toxin (PTX) was also administered intraperitoneally (*i.p.*) 2 and 24 hours after MOG/CFA injection. PTX injection opens the blood brain barrier, allowing infiltration of inflammatory MOG-specific T cells. These cells demyelinate the axons of neurons leading to loss of motor function beginning around day 9 and complete paralysis occurring by day 16. Disease severity was monitored daily by measuring body weight loss and clinical score, a measurement of the extent of paralysis: 0 – no symptoms, 1 – tail paralysis, 2 – hind limb weakness, 3 – hind limb paralysis, 4 – partial front limb paralysis, 5 – moribund. The induced mice (N=8-10 per group) were either left untreated or treated *s.c.* at the tailbase using complexes prepared in molecular biology grade water at a 2:1 $MOGR_2$:GpG ratio (actual dose: 200 µg $MOGR_2$; 85.9 µg of GpG). As indicated in the text for each study, treatment regimens consisted of either a single complex injection on day 7, or three administrations of complexes on days 6, 12, and 18. In control studies, mice were treated with 50 µg free GpG on days 5, 10, and 15.

4.2.12 Statistical analysis

One-way ANOVA with a Tukey post-test was used to compare three or more groups for materials characterization and in vitro studies, with post-test corrections for multiple comparisons. Unpaired t-tests were used to compare mean clinical score and body weight between groups at each study day. Log-rank tests were used in analysis of

disease incidence. For all tests, p values ≤ 0.05 were considered significant. For all figures: *$p < 0.05$, **$p < 0.01$, ***$p < 0.001$, #$p < 0.0001$, ns = not significant.

4.3 Results

4.3.1 MOG modified with cationic arginine residues binds GpG to form immunological polyplexes

Since GpG is a single stranded (ss) DNA molecule, and thus intrinsically anionic, we first tested if immunological polyplex-like structures could be formed using GpG and MOG modified with either one or two cationic arginine residues ($MOGR_1$, $MOGR_2$). In these studies, the mass of GpG was fixed while the mass of $MOGR_x$ was varied to form complexes over the range of 1:20 – 40:1 $MOGR_x$:GpG. These formulations corresponded to a range of charge ratios spanning highly negative to highly positive values (**Table 4.1**). DLS confirmed the formation of complexes exhibiting nanoscale hydrodynamic diameters of 117.9 ± 6.5 nm to 199.2 ± 4.1 nm (**Figure 4.1A**). These sizes were relatively uniform across the ratios tested, though for complexes formed from $MOGR_2$ at near-neutral charge ratios, the sizes increased slightly (e.g., 1:1, 2:1). The PDIs of the complexes were quite large, ranging from 0.272 to 0.533 with no correlation between number of arginine residues of mass ratio of formulation (**Table 4.2**). This result is expected due to the non-uniform preparation method of polyplexes that simply involves mixing of the two immune signals as opposed to more uniform particle preparation (i.e. PLGA MPs) that includes a homogenization step. Polyplex stability studies conducted by incubation in media with serum revealed that these sizes

did not change appreciably over at least 24 hours (**Figure 3.2**). Surface charge, however, was readily tunable as indicated by zeta potential measurements (**Figure 4.1B**). As expected, complexes formed at lower $MOGR_x$:GpG ratios (e.g., 1:20) exhibited a negative zeta potential that became positive moving toward higher $MOGR_x$: GpG ratios (e.g., 40:1). The values of these measurements ranged from -42.5 ± 0.5 mV (1:5) to 33.4 ± 0.7 mV (40:1), with a shift in zeta potential observed approximately around the zone that charge ratio analysis predicted a charge inversion (**Table 4.1**). Corresponding to these changing physicochemical properties, measurements of the actual loading of each complex formulation ranged from 0.57 µg to 9.18 µg of $MOGR_x$ and 2.18 µg to 4.88 µg of GpG as a function of ratio (**Table 4.3**).

$MOGR_x$:GpG Mass Ratio	$MOGR_1$:GpG Charge Ratio	$MOGR_1$-GpG Complex Charge	$MOGR_2$:GpG Charge Ratio	$MOGR_2$-GpG Complex Charge
1:20	0.02	-49	0.02	-41
1:10	0.04	-25	0.05	-21
1:5	0.08	-12	0.10	-10
1:2	0.20	-4.7	0.24	-3.9
1:1	0.41	-2.1	0.48	-1.6
2:1	0.81	-0.4	0.97	-0.1
5:1	2.02	+1.5	2.41	+2.0
10:1	4.05	+3.8	4.83	+4.6
20:1	8.10	+8.0	9.54	+9.4
40:1	16.2	+16	19.1	+19

Table 4.1: Charge characteristics of MOGRx-GpG complexes.

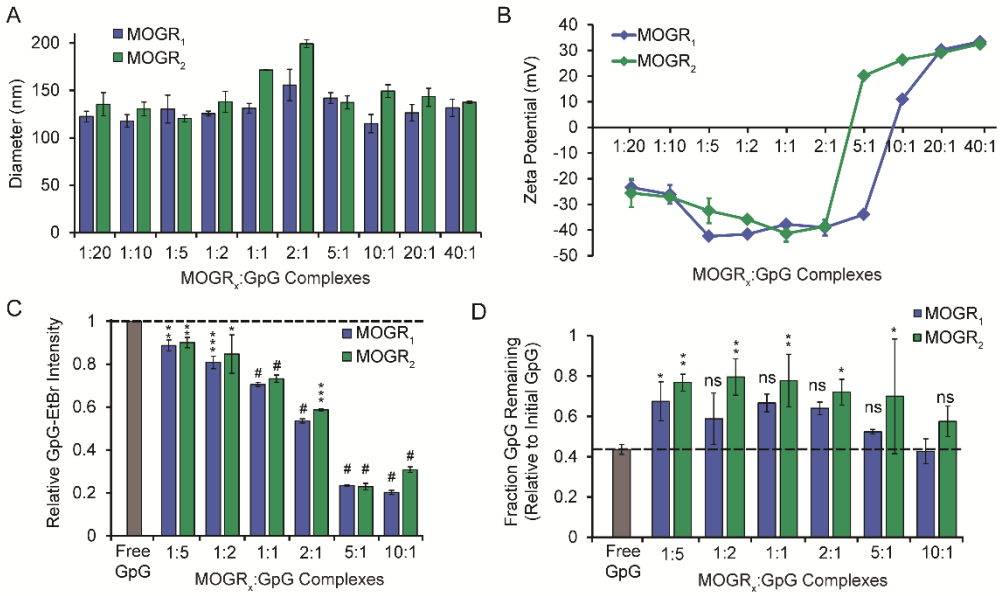

Figure 4.1: $MOGR_x$ and GpG formed complexes with controllable properties. (**A**) DLS measurements performed in triplicate showed relatively small diameters regardless of complex formulation. (**B**) Triplicate zeta potential measurements of complexes indicated controllable surface charge. (**C**) Binding of $MOGR_x$ to GpG was measured by an EtBr assay. A reduction in fluorescent intensity relative to free GpG indicated displacement of EtBr by the peptide. (**D**) Protection of GpG from degradation by $MOGR_x$ complexation was measured after incubation with DNase. *p < 0.05, **p < 0.01, ***p < 0.001, #p < 0.0001, ns = not significant. For Panels C and D, statistics are comparisons versus free GpG.

$MOGR_1$:GpG Mass Ratio	Average PDI	$MOGR_2$:GpG Mass Ratio	Average PDI
1:5	0.424	1:5	0.533
1:2	0.429	1:2	0.424
1:1	0.442	1:1	0.426
2:1	0.386	2:1	0.449
5:1	0.389	5:1	0.288
10:1	0.272	10:1	0.345

Table 4.2: Average PDI of $MOGR_x$-GpG complexes

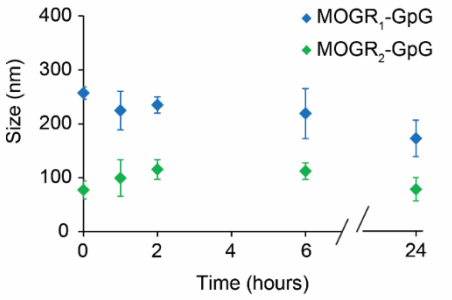

Figure 4.2: Polyplexes remained stable in serum for up to 24 hours. Hydrodynamic diameter was assessed over time as a measure of stability.

$MOGR_x$:GpG Mass Ratio	$MOGR_1$ Mass Loading (μg)	$MOGR_2$ Mass Loading (μg)	GpG Mass Loading (μg)
1:5	0.57 ± 0.06	0.67 ± 0.04	2.18 ± 0.28
1:2	2.01 ± 0.10	2.06 ± 0.03	2.97 ± 0.10
1:1	4.28 ± 0.01	4.31 ± 0.00	3.44 ± 0.13
2:1	8.61 ± 0.14	9.18 ± 0.11	4.88 ± 0.15

Table 4.3: Component loading levels of $MOGR_x$-GpG complexes.

4.3.2 Strong binding between $MOGR_x$ and GpG provides protection from enzymatic degradation

To determine the binding affinity between MOG and GpG, an ethidium bromide (EtBr) assay was performed using a subset of ratios (i.e., 1:5-10:1). For double-stranded DNA, EtBr intercalates base pairs, resulting in a significant increase in fluorescence. For ssDNA, EtBr can bind secondary and tertiary structural features where regions of local base pairing offer the stacked base pairs that support intercalation by dye molecules. [219, 220] Free GpG controls incubated with EtBr led to a high level of fluorescence (**Figure 4.1C**). Treating these mixtures with $MOGR_1$ or $MOGR_2$ at all ratios revealed that the peptides competed with and displaced the EtBr bound to GpG, decreasing the fluorescent measurements (**Figure 4.1C**). As the mass of $MOGR_x$ added to GpG increased (1:5 → 10:1), fluorescent intensity decreased (**Figure 4.1C**), indicating increasing binding affinity as the surface charge became increasingly positive over this same range (**Figure 4.1B**).

We next tested if condensation of GpG by $MOGR_x$ protects GpG from enzymatic degradation. GpG was covalently labelled with Cy5 and the fluorescence was measured

to quantify the amount of DNA prior to degradation. After incubation of free GpG with DNase for 30 minutes, less than 50% remained intact relative to the starting concentration of GpG (**Figure 4.1D**). Complexation of GpG with $MOGR_2$, which generally exhibited a slight increase in positive charge versus $MOGR_1$ (**Figure 4.1B**), significantly reduced GpG degradation at most ratios, with up to ~80% of the GpG remaining after incubation with enzyme (**Figure 4.1D**). Complexation with $MOGR_1$ resulted in a trend of protection, but these effects were only significant against free GpG at one ratio.

4.3.3 GpG complexed with $MOGR_x$ maintains the ability to restrain TLR9 signaling

We next confirmed GpG is able to blunt TLR9 signaling after complexation with $MOGR_x$. Cells were first stimulated with CpG, a strong TLR9 agonist, then treated with polyplexes or dose-matched free components (i.e., GpG or $MOGR_x$). These experiments confirmed high levels of TLR9 activity in cells receiving only CpG, while addition of GpG-containing complexes significantly reduced TLR9 signaling (**Figure 4.3A**). Although in some cases the levels of reduction observed with complexes were not as high as treatment with equivalent doses of free GpG, these experiments confirm GpG maintains the capacity to block TLR9 signaling after complexation with self-antigen. Although a small decrease in TLR9 activity was seen due to some free $MOGR_x$ treatments (grey bars), these non-specific effects were not observed for most of the ratios. Building on the TLR signaling results, we assessed the toxicity of complexes by treating primary DCs ($CD11c^+$) isolated from the spleens of mice with complexes or free controls. Flow cytometry analysis of $DAPI^-$ cells indicated only a small decrease

in cell viability (~10%), regardless of the specific complex formulation (**Figure 4.3B**). These effects were also observed in wells treated with only GpG (purple bars), but were less common in wells treated with free $MOGR_x$ (grey bars) controls (**Figure 4.3B**).

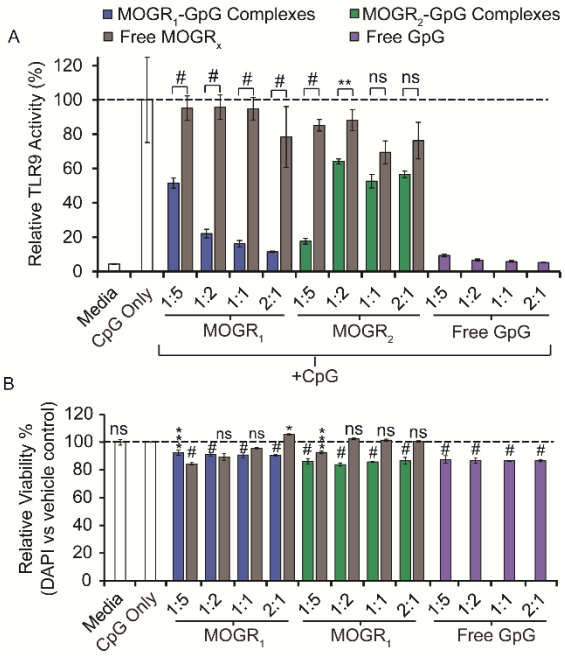

Figure 4.3: Complexes antagonized TLR9 without affecting viability. (**A**) The SEAP level induced by CpG and complex or free treatments correlates to TLR9 activity in a reporter cell line and was measured by spectrophotometry. (**B**) Viability following complex or free treatments was measured by incubation with DAPI and flow cytometry. *p < 0.05, **p < 0.01, ***p < 0.001, #p < 0.0001, ns = not significant. For Panel B, statistics correspond to comparisons against CpG only.

4.3.4 Primary DCs readily internalize $MOGR_x$-GpG complexes

Having confirmed cell compatibility and the ability of complexes to reduce TLR9 signaling, we studied the immunological processing and tolerogenic activity of complexes. To determine the ability of APCs to phagocytose these NPs, DCs were incubated with complexes formed from FITC-tagged $MOGR_x$ and Cy5-labeled GpG or free controls. Flow cytometry analysis revealed all complex formulations resulted in a significant increase in both FITC signal ($MOGR_x$; **Figure 4.4A,B**) and Cy5 signal

(GpG; **Figure 4.4C,D**) compared to vehicle treatment. Interestingly, for $MOGR_x$ peptides, uptake levels were similar regardless of whether the peptide was in a free or complexed form (**Figure 4.4A,B**). Flow cytometry measures the co-localization of signal with cells but cannot directly determine if molecules are internalized or simply bound to the cell membrane. To gain a better understanding of polyplex uptake, we incubated treated cells with trypan blue prior to flow cytometry analysis which quenches FITC signal on the cell membrane but not FITC signal that has been internalized. The level of FITC-MOG signal was comparable to treated cells that had not been incubated with trypan blue, giving one indication that the polyplexes had been phagocytosed. In contrast, GpG uptake was significantly higher when complexed with $MOGR_2$, compared to both free GpG and $MOGR_1$-GpG polyplexes (**Figure 4.4C,D**).

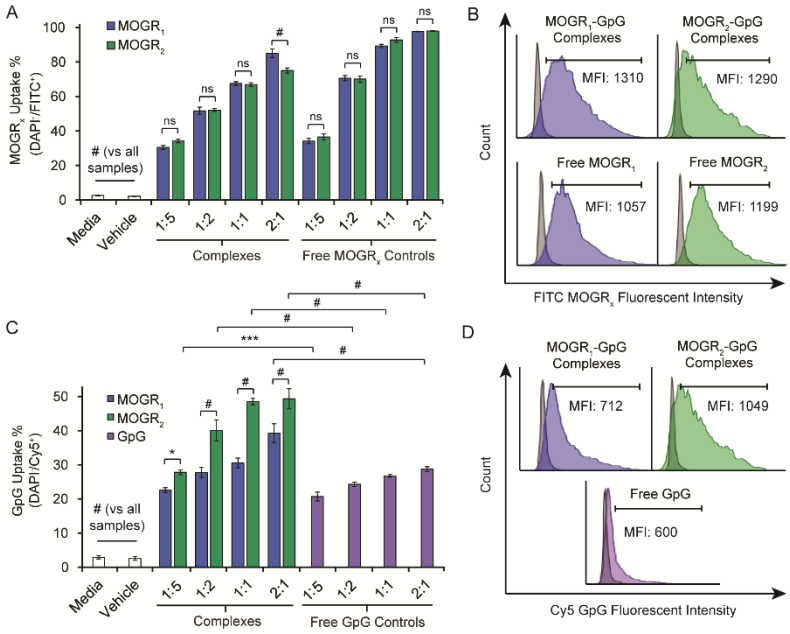

Figure 4.4: $MOGR_x$-GpG complexes were readily taken up by DCs. Uptake of complexes by primary DCs was analyzed by flow cytometry following incubation with polyplexes formed from FITC-$MOGR_x$ (**A**), (**B**) and Cy5-GpG (**C**), (**D**). *$p < 0.05$, ***$p < 0.001$, #$p < 0.0001$, ns = not significant.

4.3.5 $MOGR_x$-GpG complex treatment deactivates DCs

To determine how uptake of complexes impacts DC activation, DCs were stimulated with CpG prior to incubation with $MOGR_x$-GpG complexes or dose-matched free controls. Flow cytometry analysis revealed stimulation with CpG induced high levels of classic surface activation markers (**Figure 4.5A,B,C**). Strikingly, complexes containing GpG significantly decreased activation compared to equivalent free $MOGR_x$ controls (grey bars) by as much as 54.1%, 53.6% , and 53.1% for CD80 (**Figure 4.5A**), CD86 (**Figure 4.5B**), and CD40 (**Figure 4.5C**), respectively. However, these decreases were most evident for CD80 and CD86, with $MOGR_2$-GpG complexes generally causing greater reductions in DC activation compared with $MOGR_1$-GpG complexes (**Figure 4.5A-C**, green vs. blue series). Measurement of MFI yielded similar results (**Figure 4.6**). Importantly, DC deactivation was not seen when GpG was replaced with a control oligonucleotide (ODN), indicating the specificity of the TLR antagonist (i.e., GpG) to regulate inflammation (**Figure 4.7**). In similar studies, we tested if complexes alter the levels at which DCs secrete IFN-γ, a key inflammatory cytokine. As expected, ELISA measurements confirmed CpG-induced secretion of IFN-γ (**Figure 4.5D**). Analogous to the results of surface activation staining, $MOGR_x$-GpG complexes significantly reduced IFN-γ secretion relative to $MOGR_x$ free controls (**Figure 4.5D**).

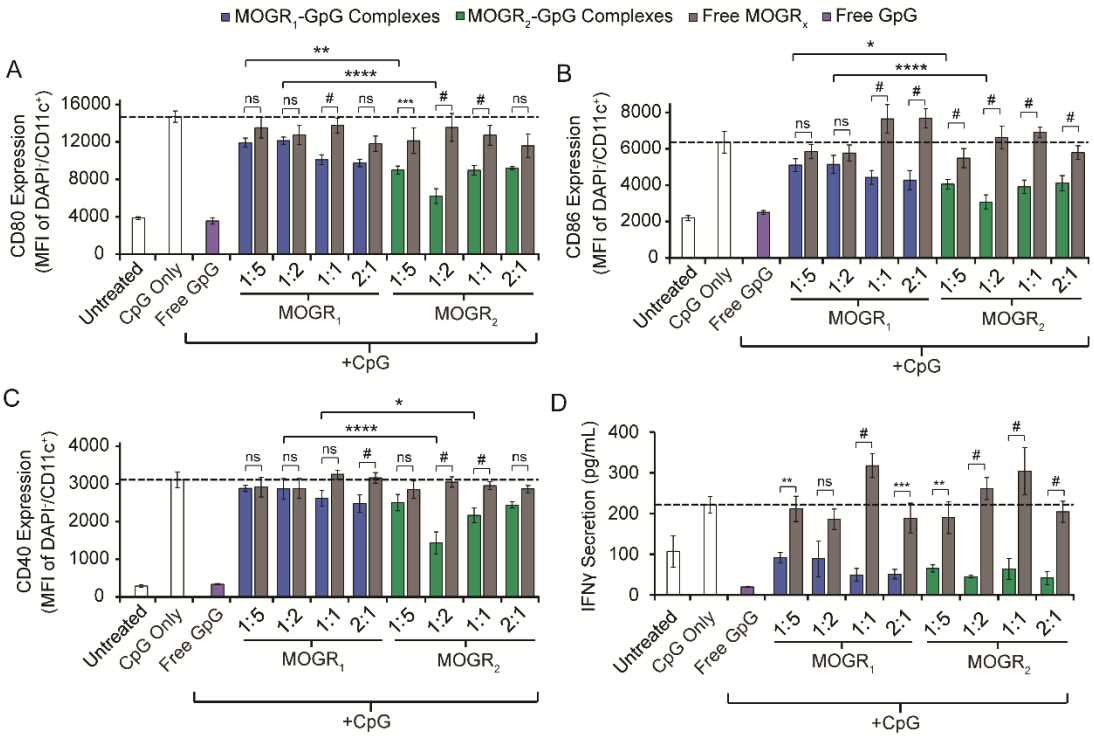

Figure 4.5: Complex treatment deactivated primary DCs. DC activation was measured following incubation with stimulatory CpG and complex or free treatments by expression levels of costimulatory markers CD80 (**A**), CD86 (**B**), and CD40 (**C**), by staining with fluorescent antibody conjugates and analysis by flow cytometry. (**D**) DC deactivation was confirmed by ELISA to measure the secretion of inflammatory cytokine IFN-g. *p < .05, **p < 0.01, ***p < 0.001, #p < 0.0001, ns = not significant.

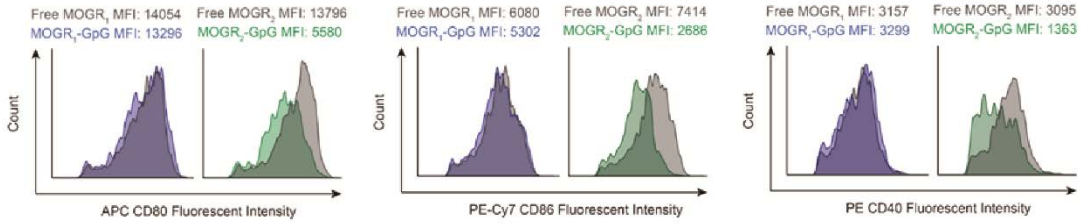

Figure 4.6*:* MOGR$_x$-GpG complexes knockdown expression of DC activation markers. DC activation following CpG stimulation and complex or free peptide treatment was analyzed by staining for the activation markers CD80, CD86, and CD40 with a fluorescent antibody conjugate. The mean fluorescent intensity of APC, PE-Cy7, and PE was measured by flow cytometry and correlates to CD80, CD86, and CD40 expression levels, respectively.

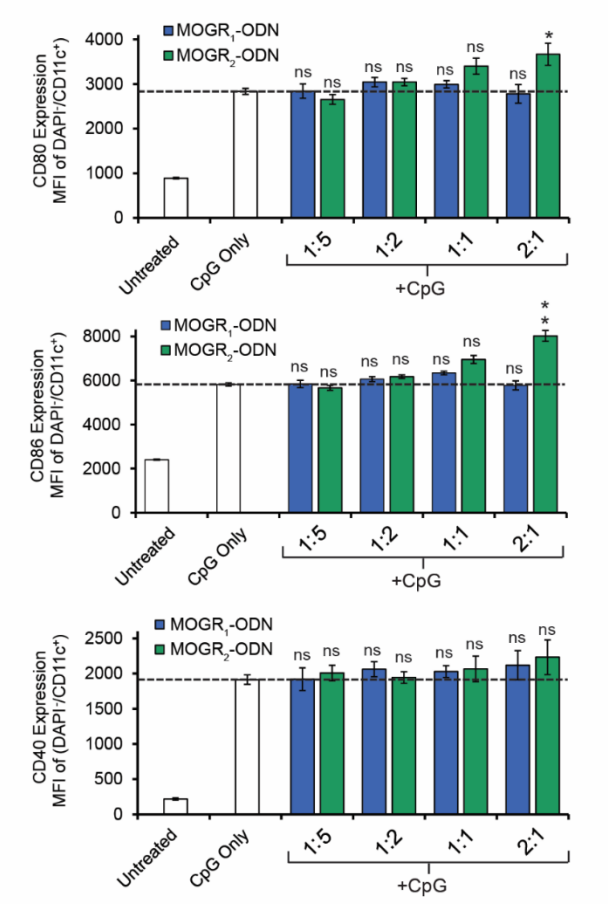

Figure 4.7: Complexes formed from MOGR$_x$ and a control oligonucleotide do not affect DC activation. DC activation was analyzed following stimulation with CpG and incubation with complexes formed from MOGR$_x$ and ODN. Fluorescent antibody conjugates were used to quantify the expression levels of CD40, CD80, and CD86 by flow cytometry. *p < 0.05, **p < 0.01, ns = not significant. For all panels, statistics correspond to comparisons against Free CpG only.

4.3.6 MOGR$_x$-GpG complexes decrease inflammatory T cell proliferation

The results above indicate that complexes containing GpG alter both the activation state of DCs and the secretion of inflammatory cytokines by these cells. Since these characteristics are critical in determining the type and magnitude of response to foreign or self-antigens, we investigated whether these complex-induced changes altered the function of myelin-specific T cells characteristic of disease in MS. In these studies, we

cultured similarly-treated primary DCs with T cells isolated from 2D2 mice. T cells from 2D2 mice exhibit transgenic T cell receptors, and thus proliferate upon encounter of APCs displaying MOG in MHC-II. After co-culturing for 48 hours, flow cytometry analysis revealed a high level of $CD4^+$ T cell proliferation in co-cultures stimulated with CpG and free $MOGR_x$, indicated by decreasing signal intensity as dye was diluted from cell proliferation (**Figure 4.8A**). Interestingly, all $MOGR_x$-GpG complex formulations greatly decreased proliferation, in some cases more than 12-fold, compared to controls containing equivalent doses of $MOGR_x$ peptide without GpG (**Figure 4.8B, Figure 4.9**). Further, since CpG alone did not cause any proliferation (**Figure 4.8B**), our results suggest complexes limit proliferation of myelin-specific T cells.

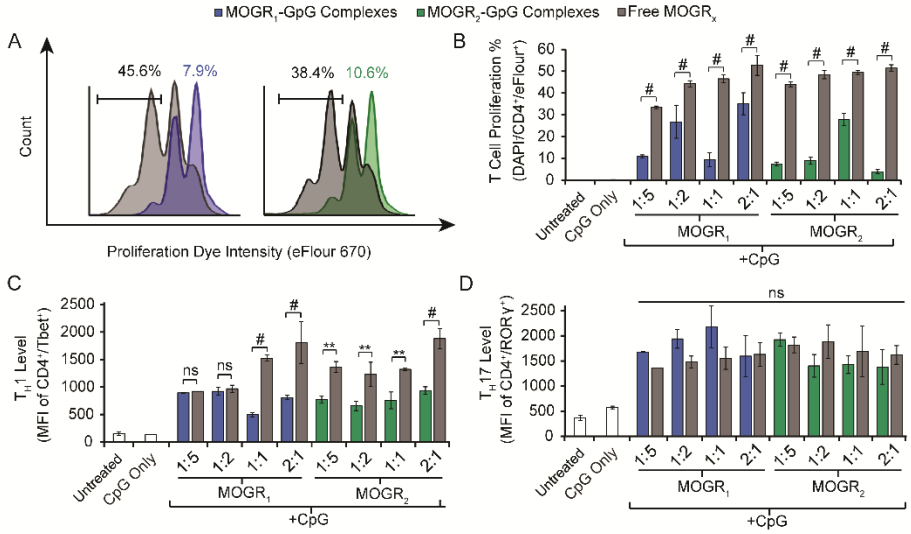

Figure 4.8: Complexes reduced the proliferation and inflammatory function of transgenic T cells displaying receptors specific for MOG presented by DCs in the MHC-II complex. Primary DCs were incubated with stimulatory CpG and complex or free treatments prior to coculture with 2D2 T cells. T cells containing a dye were used to assess proliferation by dilution of the dye between daughter cells (**A**), (**B**). T cell phenotype was assessed by staining with TH1 (**C**) and TH17 (**D**) fluorescent antibody conjugates and flow cytometry. **p < 0.01, #p < 0.0001, ns = not significant.

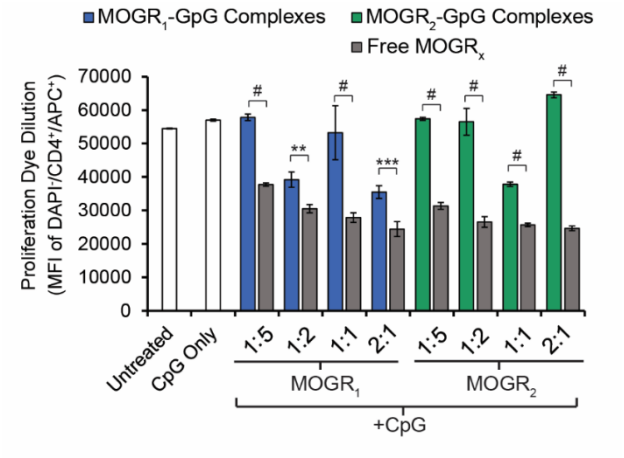

Figure 4.9: Complex incubation reduced the decrease of proliferation dye intensity. 2D2 T cells labelled with a proliferation dye were incubated with DCs that had been treated with CpG and complexes or free controls. Dilution of the dye correlates to proliferation of T cells as they dye splits between daughter cells. Flow cytometry analysis quantified the mean fluorescent intensity of proliferation dye. **$p < 0.01$, ***$p < 0.001$, #$p< 0.0001$.

To investigate if reduced proliferation also alters the phenotype of these T cells, we used flow cytometry to assess T_H1 ($CD4^+/Tbet^+$) and T_H17 ($CD4^+/ROR\gamma^+$) levels, effector populations that drive disease in human MS and mouse models of MS. Incubation with free $MOGR_x$ and CpG induced a high level of inflammatory T_H1 ($Tbet^+$) (**Figure 4.8C**) and T_H17 ($ROR\gamma^+$) cells (**Figure 4.8D**). As expected, cell numbers and T_H1 levels were only detectable in treatments containing some form of myelin peptide since 2D2 cells are specific for myelin and do not respond to other stimulus. In agreement with our proliferation data, we discovered that treating CpG-stimulated cultures with $MOGR_x$-GpG complexes significantly reduced T_H1 subsets relative to cells stimulated with CpG and free peptide (i.e., without GpG). Complexes containing either $MOGR_1$ or $MOGR_2$ drove these reductions, but the effects were more robust in $MOGR_2$-GpG complexes where significant reductions in T_H1 levels were measured for all complex ratios (**Figure 4.8C**). Regardless of peptide structure or

complex ratio, no effects were observed on T_H17 levels compared with the free controls (**Figure 4.8D**). Taken together, the data in **Figures 4.1-4.9** demonstrate that complexes reduce TLR9 signaling and deactivate DCs, while limiting myelin-specific T cell proliferation and reducing T_H1 phenotypes associated with pathogenesis during disease.

4.3.7 MOGR$_2$-GpG polyplexes improve disease progression and severity during a mouse model of MS (EAE)

Building on our *in vitro* results, we tested if complexes promote tolerance and control disease in a mouse model of MS (EAE). In these studies, mice received a single *s.c.* injection of MOGR$_2$-GpG complexes—since R_2 complexes were generally more potent than R_1 complexes during *in vitro* studies—on day 7 after EAE induction (**Figure 4.10A**). These mice, along with untreated mice induced with EAE were assessed daily using an established clinical score system and by body weight. As shown in **Figure 4.10B**, mice treated with complexes exhibited a modest, but statistically significant, improvement in disease progression. Additionally, disease severity was improved, as indicated by a significantly reduced mean maximum disease score compared to the untreated group (**Figure 4.10C**). This single complex treatment regimen also delayed onset of symptoms, with a mean time to onset of 13.6 ± 0.5 days for treated mice compared 11.6 ± 0.3 days for untreated mice (**Figure 4.10D**). We next tested if a multi-injection regimen could enhance these therapeutic effects by treating mice with complexes on days 6, 12, and 18 (**Figure 4.10E**). Strikingly, this strategy substantially enhanced efficacy, as indicated by a much greater reduction in the progression and

severity of disease in treated mice. The clinical score of treated mice was significantly lower than untreated mice throughout the course of the study (**Figure 4.10F**), with more than a 2.0-point decrease in the mean maximum disease score (**Figure 4.10G**). This three injections regimen also led to a significant decrease in weight loss (**Figure 4.11**) and disease incidence, with only 60% of mice showing symptoms at the end of the study compared to 100% of untreated mice (**Figure 4.10H**). Control studies using similar regimens, but involving three treatments of GpG alone, revealed no therapeutic effect relative to untreated mice (**Figure 4.12**).

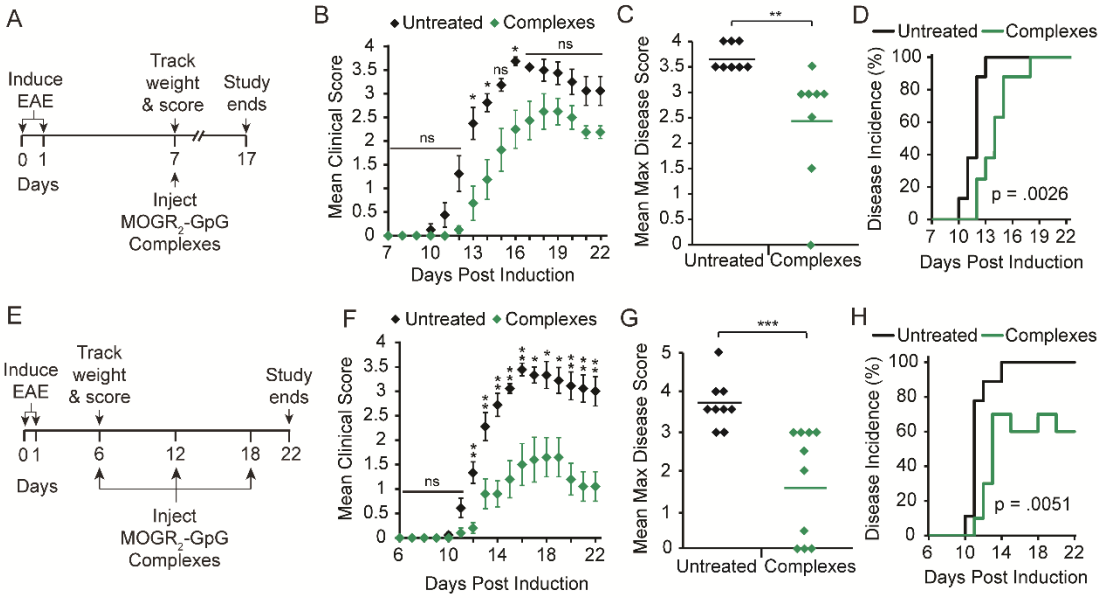

Figure 4.10: Complex treatment reduced disease severity in EAE. (**A**) In one study, mice were induced with EAE on days 0 and 1 and treated *s.c.* with complexes on day 7. (**B**) Disease progression was monitored by daily scoring of paralysis. (**C**) Comparison of disease severity was completed by averaging the maximum disease score of each mouse. (**D**) Disease onset was the first day a mouse showed symptoms. (**E**) In a similar study, mice were instead injected *s.c.* with complexes on days 6, 12, and 18. Disease progression (**F**), severity (**G**), and onset (**H**) were again measured. *p < 0.05, **p < 0.01, ***p < 0.001, ns = not significant.

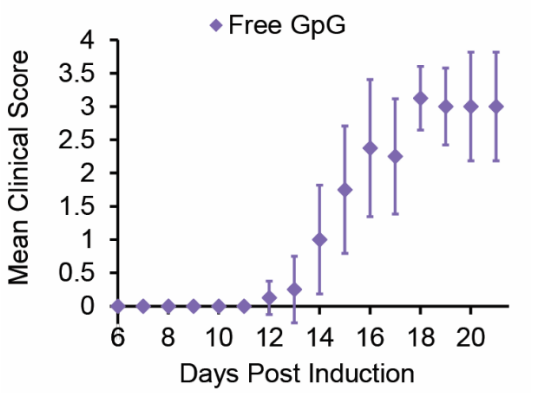

Figure 4.11: MOGR$_x$-GpG complexes halted body weight loss due to EAE induction. Loss of body weight is a measure of disease onset and severity in EAE and was monitored daily beginning at day 6 following EAE induction. **p < 0.01, ***p < 0.001, #p < 0.0001.

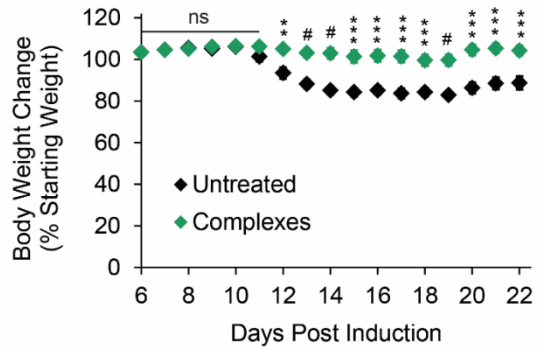

Figure 4.12: Treatment with GpG alone had no effect on disease progression. Mice were induced with EAE on days 0 and 1 and treated *s.c.* with free GpG on days 5, 10, and 15. Disease progression was monitored by daily assignment of clinical EAE scores.

4.4 Discussion

Current treatment options for MS involve the regular injection of immunosuppressive drugs or antibodies that are broadly acting. These options are not curative and can leave patients immunocompromised,[23] highlighting the need for new, more selective therapies. Despite the simplicity and unique features of polyplexes, this general approach has only recently begun to be exploited to promote tolerance. We approached the current challenges to autoimmune therapies using principles from the polyplex field

to enable co-delivery through self-assembly of myelin-derived peptide (MOG) and antagonistic ligands for TLRs—pathways increasingly implicated in both human and animal autoimmune disease.[175, 176, 178, 179, 203] Our strategy is unique in several ways. First, the reports highlighted in the introduction utilize plasmid DNA encoding regulatory signals,[212, 213] requiring internalization, endosomal escape, transcription, and translation, or DNA designed to expand T_{REGs} by avoiding PAMPs to support regulatory pathways (e.g., indoleamine 2,3-dioxygenase induction, IDO).[214-216] We have taken an alternative approach, incorporating peptide self-antigen (i.e., MOG) into polyplexes to create a direct route for generation of antigen-specific tolerance without need for gene expression. Second, we are directly targeting a new pathway, TLR signaling, to limit the pro-immune signaling during differentiation of self-reactive T cells to bias these cells away from inflammatory populations (e.g., T_H1). This is of particular relevance for the polyplexes we have designed since TLR9 is expressed in endosomes, eliminating the need for endosomal escape. [221] Along these same lines, our approach does not require transcription or translation of either a self-antigen (i.e., MOG) or a regulatory cue (i.e., GpG) since each of these components are already the active molecules. We propose that following polyplex uptake by APCs, GpG blunts inflammatory TLR9 signaling as myelin-derived peptide is being presented to naïve myelin-specific T cells (**Figure 4.13**). This altered signaling may still allow proliferation of MOG-specific T cells, but polarize these cells away from inflammatory subsets (e.g., T_H1, T_H17) and toward T_{REGs} that can migrate to the CNS or other sites of disease to control inflammation (**Figure 4.13**). Lastly, the polyplex-like structures we have developed eliminate all synthetic carrier components, and instead, are

constructed entirely from immune signals. This removes the potential for intrinsic inflammatory activity associated with many common polymers that could make disease worse while also simplifying composition since the signals are also the carriers and condensation agents.

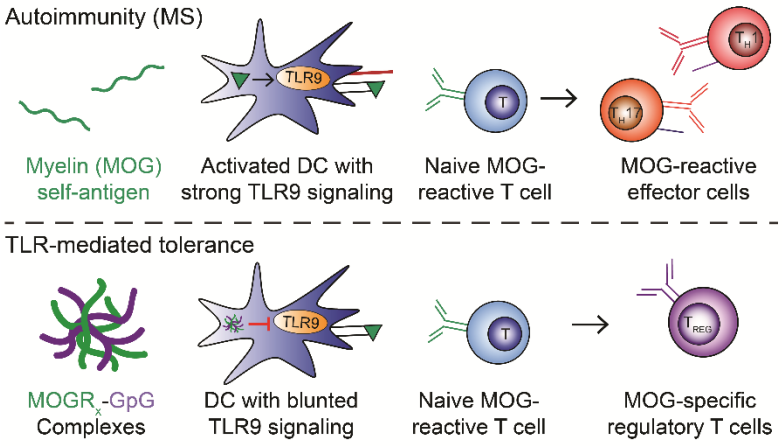

Figure 4.13: Schematic of the proposed mechanism of tolerance induced by $MOGR_x$-GpG complexes. In MS, myelin peptide is presented to naïve T cells by activated DCs with strong TLR9 signaling, leading to the proliferation of inflammatory MOG-reactive effector T cells. $MOGR_x$-GpG polyplexes are taken up by APCs. GpG blunts inflammatory TLR9 signaling as MOG is presented to naïve T cells. The combination of immune signals induces the proliferation of MOG-specific TREGs that promote tolerance.

Beyond polyplex-like materials, there are a number of exciting strategies developing at the interface of biomaterials and autoimmune therapy. One important question is how NPs are processed compared with soluble signals. Shea, Miller, and colleagues have shown that conjugation of self-antigens to polymeric NPs helps direct these particles to macrophage scavenger receptors typically involved in clearance of apoptotic cells debris, material which clearly needs to be recognized as self.[50, 53] Thus, this altered trafficking results in activation of downstream tolerance pathways including deletion, anergy, and T_{REG} expansion. The polyplex studies by the Mellor lab focus on induction of the regulatory IDO pathway through delivery of DNA that does not contain

inflammatory cues typically present in pathogens.[214-216] Instead, these particles are surveyed by the stimulator of IFN genes (STING) pathway in DCs, leading to IDO expression and T_{REG} activation. In yet a different recent study, tolerance was induced simply by altering the surface charge of synthetic polymeric particles to exhibit negative surface charge.[50] Together these examples highlight both the potential of biomaterials for studying and treating autoimmunity, as well the breadth of questions that require further study—design guidelines, roles of self-antigen and regulatory cues, the frequency of delivery and durability of tolerance, to name a few.

In cell culture, NPs formulated with self-antigen and plasmid encoding a lymphocyte attenuator have recently been used to condition DCs *in vitro* for promoting tolerance after adoptive transfer.[222] Motivated by the potential of this idea, but striving to eliminate the need for cell isolation or *ex vivo* manipulation, we began by applying classic polyplex design and characterization techniques to NPs assembled entirely from MOG-derived peptides and regulatory TLR9 antagonists. Interestingly, we discovered that the polyplexes could be formed over a range of charge ratios and surface charges (**Figure 4.1B**) without significantly altering the diameter (**Figure 4.1A**). This finding revealed some interesting implications during our *in vitro* studies. First, MOG peptide was internalized at similar levels in both free and complexed form, whereas GpG was internalized at much higher levels when complexed with $MOGR_2$ (**Figure 4.4**) This likely results from the divergent charges and molecular weights of these molecules, with $MOGR_1$ (MW = 3240.69) and $MOGR_2$ (MW = 3396.88) exhibiting total net charges of +4 and +5, respectively, while GpG (MW = 7215.8) has a charge of -22.

Thus, while free GpG is highly negatively charged, the peptide is cationic and condensation results in complexes that are less anionic. This feature of $MOGR_x$ is attractive because it supports uptake by endocytosis, and, In particular, TLR9 is expressed in endosomes. This idea also highlights the possibility of modulating immune function along another dimension by using the composition of the polyplexes to change the physicochemical properties.

In the classic polyplex field, polyplexes are often formed by mixing the components and assuming all of the molecules become complexed. In our work, we purified the polyplexes by centrifugation to allow a precise measurement of the relative composition (i.e., peptide vs. GpG content) after polyplex formulation. This methodology is important because changing the relative input of each component could lead to complexes with different compositions, subsequent changes in physicochemical properties, and ultimately, impact the types of immune responses that develop. The latter point is particularly relevant as high levels of self-antigen in isolation might create situations that could exacerbate autoimmune disease, while high doses of regulatory signals alone might drive broad suppression. In our current proof-of-principle report, the goal was to understand if self-assembled immune signals that mimic useful features of polyplexes can be used to target TLR signaling to promote tolerance. In future studies, however, teasing out the link between polyplex composition and the balance between autoimmunity and tolerance will be informative to designing therapies that are both effective and selective.

We also observed that polyplexes formed from GpG and MOG modified with R_2 generally performed better (i.e., greater uptake and DC deactivation, reduced T cell proliferation) than $MOGR_1$-GpG complexes (**Figure 4.4-4.9**). This also might be a result of the decreased negative charge, a hypothesis that could be directly tested by studying peptides modified with additional arginine residues. For example, in the polyplex field, endocytosis is typically the mechanism of cell entry, while cell penetrating peptides can enter through penetration or other energy-independent mechanisms.[223-225] The latter molecules are characterized by short stretches of mostly cationic amino acids, so appending such sequences to peptides might allow enhanced uptake; perhaps these phenomena even occur in the case of $MOGR_2$, though mechanistic studies blocking specific internalization routes will be required to elucidate this possibility. Charge can also greatly affect the ability of polyplexes to escape endosomes following cell entry, with a classic motivation for studying polyplexes as gene delivery agents being the buffering capacity of polycations to exploit endosomal acidification and promote endosomal escape by the "proton sponge effect".[226-228] Although TLR9 is expressed in endosomes, facilitating our current work, future studies could exploit these materials to target cytosolic receptors through endosomal escape or through cell penetration. Future studies will leverage controllable surface charge to compare uptake and trafficking to other organelles as a function of the properties of polyplexes assembled from immune signals. From an immunological or therapeutic perspective, the high and tunable levels of GpG carried into cells through $MOGR_x$ complexation could be important in explaining the ability of complexes to control the inflammatory response to myelin, as a higher amount of GpG entering cells should

have a greater effect on inhibiting TLR9 signaling during differentiation of spleen- or LN-resident T cells. Since surface charge appears to play a direct role in tolerance,[50] and certainly impacts particle uptake,[6, 229] tunable control over charge could also be useful in optimizing immunological processing or efficacy.

We also observed some interesting differences in how GpG behaved in complexes versus free form. During the TLR9 signaling studies, free GpG reduced TLR9 signaling more than complexed GpG (**Figure 4.3A**). One potential explanation is the strong binding between $MOGR_x$ and GpG (**Figure 4.1C**), which could require a longer time for binding and processing of GpG to TLR9 receptors. Supporting this possibility, $MOGR_2$—which protected GpG from degradation better than $MOGR_1$ (**Figure 4.1D**)—did not suppress TLR9 signaling as much as $MOGR_1$, though we only studied these effects at a single time point (**Figure 4.3A**). Surprisingly, despite better protection from enzymes (**Figure 4.1D**), the EtBr assay suggested similar binding levels (**Figure 3.1C**), so more sensitive measurements of binding affinity might provide additional insight into some of the different effects we observed from GpG as a function of which $MOGR_x$ structure was used to complex GpG. Despite the less efficient suppression of TLR9 signaling when GpG was complexed at some ratios, both complex formulations (i.e., using $MOGR_1$ or $MOGR_2$) greatly reduced TLR9 activity, and further, provide other benefits such as improved uptake and protection from enzyme. Importantly in our studies, treatment of cells with free $MOGR_x$ or $MOGR_x$-ODN polyplexes (**Figure 4.7**) generally had no effect, directly demonstrating the role of GpG and TLR9 signaling in the observed effects. Further, free GpG had no therapeutic effect when injected alone

into mice induced with EAE (**Figure 4.11**). Similarly, in co-culture studies, CpG alone did not cause proliferation, while proliferation was observed during treatment with free $MOGR_x$ (**Figure 4.8B**). When GpG was complexed with these peptides, proliferation was greatly diminished. This result indicates that $MOGR_x$-GpG complexes alter the function of myelin-reactive cells in a myelin-dependent manner, a feature that is important in therapies that might offer antigen-specific control of autoimmune disease. Taken together, these results support an important role for co-delivery of both the self-antigen and the regulatory signal in the polyplex to induce tolerance.

Our approach reveals several important follow-on questions. First, we prepared polyplexes containing a single antigen, but in human disease, multiple epitopes are attacked initially and through the process of epitope spreading. Future studies will need to investigate induction of tolerance against other self-antigens alone or in combination. Along these same lines, the EAE model itself is limited in the reactivity and range of epitopes attacked.[230] Therefore there is also motivation to test polyplexes and other therapeutics in multiple models of autoimmunity. Additionally, we are currently investigating the trafficking and stability of complexes upon cell entry as a function of polyplex composition and the number of arginine residues on the peptide, which could modulate the route of update. These concepts are particularly important in therapeutics involving TLRs as these receptors are differentially expressed in different cell components (e.g., endosomal, cytosolic). Lastly, from a materials perspective, our approach relies on electrostatic assembly, so some self-antigens may require appending charged amino acid anchors if they do not exhibit sufficient inherent charge.[148, 231,

232] Not-withstanding these limitations, there is great recent excitement for translation of antigen-specific therapies. For example, a recent clinical trial with human MS patients involved administration of a cocktail of seven myelin peptides coupled to autologous cells as a possible approach to promote myelin-specific tolerance.[12, 193]

4.5 Conclusion

In this report we demonstrate that immune signals assembled into polyplex-like structures exhibit many cardinal features of traditional polyplexes, but eliminate carrier components. Our results show that GpG suppresses TLR9 signaling during complexation and that GpG is more efficiently internalized when in a complexed form. This enhanced delivery deactivates DCs and limits cytokines (IFN-γ) and proliferation of myelin-specific cell populations (e.g., T_H1) implicated in human MS and animal models. In mice, these complexes improve disease progression, severity, and incidence. Future studies will elucidate the mechanisms of uptake and trafficking in immune cells, as well as the underlying mechanisms of tolerance. Ultimately, this simple approach could contribute to more specific treatment options based on self-assembly of immune signals into structures that offer attractive features of biomaterials, enabling co-delivery of self-antigens and regulatory ligands that block TLR signaling to bias differentiating T cells toward regulatory populations instead of inflammatory effector subsets.

The following chapter describes another material-based strategy for delivering MOG, in an attempt to induce tolerance in EAE. This platform features one of the inorganic materials described in **Chapter 3** (QDs) and is based on the approach discussed in

Chapter 2 to alter the trafficking and processing of self-antigen through particle-based delivery. In particular, **Chapter 5** investigates key parameters for inducing tolerance such as peptide dose and density.

Chapter 5: Engineering immunological tolerance using quantum dots to tune the density of self-antigen display[3]

5.1 Introduction

In MS, self-reactive antibodies and T cells attack the myelin sheath insulating the CNS.[17, 18] Existing therapies can suppress these effects, but are not curative and leave patients immunocompromised.[23, 233] One promising strategy to overcome these hurdles is generation of T_{REGs}. These cells can act in a myelin-specific manner to restrain the inflammatory response against myelin without non-specific suppression.[12, 183, 201] New studies focused on more specific treatments reveal that the development of inflammation or tolerance against self-molecules is influenced by the concentration and form of antigen reaching the tissues that coordinate immune function, namely, LNs and the spleen.[12, 48, 49, 62, 234] Thus, tunable control over the display of these self-ligands could enable more specific and effective therapies.[47] Along these lines, three recent discoveries motivated our strategy to test QDs as a nanoscale scaffold to promote tolerance. First, several reports demonstrate sub-30 nm NPs drain very efficiently through lymphatic vessels and accumulate in LNs.[4, 5] Second, new studies reveal that changing the way myelin is processed and presented to the immune system can drive tolerance instead of inflammation.[25, 53, 54, 192] For example, one group induced T cell tolerance by treatment with large MPs decorated with myelin peptide that trafficked to macrophages expressing a scavenger receptor

[3]Adapted from **KL Hess**, LH Tostanoski, JI Andorko, K Susumu, JR Deschamps, IL Medintz, and CM Jewell; "Engineering Immunological Tolerance Using Quantum Dots to Tune the Density of Self-Antigen Display", *Advanced Functional Materials* **2017**, 27 (22):1700290 (cover article)

(MARCO) normally involved in uptake and removal of particulate debris.[53] This altered trafficking activates apoptotic clearance pathways that bias responses against these peptides toward tolerance. Lastly, two seminal papers reveal direct connections between LNs and the CNS.[235, 236] This discovery suggests engineering the response to self-antigens in LNs during T cell priming could provide a direct route to generate T_{REGs} that subsequently migrate to the CNS to control pathogenic T cells (e.g., T_H1, T_H17) attacking myelin.

QDs offer many attractive properties to achieve the goals above.[237] Their broad absorption, tunable photoluminescence, and strong resistance to photobleaching enable powerful deep-tissue imaging.[238-240] Structurally, QDs serve as a central platform for high-avidity display of biomolecules.[74] We recently showed QDs remain bright while displaying controlled numbers of peptides in cells and complex tissues (e.g., brain) with no overt toxicity,[241, 242] similar to other QD toxicity studies.[243, 244] Of note, QDs allow facile tracking and drainage through lymphatics.[245] We thus hypothesized that QDs displaying defined densities of the MOG peptide (MEVGWYRSPFSRVVHLYRNGK) – a self-peptide sequence attacked during MS – would allow efficient visualization of trafficking to lymphoid tissues, while altering the processing and trafficking of MOG to promote T_{REGs} that control disease in a mouse model of MS.

QDs modified with myelin or control peptides exhibited tunable, uniform features – peptide display density and size, for example. These materials were non-toxic to

primary immune cells and did not trigger any intrinsic inflammatory responses. In mice, the peptide-QDs rapidly drained to LNs following injection, and were co-localized with macrophages expressing scavenger receptors involved in tolerance. MOG-QD treatment in mice induced with a mouse model of MS drastically reduced disease severity and incidence, while QDs modified with control peptide sequences did not. Importantly, these therapeutic effects were tunable and directly correlated with not just the dose, but with the density of MOG ligands assembled on the QD surfaces.

5.2 Materials and Methods

5.2.1 Materials

MOG modified for attachment to QDs (HHHHHSAAAAAGMEVGWYRSPFSRVVHLYRNGK, denoted "MOG" in the text) and a similarly-modified control peptide from OVA (HHHHHSAAAAAGISQAVHAAHAEINEAGR; denoted "CTRL" in text) were synthesized by Genscript (Piscataway, NJ). Molecular Biology Grade Water and RPMI-1640 media were purchased from Lonza (Allendale, NJ). Fetal bovine serum (FBS) was supplied by Corning (Tewksbury, MA). 2-Mercaptoethanol and Amicon Ultra Centrifugal Filters were purchased from Sigma Aldrich (St. Louis, MO). HEPES, non-essential amino acids, and 40 μm cell strainers were purchased from VWR (Radnor, PA). OPC oligonucleotide purification cartridges, L-Glutamine, Penicillin-Streptomycin, and 4',6-diamidino-2-phenylindole (DAPI) were purchased from Thermo Fisher Scientific (Grand Island, NY). Spleen Dissociation Medium and CD4

negative selection kits were from STEMCELL Technologies (Vancouver, British Columbia, Canada). CD11c microbeads were purchased from Miltenyi Biotec (Cambridge, MA). CpG adjuvant (5'-TCC ATG ACG TTC CTG ACG TT-3') was synthesized by IDT (Coralville, IA). Fluorescent antibody conjugates for flow cytometry were purchased from BD (San Jose, CA). eFlour 670 proliferation dye was supplied by affymetrix eBioscience (San Diego, CA). FITC CD45R/B220 (BD), CD3e (abcam, Cambridge, MA), DL405 IgG (Jackson Immunoresearch, West Grove, PA), F4/80 (BD), Biotinylated MARCO (R&D Systems, Minneapolis, MN), and Streptavadin Alexa 488 (Jackson Immunoresearch) were used for immunohistochemical staining of iLN sections. EAE induction kits were supplied by Hooke Laboratories (Lawrence, MA).

5.2.2 Cells and animals

All primary cells were harvested from female C57BL/6 mice (4-12 weeks, stock #000664) and male C57BL/6-Tg(Tcra2D2,Tcrb2D2)1Kuch/J (2D2) mice (10-16 weeks, stock #006912) purchased from Jackson Laboratories (Bar Harbor, ME). 2D2 mice display transgenic $CD4^+$ T cell receptors specific for MOG residues 35-55. Mice induced with EAE were female C57BL/6 mice (10-12 weeks, stock #000664). All animals were cared for in compliance with Federal, State, and local guidelines, and using protocols reviewed and approved by the University of Maryland's Institutional Animal Care and Use Committee (IACUC).

5.2.3 Characterization of quantum dots and peptide-QD assemblies

The 625 nm emitting QDs and their cap-exchange with CL4 ligands have been previously described.[246] Peptides were desalted prior to QD conjugation as previously described.[247] Briefly, an oligonucleotide purification cartridge is charged with acetonitrile (MeCN) and triethylamine acetate (TEAA). Peptide that has been dissolved in molecular biology grade water is then passed through the cartridge approximately 20 times, prior to being eluted by MeCN. The resulting solution is then lyophilized. MOG peptide has a net charge of +4 at pH 7. MOG and CTRL were assembled on QDs by mixing solutions of desalted peptide in molecular biology grade water with QDs at defined molar ratios. TEM, gel electrophoresis, and DLS analysis were performed as described.[246]

5.2.4 Quantification of peptide loading on QDs

We utilized an established fluorescence method to verify peptide binding to QDs by the same mechanism.[248] A Cy3-labeled peptide terminating in a (His)6 motif was self-assembled to the QDs across a range of ratios including 0, 10, 25, 50, 75, 100, 125, and 150 peptides/QD in 100 µL of PBS. Equal amounts of free dye-labeled peptide without QD were added to the same volume of PBS as controls. Following self-assembly, all samples were loaded into 0.5 mL Amicon Ultra Centrifugal Filters with a 50,000 NMWL and centrifuged at 14,000×g for 10 min. The amount of free dye-labeled peptide from the QD samples was then compared to that from the unbound dye-labeled peptide only control samples using UV absorbance.

5.2.5 Simulation of MOG-QD peptide assembly

The MOG-QD peptide assembly was simulated in silico in a manner similar to that we described previously for other peptides.[249-253] These structures and calculations were prepared using Chimera and Chem-3D Ultra 11.0. Energy was minimized using the MM2 module and the most probable conformation when attached to the QD were selected. A hard sphere was used to represent the QD core/shell structure, which was covered with the surface-functionalizing ligand at an extension estimated from DLS measurements and energy minimization. The core MOG peptide structure was taken directly from the crystallographic structure 1PKO in the Protein Data Bank.[254] The remaining $(His)_5S(Ala)_5G$ N-terminal portion was docked to the QD surface via the $(His)_5$ sequence with the $(Ala)_5G$ portion in an energy-minimized alpha helical conformation. Probabilities for peptide ligand density distributions were calculated using a Poisson distribution as previously described and confirmed experimentally.[255]

5.2.6 Dendritic cell isolation and flow cytometry

$CD11c^+$ DCs were isolated from the spleens of female C57BL/6 mice through positive selection with Spleen Dissociation Media (STEMCELL) and CD11c Microbeads (Miltenyi). DC purities after isolation varied slightly across experiments, but were 90% or greater. DCs were plated in a 96 well plate at 100,000 cells per well and cultured in RPMI 1640 media supplemented with 10% FBS, 2 mM L-glutamine, 1x non-essential amino acids, 10 mM HEPES buffer, 1x penicillin and streptomycin, and 55 μM β-mercaptoethanol at 37°C and 5% CO_2. For uptake studies, DCs were incubated with

150:1 MOG-QDs for 2 hours, stained with DAPI, and examined by flow cytometry (BD Cantoll, San Jose, CA) for presence of MOG-QDs and viability. Viability was determined by cells staining negative for DAPI. Data were analyzed with FlowJo v.10 (TreeStar, Ashland, OR).

5.2.7 DC activation, T cell coculture, and flow cytometry

Isolated DCs were treated with CpG to induce the expression of costimulatory factors and either MOG or CTRL in soluble or QD-conjugated form and cultured for 24 hours. DC activation was then analyzed by staining for CD40, CD80, and CD85 markers. Stained cells were analyzed by flow cytometry. $CD4^+$ T cells were then isolated from the spleens of 2D2 mice via a negative selection kit (STEMCELL) and labelled with eFlour 670 proliferation dye. 300,000 T cells were then added to the wells containing treated DCs. After 72 hours, cell viability was assessed by DAPI staining and T cell proliferation was analyzed by a decrease in fluorescent signal as dye is diluted in daughter cells during successive generations. Cells in all *in vitro* studies were treated with a dose of QDs ranging from 0.44 to 40 picomoles and a dose of MOG ranging from 0.25 to 10 µg.

5.2.8 Analysis of QD drainage in mice

Mice were injected with MOG-QDs and 24 hours later, the draining and non-draining iLNs were harvested for analysis. LNs were passed through a 40 µm strainer to create a single cell suspension. Cells were then stained with DAPI and analyzed by flow

cytometry for viability (i.e., $DAPI^-$) and presence of fluorescent MOG-QDs. Additional iLNs were frozen, sectioned, and fixed for staining. In one analysis, sections were stained for T cells (CD3e) and B cells (B220). In an additional study, sections were stained with antibodies for macrophages (F4/80) and the scavenger receptor MARCO. iLN sections were visualized by fluorescent microscopy (Olympus IX-83) for presence of MOG-QDs, T cells, B cells, macrophages, and MARCO. ImageJ was used for image processing and analysis. All images in a particular study were analyzed in an identical manner that was applied to the entire image area.

5.2.9 EAE induction and monitoring

C57BL/6 mice (female, 10-12 weeks) were induced with EAE following a defined protocol from Hooke Labs. Briefly, mice were injected *s.c.* with an emulsion of MOG and complete Freund's adjuvant (CFA) at the upper and lower back on day 0. Pertussis toxin was also administered *i.p.* 2 and 24 hours after MOG/CFA injection. Beginning at day 7, mice were weighed to detect changes from day 0 body weight (a symptom of disease) and scored for disease severity with respect to paralysis. A standard clinical scoring rubric was used: 0 – no symptoms, 1 – limp tail, 2 – weakness of hind legs, 3 – hind limb paralysis, 4 – hind limb paralysis and partial front limb paralysis, 5 – moribund.[53, 183, 201] Disease incidence was defined as the first day a mouse displayed symptoms of paralysis.

5.2.10 MOG-QD treatment

Mice induced with EAE were randomly divided into groups of 8-10 mice each. A control group was left untreated in each experiment. In one experiment, additional groups were treated by *s.c.* injection at the tailbase with 0.2 nanomoles QDs, 70 μg MOG, 70 μg CTRL peptide on 0.2 nanomoles QDs (100:1), or 70 μg MOG peptide on 0.2 nanomoles QDs (100:1). Similar experiments contained two treatment groups: 14.3 μg MOG on 0.4 nanomoles QDs (17:1) or 73 μg MOG on 0.2 nanomoles QDs (52:1). The final experiment design contained three treatment groups: 70 μg MOG on 0.5 nanomoles QDs (25:1), 70 μg MOG on 0.4 nanomoles QDs (52:1), or 70 μg MOG on 0.3 nanomoles QDs (65:1).

5.2.11 EAE T cell readout

Mice were induced with EAE and treated with MOG-QDs as described above. On day 9, the iLNs were removed for analysis by flow cytometry. iLNs were mashed through a 40 μm strainer to create a single cell suspension and stained for T cell surface markers ($CD4^+$, $CD25^+$) and transcription factors ($Tbet^+$, $Foxp3^+$). Tbet and Foxp3 are common transcription factors used to identify T_H1 and T_{REG}, respectively. Cells were examined with flow cytometry and data were again analyzed with FlowJo v.10.

5.2.12 Statistics

One-way ANOVA with a Tukey post-test was used to compare three or more groups for *in vitro* studies and overall disease metrics from *in vivo* studies. For *in vivo* studies, two-way ANOVA was used to compare three groups monitored over time, with post-

test corrections for multiple comparisons. Log-rank tests were used in analysis of disease incidence. For all tests, p values ≤ 0.05 were considered significant. For all figures, *p < 0.05, **p < 0.01, ***p < 0.001, ****p < 0.0001, $^{\#}$p < .05.

5.3 Results and Discussion

5.3.1 Self-peptides can be assembled at high densities on QD surfaces

We began our studies using 625 nm emitting CdSe/ZnS core/shell QDs (**Figure 5.1**) with a diameter of 9.2 ± 0.8 nm (**Figure 5.2A**). We have previously shown this system is useful in biological contexts because these QDs can be made biocompatible using the zwitterionic CL4 ligand (**Figure 5.3**).[242] For peptide assembly, we employed metal-affinity driven coordination to the QD surface (K_d~10^{-9} M), which is nearly instantaneous upon simple mixing of QDs with peptide.[74] Since this assembly follows a Poisson distribution, the actual number of peptides loaded per QD is close to the input peptide:QD ratio, except at very low densities (<4 peptides/QD).

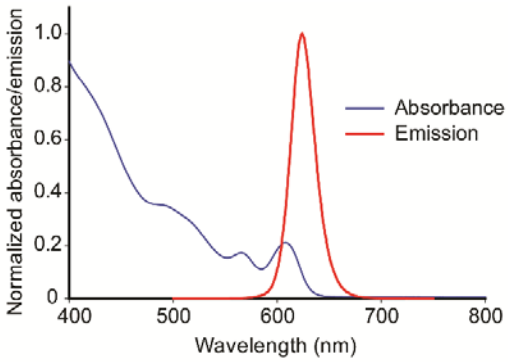

Figure 5.1: Normalized absorbance (blue) and emission (red) curves of 625 nm QDs. Intrinsic fluoresnce

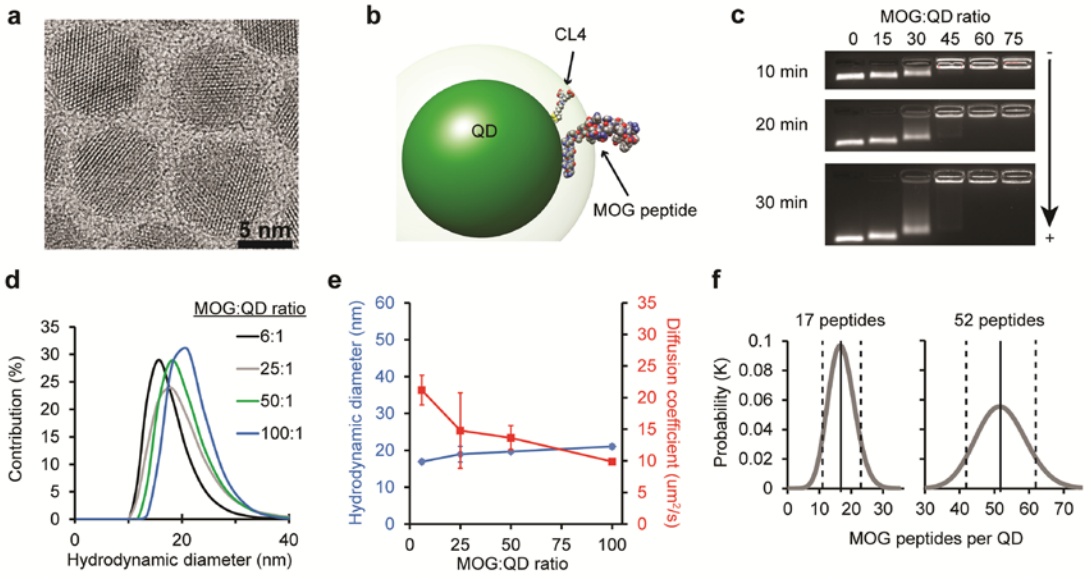

Figure 5.2: MOG-QDs offer tunable display of MOG peptide ligands. (**A**) TEM image of 9.2 ± 0.8 nm CdSe/ZnS core/shell 625 nm emitting QDs. (**B**) Structural simulation of the MOG-QD to scale with an energy minimized CL4 ligand attached to the surface with an extension of ≈1.1 nm. (**C**) Electrophoretic mobility of MOG-QDs was assessed in a 1% agarose gel run in 1× TBE buffer. (**D**) MOG-QD size was measured by DLS. (**E**) MOG-QD size was compared to rate of diffusion. (**F**) Simulation was used to confirm MOG loading densities. Data in (E) represent mean ± s.d.

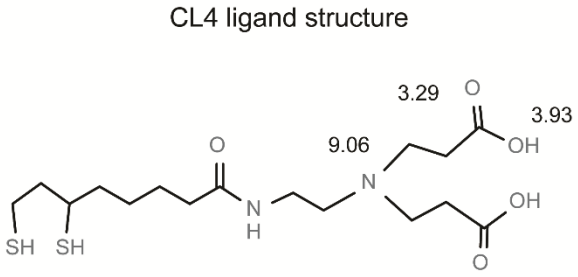

Figure 5.3: CL4 ligand structure with estimated pKa values.

To facilitate assembly, MOG was synthesized with an N-terminus sequence of HHHHHSAAAAAG, where $(H)_5$ participates in Zn-coordination, S acts as a flexible hinge to display the peptide away from the QD surface, and $(A)_5$ forms a rigid alpha-helical spacer terminated by the G residue. These interactions were simulated using an

energy-minimized approach, revealing the conformation in **Figure 5.2B**. Although many conformations for the $(His)_5S(Ala)_5G$ N-terminal portion are possible, the outcome for this segment of the full-length peptide attached to the QDs has been confirmed experimentally in our previous work by Förster resonance energy transfer (FRET).[74, 241, 249, 250, 256, 257] With respect to the peptide attachment point on the QD surface, previous FRET studies in conjunction with modeling have confirmed that the peptides distribute around the QD surface in a random manner and do not disproportionally assemble in any given area.[258] Thus this system creates an opportunity to understand the role of ligand density on the induction of tolerance. To confirm this capability experimentally, QD modification was carried out at increasing ratios of fluorescent MOG peptide, then purified by ultracentrifugation, and quantified by fluorimetry. These studies revealed tunable modification of QDs up to a density of 150 MOG peptides per QD (**Figure 5.4**).

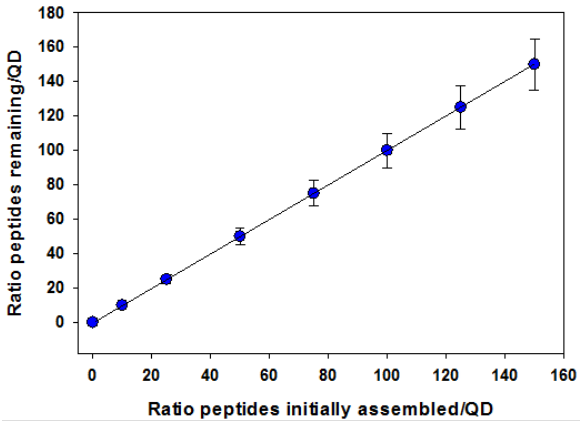

Figure 5.4: Cy3-labeled peptide loading experiments suggest 100% loading up to 150:1 peptide:QD.

5.3.2 MOG-QDs exhibit uniform diameters ideal for lymphatic trafficking

We next characterized how different levels of modification of QDs with MOG self-antigens impacted particle size and mobility. Electrophoretic mobility in agarose gels confirmed an inverse relationship between the MOG:QD conjugation ratio and migration (**Figure 5.2C**). Since MOG peptide has a net charge of +4, the observed patterns are consistent with a less negative charge as the MOG:QD ratio increases until charge balance is approached and migration stops. These effects were further confirmed with zeta potential measurements that revealed less negative charges as a function of increasing MOG:QD ratios (**Figure 5.5**). DLS indicated MOG-QD conjugates were monodisperse (**Figure 5.2D**), with control over MOG conjugation to QDs further shown by hydrodynamic diameters (H_D) increasing from 15.0 ± 0.24 nm to 21.0 ± 0.63 nm over MOG:QD functionalization ratios of 1:1 to 100:1 (**Figure 5.2E**, blue). The diffusion coefficient decreased correspondingly over this same set of ratios (**Figure 5.2E**, red). MOG-QDs prepared at ratios up to 100:1 exhibited H_D of approximately 20 nm, optimal for drainage to LNs.[4, 5] Thus, within an immunologically-relevant size range, QDs with a variety of ligands densities could be generated. In particular, in the cell and animal studies below, a range of 17:1 to 65:1 MOG:QD ratios were used. Experimental measurements of the density of peptide ligands displayed on the QDs (**Figure 5.4**) were also in good agreement with simulations of peptide-QD assembly for ratios of 17:1 and 65:1, corresponding to conjugates with 17 ± 4 peptides and 52 ± 7 peptides assembled per QD (**Figure 5.2F**).

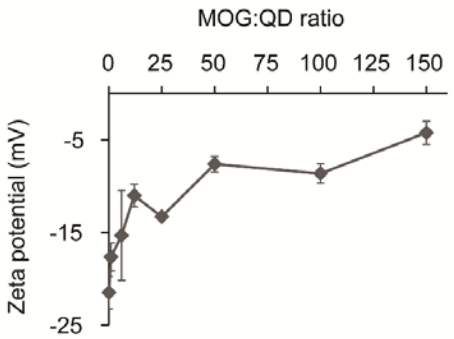

Figure 5.5: Zeta potential of MOG-QDs increases as more MOG peptide is conjugated to the QDs.

While recent studies aimed at inducing tolerance have used MPs or larger NPs (~100-500 nm),[53, 183, 192] the results above highlight unique features of QDs, including 5-50 fold smaller diameters (<20 nm) for efficient concentration in LNs. This size range is particularly noteworthy in the context of lymphatic drainage. Seminal work has shown that even particles on the size range of 100 nm drain inefficiently to LNs, while a diameter of 20 nm dramatically improves lymphatic trafficking.[4] Further, MOG-QD particles also self-assemble, allowing facile administration without need for complicating stabilizers, reactions, or purification steps. With respect to loading, in contrast to the typical loading levels of several or tens of micrograms of peptide per milligram of NP carrier, the MOG-QDs above offer loading as high as 550 μg peptide / mg QD for 130:1 MOG:QD, as well as direct tuning of surface display density. Using QDs as shuttles for self-peptides also opens a new dimension as a tool for autoimmune research, enabling visualization and tracking of therapeutic conjugates without photobleaching, additional probes, or dissociation of dyes from a carrier.

5.3.3 MOG-QDs drive efficient presentation of self-antigen to T cells without inflammation

To exploit the unique features of QDs for modulating immunity, we first investigated uptake and antigen processing of MOG-QDs using conjugates at the highest antigen density we characterized, 150:1 (**Figure 5.5**, **Figure 5.6**). DCs isolated from mouse spleens were incubated with MOG-QDs or co-cultured with MOG-QDs and transgenic T cells recognizing MOG when displayed by DCs (**Figure 5.7A**). As expected, flow cytometry analysis of DC cultures revealed efficient, dose-dependent uptake of QDs (**Figure 5.7B**, **Figure 5.8**), but these conjugates – lacking inflammatory signals – did not activate DCs, as indicated by the expression levels of CD40 (**Figure 5.7C**), CD86 (**Figure 5.7D**), and CD80 (**Figure 5.9**). This finding is important because many common polymeric carriers (e.g., poly(lactide-co-glycolide)) exhibit intrinsic features – such as charge or repetitive monomers – that can activate innate immune pathways and cause inflammation.[7] These outcomes could worsen disease in the context of autoimmunity.

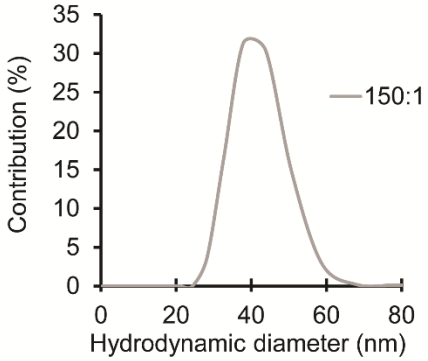

Figure 5.6: Size distribution of 150:1 MOG:QDs measured by DLS.

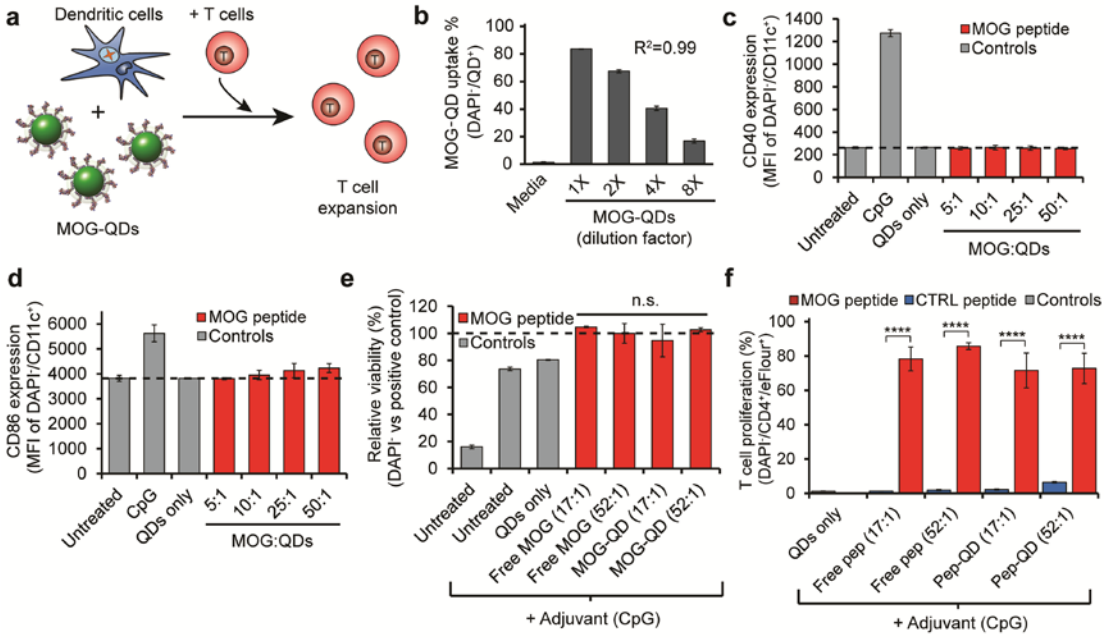

Figure 5.7: DCs can phagocytose MOG-QDs and process and present MOG to T cells. (**A**) DCs were incubated with MOG-QDs and transgenic 2D2 T cells that proliferate in response to MOG. (**B**) DC uptake of MOG-QDs was quantified by fluorescent intensity via flow cytometry. DC activation was measured by expression of (**C**) CD40 and (**D**) CD86 activation markers. (**E**) Viability was assessed by DAPI staining 72 h after cell treatment. (**F**) 2D2 T cell proliferation was quantified by proliferation dye dilution via flow cytometry. Data in (**B**)–(**F**) represent the mean (N = 3) ± s.d. Statistical significance was determined by one-way ANOVA with p-values ≤ 0.05 considered significant (****p < 0.0001; ns = not significant).

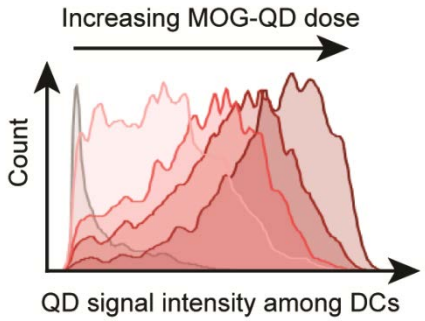

Figure 5.8: Representative histograms demonstrating DC uptake of MOG-QDs.

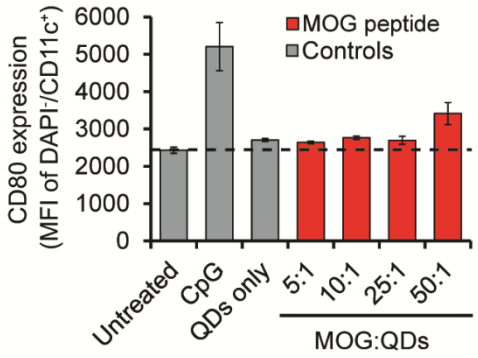

Figure 5.9: DC activation was measured by expression of CD80 activation marker.

We next tested if MOG displayed on QDs is processed and presented in a manner that is accessible to myelin-reactive $CD4^+$ T cells from 2D2 transgenic mice. When 2D2 T cells encounter MOG presented by DCs with the correct co-stimulatory signals, these cells proliferate. In these studies, DCs were incubated with a fixed number of QDs, but displaying different densities – either 17 or 52 peptides per QD – of MOG ligand or an irrelevant peptide ligand from OVA (CTRL). To drive co-stimulatory signaling, DCs were also treated with a common molecular adjuvant (CpG). DAPI staining was used to evaluate the effect of MOG-QD treatment on cell viability in co-cultures relative to treatment with free MOG (**Figure 5.7E**). This DNA binding stain enters leaky (i.e., damaged) cell membranes more efficiently than cells with intact membranes. Thus **Figure 5.7E** suggested MOG-QDs did not cause toxicity by this measure. During T cell co-culture, MOG-QDs caused high levels of proliferation, indicated by a dramatic dilution of signal from a fluorescence reporter as successive generations of T cells divided (**Figure 5.7F**, **Figure 5.10**). These levels were equivalent to values measured for free MOG, while neither CTRL-QDs nor free CTRL peptide caused proliferation (**Figure 5.7F**). This result demonstrates that conjugation of MOG to QDs does not

interfere with the ability of DCs to process and present peptides, and that these materials can support antigen-specific T cell proliferation. In mice and humans, naïve MOG-specific $CD4^+$ T cells have the capacity to develop into either inflammatory phenotypes (e.g., T_H1, T_H17) or T_{REGs}, depending on the form of antigen presentation (e.g., soluble vs. particulate) and the other signals encountered during T cell differentiation.[12, 233, 234] Thus, we next employed a common mouse model of MS to test if MOG-QDs traffic to tolerogenic domains of LNs and polarize T cells to promote tolerance as a function of the density of ligands displayed.

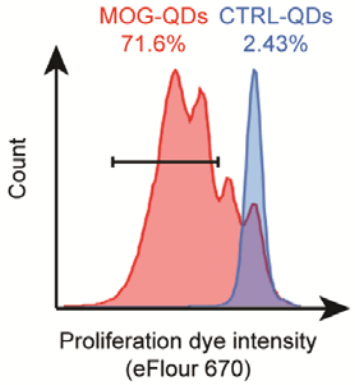

Figure 5.10: Histograms showing proliferation dye dilution representing generations of T cell proliferation in response to antigen recognition.

5.3.4 Draining lymph node imaging and analysis

We began by administering MOG-QDs to C57BL/6 mice by *s.c.* injection, then used fluorescence microscopy to assess lymphatic drainage. After 24 hours the draining and non-draining inguinal LNs (iLNs) were harvested, sectioned, and stained for common lymphocytes (B cells, B220; T cells, CD3). The draining iLN from injected mice exhibited striking levels of MOG-QDs in the medullary sinus (asterisk) and subcapsular sinuses (arrows), as well as less concentrated, widespread distribution in the T cell

zone/paracortex (**Figure 5.11A**). The non-draining iLN showed a miniscule, but detectable, level of MOG-QD fluorescence, while signal was absent in iLNs from untreated mice (**Figure 5.11A**). Flow cytometry confirmed these results, revealing high levels of MOG-QDs only in the draining iLNs (**Figure 5.11B,C**). Further, there was no difference in DAPI staining levels in the cells of tissues containing MOG-QDs compared to LNs of untreated mice (**Figure 5.11D**).

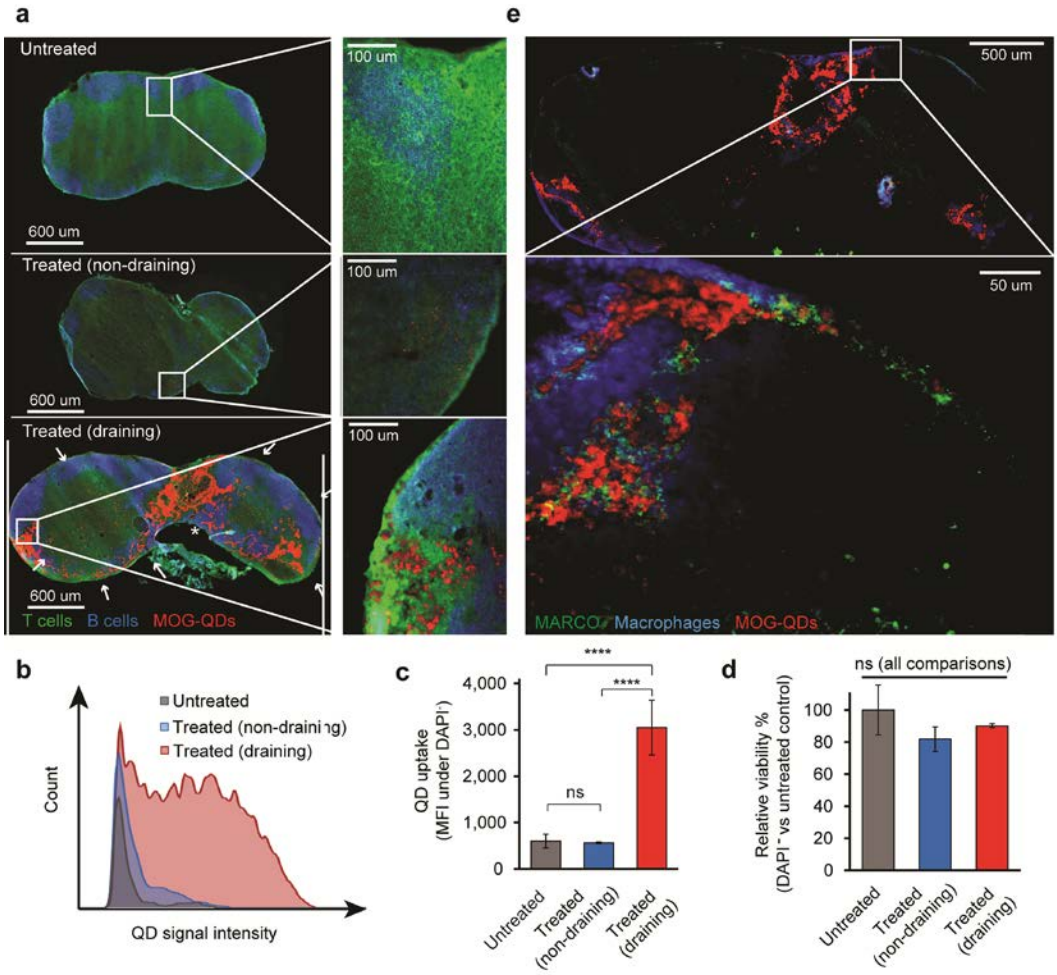

Figure 5.11: MOG-QDs drain to the iLN and induce tolerance in EAE. (**A**) iLNs were removed 24 h after MOG-QD injection, stained for T and B cells, and visualized by fluorescent microscopy. (**B,C**) MOG-QD signal in iLNs was quantified by flow cytometry. (**D**) Viability of the LNs following MOG-QD injection was assessed by DAPI staining. (**E**) iLN sections from this study were additionally stained for macrophage markers and the scavenger receptor MARCO. Data in (C) and (D) represent samples (N = 3) ± s.d., with statistical significance determined by one-way ANOVA with post-test corrections for multiple comparisons. p-values ≤ 0.05 were considered significant (****$p < 0.0001$; ns = not significant).

To determine if MOG-QDs might traffic to marginal zone macrophages and tolerance-inducing scavenger receptors, we stained iLNs for F4/80 and MARCO, respectively. Interestingly, MOG-QDs were frequently co-localized with both macrophages and MARCO throughout the iLN (**Figure 5.11E**). This co-localization was also observed among the low levels of QDs in non-draining iLN, while QD signal was absent in control iLNs from untreated mice (**Figure 5.12**). These experiments support an intriguing idea arising in the field, that altering the trafficking of self-antigen can promote tolerance by directing self-peptides to tissues and pathways (e.g., MARCO) already primed to generate regulatory responses, instead of inflammatory responses. Recent studies with large polymer NP or MPs conjugated with self-antigen reveal this conjugation leads to trafficking to macrophages expressing MARCO.[53, 54, 192] This discovery is supported by natural immune mechanisms that direct fragments from apoptotic cells to particular regulatory microdomains in LNs that help maintain tolerance against self-cells (e.g. recycling red blood cells).[259] Our findings demonstrate that MOG-QDs drain very efficiently through lymphatics, allowing direct visualization of co-localization with macrophages and scavenger receptors involved in apoptotic clearance and promotion of tolerance against antigens reaching these domains.[260]

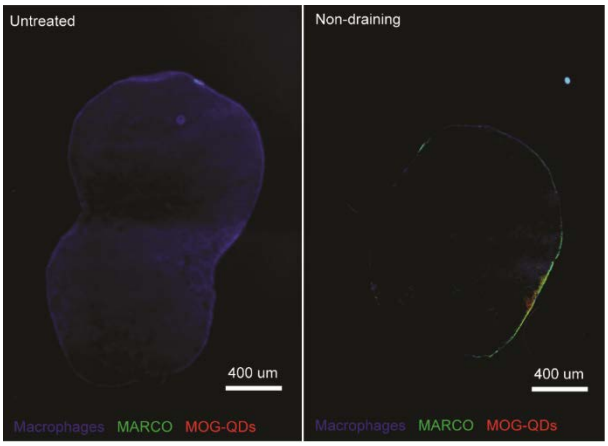

Figure 5.12: QD signal in an untreated and a non-draining LN. An untreated iLN shows positive staining for macrophages and minimally, the scavenger receptor MARCO. The non-draining iLN of a mouse treated with MOG-QDs shows a small amount of MOG-QD fluorescence that is colocalized with macrophages and MARCO.

5.3.5 MOG-QDs improve EAE, while QDs alone, MOG alone, or CTRL-QDs do not

To provide an initial indication of the therapeutic potential of MOG-QDs, we first induced mice with EAE, a myelin-driven model of MS that results in loss of motor function and development of total paralysis over 2-3 weeks.[183, 201, 261] Two days later, mice received a single *s.c.* injection of MOG-QDs or one of several control treatments: free MOG, CTRL-QDs, or QDs only (**Figure 5.13A**). The groups were then monitored daily for both paralysis and weight loss, a common symptom of disease. Paralysis was measured using a standard clinical disease scoring rubric in which increased clinical score corresponds to more severe paralysis. Compared with untreated mice and control groups receiving QDs only, free MOG, or CTRL-QDs, the MOG-QDs conferred a striking therapeutic effect on both disease progression (**Figure 5.13B**) and weight loss (**Figure 5.14**). For clarity, statistics are only shown comparing MOG-QDs against the untreated control group. Regardless of time point, however, none of the groups except MOG-QDs caused significant differences in clinical scores when

comparing treatments. Mice treated with MOG-QDs also exhibited substantially decreased disease incidence (**Figure 5.13C**). Further, there were no differences in disease incidence between untreated mice and those receiving the other treatments. Importantly, the lack of efficacy with the CTRL-QDs suggests MOG-QDs promote tolerance in a myelin-dependent manner. With clear indications of the role of each component, we sought to understand how the density of peptide displayed by QDs impacted T cell function, tolerance, and therapeutic effect.

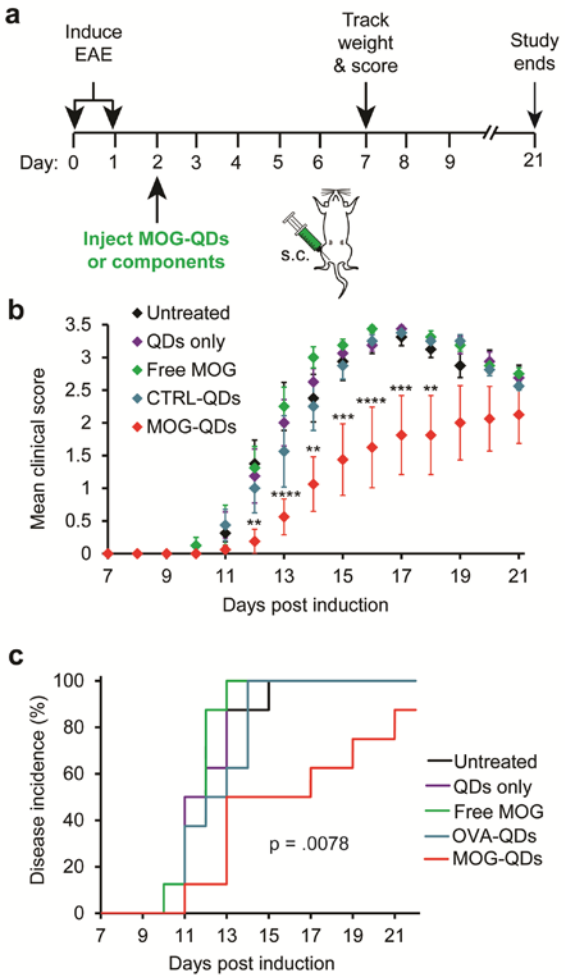

Figure 5.13: MOG-QDs decrease disease severity in EAE, but the individual components do not. (**A**) Mice were induced with EAE on days 0 and 1 and injected with MOG-QDs or component controls on day 2. (**B**) Disease progression was monitored by clinical score through day 21. (**C**) Disease onset was defined as the first day a mouse displayed symptoms. Incidence was tracked through day 21. Data in (B) represent samples (N = 8) ± s.e.m. p-values ≤ 0.05 were considered significant (**p < 0.01, ***p < 0.001, ****p < 0.0001).

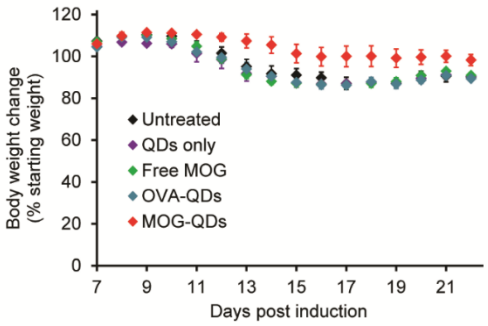

Figure 5.14: Body weight change was measured daily as an indicator of disease severity for mice receiving MOG-QDs or control treatments.

5.3.6 MOG-QDs control disease in a dose-dependent manner

We first investigated the role of MOG dose on the extent of tolerance induced by MOG-QD treatment. Mice were again induced with EAE and received an injection of MOG-QDs on day 2 (**Figure 5.15A**). While the mass of QD was fixed in these studies, two different MOG ligand densities, 17:1 and 52:1 (MOG:QD), were displayed on these QD, altering the dose of MOG while keeping the number of QDs constant. Compared with untreated mice, both MOG-QD treatments conferred therapeutic effects. Interestingly, the higher dose nearly eliminated disease-induced paralysis, as indicated by a markedly lower clinical score (**Figure 5.15B**), while the lower dose caused a significant, but lesser therapeutic effect. Relative to this lower dose, the higher MOG dose conferred efficacy that was statistically significant at several points during peak disease (e.g., day 17, day 19). The higher MOG dose (MOG-QD 52:1) also drove a 10-fold reduction in disease incidence – 1 out of 10 mice – compared to 100% incidence in untreated mice, and 40% incidence in mice treated with the lower MOG dose (MOG-QD 17:1) (**Figure 5.15C**). Compared to untreated mice, the incidences at the end of the study were significantly lower for both the 17:1 ($p<.01$) and 52:1 treatments

(p<.0001). At the peak of disease (day 17), untreated mice exhibited a mean clinical score of 3.0 (complete hind limb paralysis), while mice treated with QD formulations exhibited mean scores of 1.0 (loss of tail function) and 0.5 (limp tip of tail), for the low and high ligand densities, respectively (**Figure 5.15D**). MOG-QD treatment also significantly reduced weight loss (**Figure 5.16**).

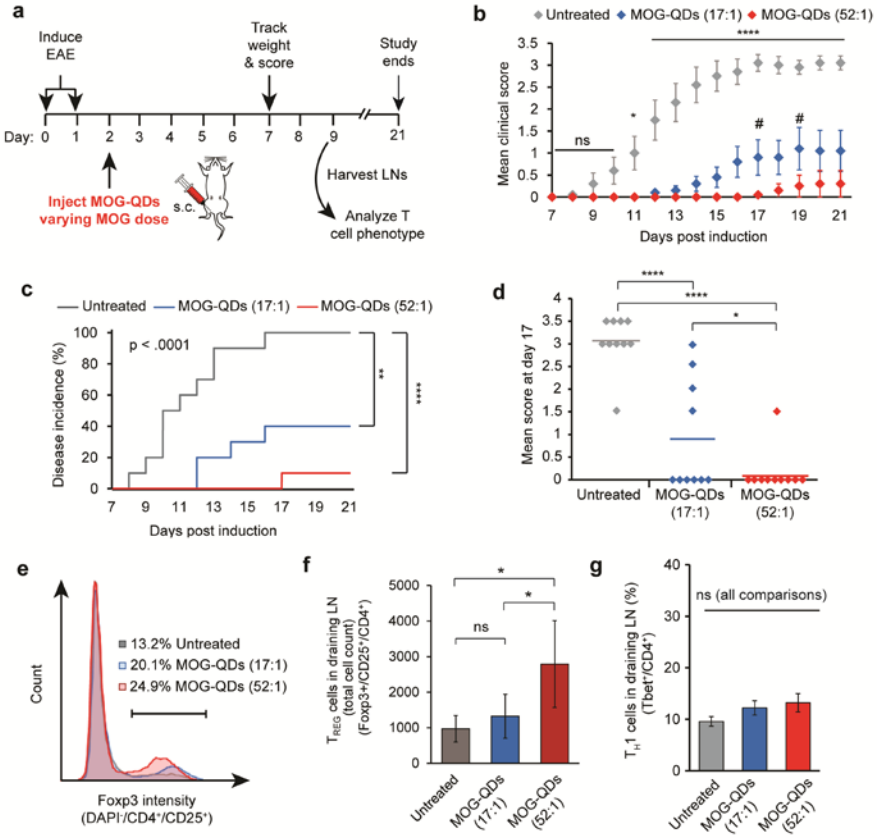

Figure 5.15: MOG-QD treatment expands T_{REGs} and increased MOG dose enhances tolerance. (**A**) Mice were induced with EAE and treated with MOG-QDs (17:1 or 52:1). (**B**) Mice were monitored daily using a standard clinical EAE scoring rubric, (**C**) where disease onset is the first day that symptoms arise. (**D**) At peak disease (day 17), mean score was compared between groups. In a separate similar experiment, the iLNs of mice were harvested to stain for (**E,F**) T_{REGs} and (**G**) the TH1 phenotype. Data in (B)–(D) represent the mean (N = 10) ± s.e.m. Data in (F) and (G) represent the mean (N = 5) ± s.d. Statistical significance for (B) was determined by two-way ANOVA with post-test corrections for multiple comparisons. For day 21 in (C), (D), (F), and (G), one-way ANOVA with post-test corrections for multiple comparisons was used. Log-rank tests were used in analysis of disease incidence in (C). For all tests, p-values ≤ 0.05 were considered significant (*p < 0.05, **p < 0.01, ****p < 0.0001; ns = not significant). In (B), all asterisks indicate statistical significance for comparisons of either MOG-QD treatment group against untreated mice. # indicates significance of p < 0.05 for comparisons of MOG-QD (17:1) against MOG-QD (52:1).

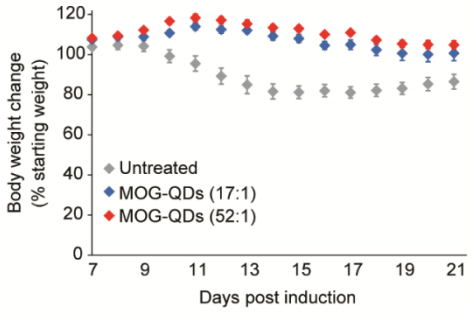

Figure 5.16: Body weight change was measured daily as an indicator of disease severity for mice receiving MOG-QDs treatments of 17:1 or 52:1.

5.3.7 MOG-QDs expand regulatory T cells without increasing inflammatory $T_H1$cells

We hypothesized that efficacy in controlling disease might result from MOG-QD driven expansion of T_{REGs} ($CD4^+/CD25^+/Foxp3^+$). Thus mice with EAE were treated with MOG-QDs (17:1 or 52:1) on day 2 as in **Figure 5a**, then iLNs were harvested and analyzed by flow cytometry on day 9. As hypothesized, MOG-QDs significantly expanded the number of T_{REGs} at the higher density, and caused an upward trend at the lower density (**Figure 5.15E,F**). Similar results were measured in the frequency of T_{REGs} (**Figure 5.17**). Since uncontrolled delivery of myelin peptides during autoimmunity could exacerbate disease,[12] we sought to confirm MOG-QDs do not expand inflammatory T_H1 cells (i.e., $Tbet^+$ among $CD4^+$ T cells). These studies revealed no significant increases in T_H1 populations between treated and untreated groups (**Figure 5.15G**).

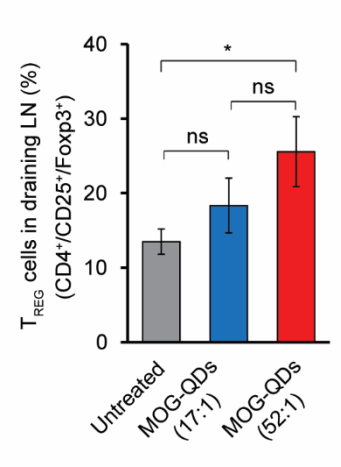

Figure 5.17: The percentage of T_{REG} cells in the draining LN was measured by flow cytometry as $Foxp3^+$ of $CD25^+$ of $CD4^+$ T cells.

5.3.8 Tolerance and efficacy during EAE correlates inversely with peptide display density

To directly investigate the role of ligand density, we next prepared MOG-QDs at three ligand densities, then injected groups of mice with EAE using constant masses of MOG, but displaying these doses on different numbers of QDs (i.e., fixed dose of MOG, varying number of QDs) (**Figure 5.18A**). Intriguingly, over the course of the study, mice receiving a 25:1 MOG:QD dose (i.e., the fewest number of peptides per QD) exhibited the lowest clinical scores, with scores increasingly in order for 52:1 and 65:1 (i.e., the greatest number of peptides per QD) (**Figure 5.18B**). These differences were statistically significant at several points, including the peak of disease (day 17). At this time, mice receiving 25:1 MOG:QDs exhibited a mean score 3-fold lower than mice treated with 65:1 MOG:QDs (**Figure 5.18C**). Additionally, mice injected with the lowest ligand density of MOG:QDs showed both delayed disease onset and lower incidence compared with all other groups (**Figure 5.18D**). An additional indicator of

EAE severity is body weight loss. For this metric, a similar trend to that measured for clinical score was observed, where mice treated with 25:1 MOG:QDs maintained the highest percentage of original body weight, and weight loss increased as the number of MOG peptides per QD increased (**Figure 5.18E**).

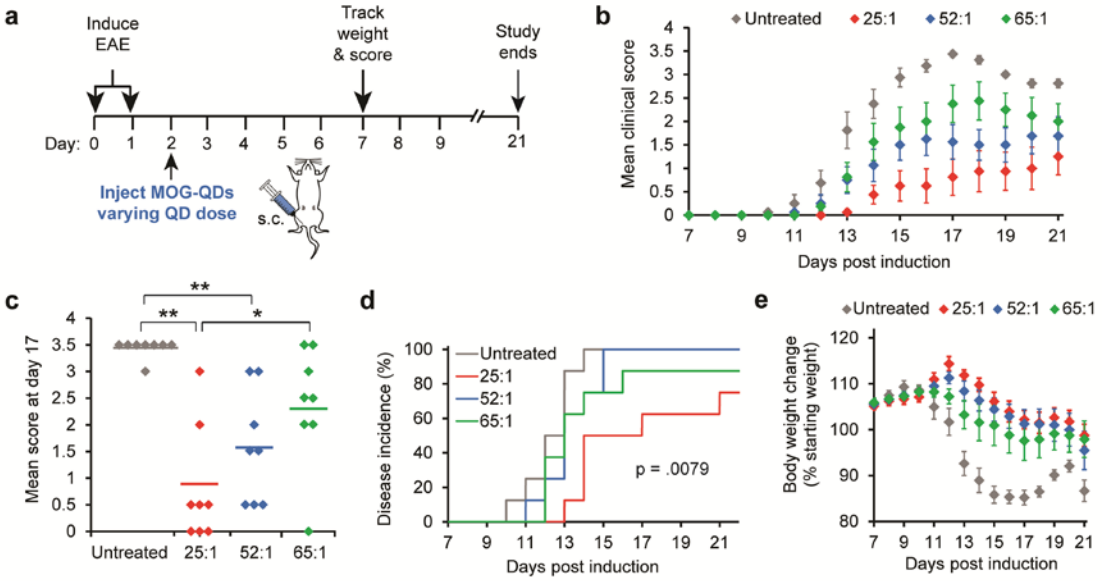

Figure 5.18: Tolerance is dependent on MOG ligand density. (**A**) Mice were induced with EAE on days 0 and 1, followed by treatment with MOG-QDs of varying QD dose on day 2. (**B**) Disease progression was again monitored by clinical score and (**C**) peak disease was compared at day 17. (**D**) Disease incidence was assessed by onset of symptoms and (**E**) body weight loss was tracked through day 21. Data in (B)–(E) represent the mean (N = 5) ± s.e.m. Statistical significance for (C) was determined by one-way ANOVA with post-test corrections for multiple comparisons and log-rank tests were used in (D). For all tests, p-values ≤ 0.05 were considered significant (*p < 0.05, **p < 0.01).

Because most therapies for MS and other autoimmune diseases are broadly suppressive, there is intense research to generating more selective therapies. The immune system offers this potential, and the control biomaterials could provide toward this goal has spurred great interest at this interface. However, fundamental questions, such as what delivery kinetics, combinations and densities of cargos, and tissues to

target are just arising.[62] Thus, in addition to the specific innovation using QDs to tune tolerance – and the potential for future theranostic applications, our work adds a fundamental discovery to the field: that a higher number of tolerogenic particles displaying lower levels of self-peptide is more effective for inducing tolerance than fewer particles displaying high densities of peptide. This finding provides guidance for future strategies that a large number of low-density/dose events may lead to more effective control of autoimmune or inflammatory reactions then larger doses distributed among fewer particles or carriers.

5.4 Conclusions

Our studies show for the first time that QDs can be harnessed to promote tolerance by designing peptide-QD displaying self-antigen at tunable densities. Importantly, the extent of efficacy is directly linked to the density of peptide ligands on the QD, with lower levels of self-antigen displayed on a larger number of QDs driving the most efficient tolerance. Since LNs, spleens, and other immune tissues integrate local signals across the body, this finding may reflect a mechanism achieved by providing a large number of therapeutic events, even if each QD only displays a low level of the self-antigen. These outcomes, along with the antigen-specific expansion of myelin-reactive T cells in co-culture studies – and the lack of efficacy using CTRL-QDs - suggest that the tolerance generated by MOG-QDs is myelin-specific. Since we observed strong local expansion of T_{REGs} in LNs, a possible mechanism for tolerance is the migration of these cells to the CNS to control inflammatory T_H17 and T_H1 cells.[12, 17, 19] Mechanistic studies will need to confirm the myelin-specific nature of tolerance, and

test if this approach can be used to reverse paralysis once disease is already established. However, our current findings support QDs as a powerful experimental tool to track vaccine-like autoimmune therapies through the lymphatic system while simultaneously promoting tolerance with tunable control. Such features could enable approaches that provide new insight into how immune cells migrate or are sequestered to tolerogenic agents, and to precisely tune the level of tolerance needed for a particular autoimmune disease while minimizing the dose or level of immune modulation needed for efficacy.

This chapter has demonstrated that parameters of self-antigen display (i.e. ligand dose and density) directly impact tolerance induction, including the development of T_{REGs}. **Chapter 6** dives further into this topic, seeking to answer questions that address the gap in knowledge about particle parameters necessary for inducing tolerance. The studies below assess how one parameter shown to have an effect on tolerance (i.e. self-peptide density) impacts draining to different LNs and how particle accumulation impacts cell infiltration, migration, or proliferation.

Chapter 6: Quantum dots as a tool for defining parameters of tolerance induction strategies

6.1 Introduction

Vaccines work by generating an extremely specific immune response against foreign antigens that leads to destruction of pathogens of infected cells without impacting host cells. Therapeutic vaccines aim to provide the same selectivity to generate tolerance rather than inflammation towards self-antigens attacked in autoimmunity, eliminating the broad suppression hindering current therapies. Biomaterials can improve the design of therapies directed at autoimmune diseases because of desirable features such as targeted delivery, encapsulation of multiple signals, and protection from degradation. The field currently lacks fundamental insight into the design parameters necessary for the use biomaterials-based technologies to promote immunological tolerance.[64] There are two approaches towards this goal that have emerged in the literature: 1) delivering the self-antigen attacked in an autoimmune disease along with a regulatory immune signal to change the way the immune system responds to it, or 2) delivering a particle loaded with the self-antigen alone to alter the way it is taken up and processed by immune cells.[170, 262] The second strategy is based on results showing that particle-based delivery of self-antigen may promote accumulation in domains of the LNs that are implicated in tolerance.[50-54] Design parameters, such as self-peptide ligand density, can control the balance between tolerance and inflammation, but have not yet been investigated. In this work we used QDs exhibiting intrinsic fluorescence

and functionalized with tunable densities of self-antigen as tools to generate this new insight.

As mentioned, the LN domains in which NPs accumulate are important in the type of immune response that is generated. APCs present antigens to T and B cells in specific microdomains that allow interactions between immune cells and promote immunity or tolerance.[3, 263] For example, recent reports have shown that naïve T cells migrate to specific microdomains where they interact with DCs that promote T_{REGs}.[259, 264, 265] Additionally, the structure of LNs changes when a response is being generated. In a resting state (i.e., no vaccination or infection), there are distinct T and B cell zones (**Figure 6.1A**). When antigen and adjuvant activate LNs, they reorganize to promote intermingling of T and B cells (**Figure 6.1B**). By comparison, the ER-TR7 network created by fibroblastic reticular cells expands during tolerance and laminin α4 increases, while laminin α5 decreases (**Figure 6.2**).[259] The converse is true in a state of inflammation.

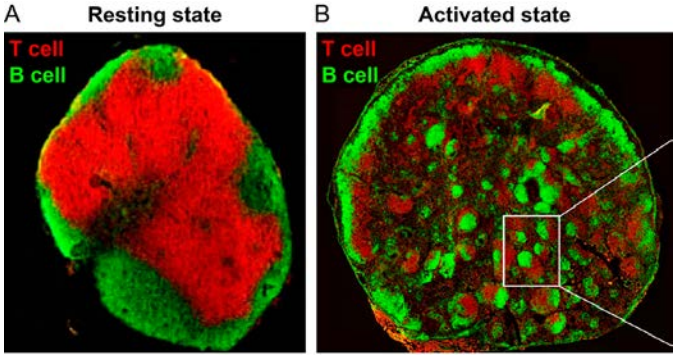

Figure 6.1: LNs reorganize during the generation of an immune response. A) Separate T and B cells zones are visible in resting state. **B**) Following delivery of antigen and a strong adjuvant, the LN reorganizes to promote T and B cell intermingling. Adapted with permission from.[266]

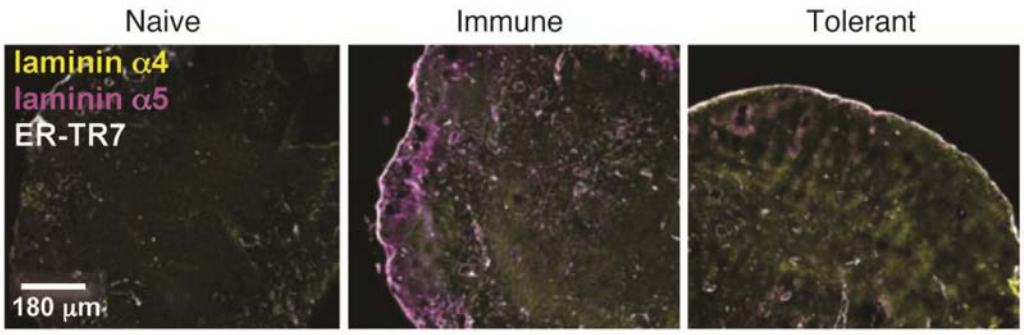

Figure 6.2 Laminins are differentially expressed in states of tolerance versus inflammation. Laminin α4 staining is enhanced in cortical ridge of tolerant LNs compared naive or inflammatory LNs. Reprinted with permission from [259].

The formations of specialized domains that promote immunity or tolerance require immune signals to reach LNs, and the type of response that develops is dependent on the balance of these signals. In particular, an initial step in the immune cascade involves phagocytosis of an antigen by a DC which then processes it and presents it on the cell surface. If the DC also encounters an adjuvant or a danger signal, activation markers are upregulated. When a naïve T cell interacts with a DC presenting both signals, it will polarize towards an inflammatory phenotype. If, however, the T cell only encounters antigen with no costimulatory molecules, polarization towards a regulatory phenotype may occur.[267] This is the case when DCs present self-antigen and immunological tolerance is functioning properly. QDs allow precise control over self-antigen display, enabling isolation of how number, density, and sequence of self-peptide impact NM trafficking, APC interactions, and subsequent T cell polarization.

As mentioned, the autoimmune response in MS is complex, being carried out by innate immune cells, myelin-reactive $CD4^+$ and $CD8^+$ T cells, and even antibodies secreted by B cells.[17, 18] These cells first develop in LNs where signals are presented, and

then migrate to the CNS where myelin-based antigens are located.[19-21] The ultra-small size of QDs allows rapid drainage to LNs, allowing an opportunity to generate T_{REGs} in LNs that migrate out and control self-reactive cells. The specific design features necessary for the induction of immunological tolerance, however, remain unknown. The already mentioned advantageous properties of QDs, along with the intrinsic fluorescence that allows tracking, make them a useful tool to probe how materials displaying self-antigen interact with immune cells, drive LN reorganization, and promote the generation T_{REGs}. The following work explores the biodistribution of myelin peptide-decorated QDs in LNs, and the effect of the particles on immune cell trafficking and function within these tissues.

6.2 Materials and Methods

6.2.1 Materials

MOG_{35-55} peptide (HHHHHSAAAAAGMEVGWYRSPFSRVVHLYRNGK, denoted "MOG" in the text) and a control peptide from OVA (HHHHHSAAAAAGISQAVHAAHAEINEAGR; denoted "CTRL" in text), both modified for optimal attachment to QDs, were synthesized by New England Peptide (Gardner, MA) and Genscript (Piscataway, NJ), respectively. OPC oligonucleotide purification cartridges, RPMI-1640 media, L-Glutamine, Penicillin-Streptomycin, and 4',6-diamidino-2-phenylindole (DAPI) were supplied by Thermo Fisher Scientific (Grand Island, NY). Fetal bovine serum (FBS) was purchased from Corning (Tewksbury, MA). Bovine serum albumin (BSA) and 2-Mercaptoethanol were from

Sigma Aldrich (St. Louis, MO). Molecular Biology Grade Water, HEPES, non-essential amino acids, and 40 μm cell strainers were supplied by VWR (Radnor, PA). Spleen Dissociation Medium and CD4 negative selection kits were purchased from STEMCELL Technologies (Vancouver, British Columbia, Canada). CD11c microbeads were supplied by Miltenyi Biotec (Cambridge, MA). Fluorescent antibody conjugates for flow cytometry were purchased from BD (San Jose, CA). EAE induction kits were synthesized by Hooke Laboratories (Lawrence, MA).

6.2.2 Cells and animals

Female C57BL/6 mice (9-12 weeks, stock #000664) were used for all experiments. All animals were cared for in compliance with Federal, State, and local guidelines, and using protocols reviewed and approved by the University of Maryland's Institutional Animal Care and Use Committee (IACUC).

6.2.3 Assembly of peptide-QDs

Synthesis of 625 nm emitting QDs and cap-exchange with CL4 ligands have been previously described.[246] Both MOG and CTRL peptides were desalted prior to QD conjugation as described in previous works.[247] Briefly, an oligonucleotide purification cartridge is charged prior to use with acetonitrile (MeCN) and triethylamine acetate (TEAA). Peptide is then pushed through the charged cartridge approximately 20 times, and is finally eluted by MeCN. The eluted peptide solution is

then lyophilized. QDs are decorated with peptide by mixing defined ratios of solutions of desalted peptide in molecular biology grade water with QDs.

6.2.4 LN harvesting and cell staining

Mice were injected with peptide-decorated QDs *s.c.* on the "left" side of the tailbase. Inguinal, axillary, and brachial LNs were then harvested from the mice at pre-determined time points post injection (*p.i.*). LNs were mashed through a 40 μm strainer to create a single cell suspension in buffer (1% BSA in 1X PBS). Cells were then incubated in Fc block for 10 minutes. When analyzing tissue composition, cells were incubated with fluorescent antibody conjugates for CD3e, B220, F4/80, CD11c, and CD11b for 20 minutes. To analyze DC activation, cells were incubated with fluorescent antibody conjugates for CD40, CD80, and CD86 for 20 minutes. For the T cell phenotype panel, cells were incubated for 30 minutes with fluorescent antibody conjugates for extracellular markers CD4 and CD25. Cells were then fixed and permeabilized for 2 hours prior to overnight incubation with fluorescent antibody conjugates for intracellular transcription factors Tbet, RORγt, and Foxp3. Cells from any of the described staining panels were then washed with buffer prior to analysis. Cells were examined by flow cytometry on a FACS CANTO II and data were analyzed with FlowJo v.10.

6.2.5 Tissue staining and imaging

QD signal in harvested LNs could be directly visualized under brightfield with a dissection microscope. Additional LNs were frozen in optimal cutting temperature compound by dry ice, sectioned at 6 µm on a cryostat, and fixed for staining with ice-cold acetone. In one analysis, sections were stained with primary antibodies for T cells (CD3e), B cells (B220), and fibroblasts (ER-TR7). In another panel, sections were stained with primary antibodies against DCs (CD11c), macrophages (F4/80), and the scavenger receptor MARCO. Secondary antibodies labelled with FITC, APC, and DAPI were then added for imaging purposes. LN sections were visualized by fluorescent microscopy and ImageJ was used for image processing and analysis. All images in a particular study were analyzed in an identical manner that was applied to the entire image area.

6.2.6 EAE induction and monitoring

Mice were induced with EAE following a protocol from Hooke Labs. On day 0, mice are injected *s.c.* at the upper and lower back with an emulsion of MOG and complete Freund's adjuvant (CFA). Pertussis toxin (PTX) is then administered *i.p.* 2 and 24 hours after the MOG/CFA injections. To monitor disease progression, mice are weighed to detect changes from initial body weight (a symptom of disease) and severity of paralysis is scored. Clinical score is defined by: 0 – no symptoms, 1 – limp tail, 2 – weakness of hind legs, 3 – hind limb paralysis, 4 – partial front limb paralysis, 5 – moribund.[53, 183, 201] Disease incidence is defined as the first day a mouse displays the described symptoms.

6.2.7 Statistics

One-way ANOVA with a Tukey post-test was used to compare three or more groups. P values ≤ 0.05 were considered significant. For all figures, *p < 0.05, **p < 0.01, ***p < 0.001, ****p < 0.0001, $^{\#}$p < .05.

6.3 Results and Discussion

6.3.1 MOG-QD accumulation in LNs results in a visible color change

We were first interested in assessing the biodistribution of self-antigen-decorated particles. Results from our previous studies indicated that the level of tolerance induced by QD treatment is inversely correlated with ligand density.[52] In the mouse model of MS, EAE, all mice were treated with the same dose of MOG peptide but spread out over varying numbers of QDs. Interestingly, when MOG density was the lowest, disease severity was also the lowest. We therefore wanted to study differences in biodistribution due to peptide ligand density. We began by injecting MOG-QDs, *s.c.* at tailbase of naïve C57BL/6 female mice, comparing the ratios 25:1, 52:1, and 65:1. After four days, three sets of LNs were harvested from the mice: left and right inguinal, left and right axillary, and left and right brachial (**Figure 6.3**).

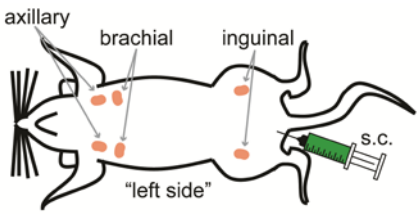

Figure 6.3: Schematic showing MOG-QD injection site and harvest LNs. In biodistribution studies, MOG-QDs were injected *s.c.* on the left side of the tailbase. Three sets of LNs were harvested at various time points *p.i.* including inguinal, axillary, and brachial.

When LNs are removed from naïve, untreated mice, they appear translucent (**representative images appear in Figure 6.4**). In mice that had been treated, the LNs were visibly orange, indicating the presence of MOG-QDs. The treatment with the lowest ligand density had the highest mass of QDs and accordingly, the left inguinal LN from mice that were treated with 25:1 MOG:QDs were brighter than those injected with 65:1 MOG:QDs. In these experiments, the dose of MOG was kept constant but varied over different numbers of QDs. As seen in **Figure 6.3**, the left inguinal LN is closest to the injection site and is therefore referred to as the "draining" LN. We expected that particles would first accumulate in the draining LN before travelling into other LNs, and accordingly, the signal in left inguinal LNs appeared brightest. It is interesting to note that some of the "non-draining" LNs (e.g. left axillary, right inguinal) from mice receiving the highest QD dose (i.e., 25:1) also appeared visibly brighter than those that were injected with a lower QD dose. This could be an important consideration when designing therapeutics for diseases that occur at one site or those that are system-wide. For example, a recent study revealed that a cocktail of OVA-decorated and CpG-decorated AuNPs largely accumulated in liver-draining LNs after infection.[121] The authors therefore applied to platform to a liver infection, a model that requires a local immune response, rather than a system one. Conversely, in cancer, it may be desirable for particles to reach LNs throughout the body in order to mount an immune response against both the primary tumor and metastases.

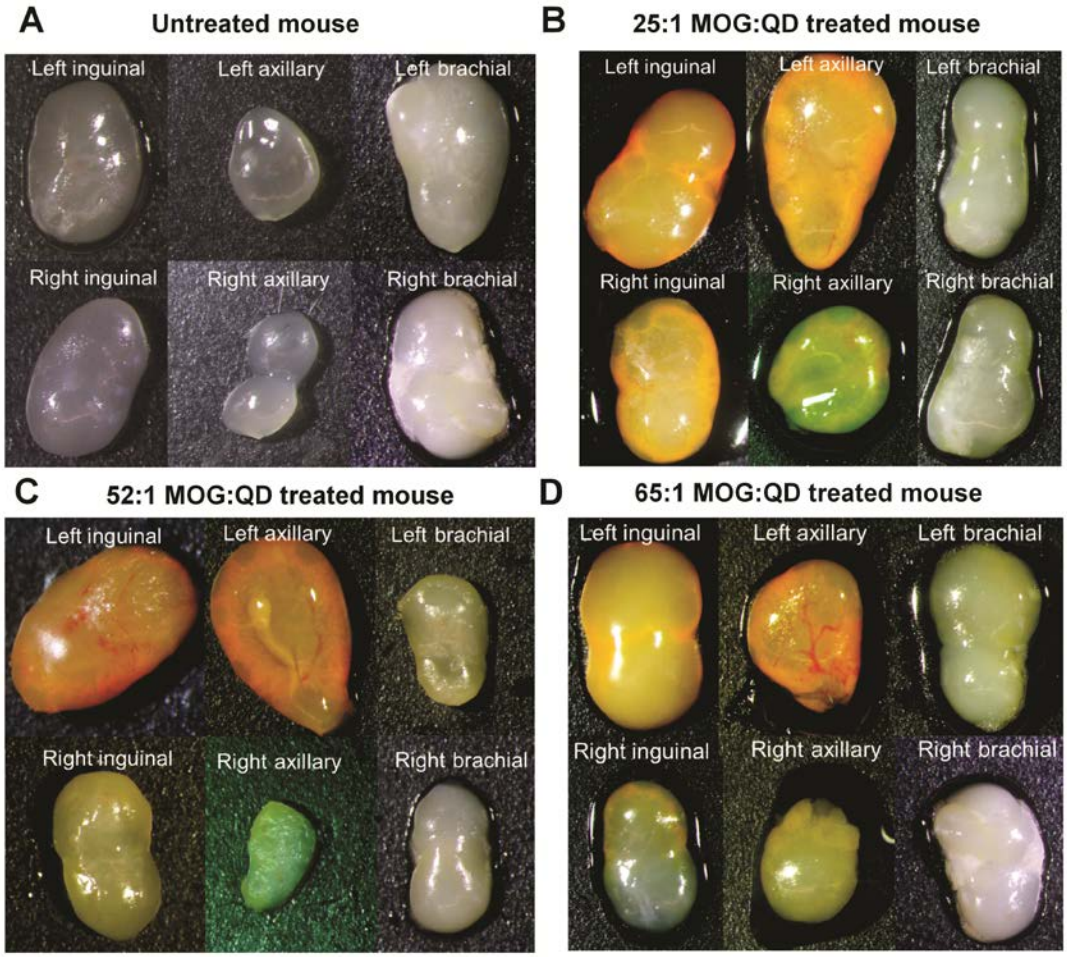

Figure 6.4 Accumulation of MOG-QDs in LNs causes a visible color change in the tissue. LNs from untreated mice appear translucent when imaged with a dissection microscope (**A**). LNs rom MOG-QD treated mice were harvested 4 days *p.i.* appear a brighter color orange as dose increases from 65:1 (**D**) to 52:1 (**C**) to 25:1 (**B**).

6.3.2 MOG-QDs drain to and persist in LNs for at least one week

As the images discussed in the previous section are qualitative, we next sought more quantitative results. We began by injecting naïve mice with the same MOG-QD dose (25:1, 52:1, and 65:1). At time points 1 day, 3 days, 5 days, and 7 days *p.i.* we harvested the LNs for analysis of QD signal. We next created a single cell suspension from the tissues for analysis with a flow cytometer. When broadly looking at all cells within the

draining left inguinal LN, signal was detectable after just 24 hours, and peaked 3 days after treatment (**Figure 6.5A**). Interestingly, despite the visible changes in **Figure 6.4**, there were no significant differences between groups at any time point. It is important to remember that these mice were healthy, and that differences between groups may be seen in a diseased state where MOG is presented in LNs.

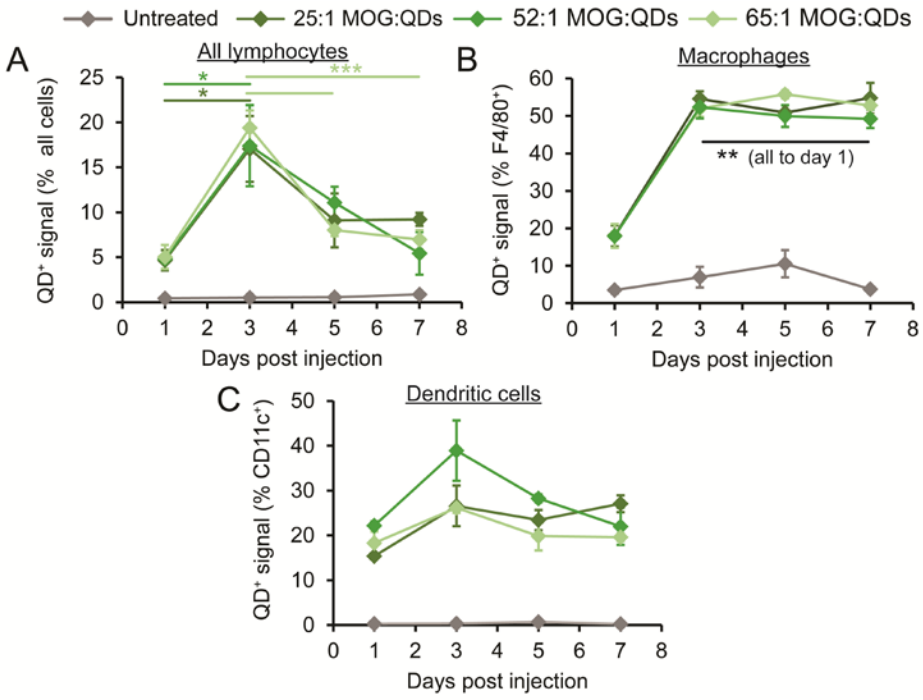

Figure 6.5 Robust and sustained MOG-QD signal is measurable for at least one week after injection. QD signal was measured by flow cytometry in left inguinal LNs at days 1, 3, 5, and 7 *p.i.* in all lymphocytes (**A**), macrophages ($F480^+$, **B**), and DCs ($CD11c^+$, **C**). Comparisons were made between time points for each group: *p < 0.05, **p < 0.01, ***p < 0.001.

It is also important to understand the types of cells that both take up QDs near the injection site and bring them to LNs or cells that phagocytose the particles once they accumulate in the LN. Two important cell types that can perform these functions are macrophages and DCs. At the initial time points, the profile of macrophage uptake in the left inguinal LNs looked similar to that in **Figure 6.5A**, with a large increase (from

below 20% to over 50%) of macrophages positive for QD signal between days 1 and 3 (**Figure 6.5B**). After this, however, signal was much more sustained for up to 7 days *p.i.* There were again no significant differences between the groups receiving MOG-QDs at different peptide ligand densities. We hypothesize that differences due to self-peptide ligand density may only be seen in mice that have been induced with an autoimmune disease. Another important type of APC, DCs, engulfed MOG-QDs in just 24 hours (**Figure 6.5C**). Like the overall signal in lymphocytes, QD signal in DCs in the draining LNs peaked 3 days *p.i.* Presentation of antigen by APCs to T cells can result inflammatory or regulatory polarization. Further analysis into the specific phenotypes of cells that take up MOG-QDs must be performed in order to predict what type of response will develop. For example, macrophages expressing the MARCO receptor are known to be tolerogenic as they are involved in the clearance of apoptotic cell debris.[53]

At the same time points mentioned above, LNs from the 25:1 MOG:QD treatment group were sectioned, fixed, and imaged on a fluorescent microscope. Strong QD signal was visible in both the left inguinal and left axillary LNs of treated mice 24 hours after injection (**Figure 6.6**). In both of these tissues, the signal then waned through day 7 when it became barely detectable. In contrast, a low level of QD signal was visible in the right inguinal LN one day *p.i.* that increased and peaked at day 5. In the right axillary LN, QD signal was almost imperceptible by fluorescent microscopy. These results were compared to the quantitative results of flow cytometry, which confirmed a very low level of uptake in the lymphocytes of the right axillary LN of 25:1 MOG:QD

treated mice (**Figure 6.7**). The increase in signal up seen up to day 5 in images of the right inguinal LN was also confirmed by flow cytometry. The images in **Figure 6.6** suggest that QD accumulation on the injection side ("left") is highest at day 1 *p.i.* and signal persists in the left axillary LN longer than in the left inguinal LN. The profiles seen in **Figure 6.7** suggest a similar trend, but with a peak at day 3. This difference may be due to the quantitative nature of microscopic analysis. In particular, each image represents only a 6 μm section of the tissue. Understanding the dynamic nature of particle biodistribution is important to the rational design of immunotherapies. The innate and adaptive immune responses occur over a precise number of days, making the time it takes for a "vaccine-like" treatment to reach various SLOs critical.[2]

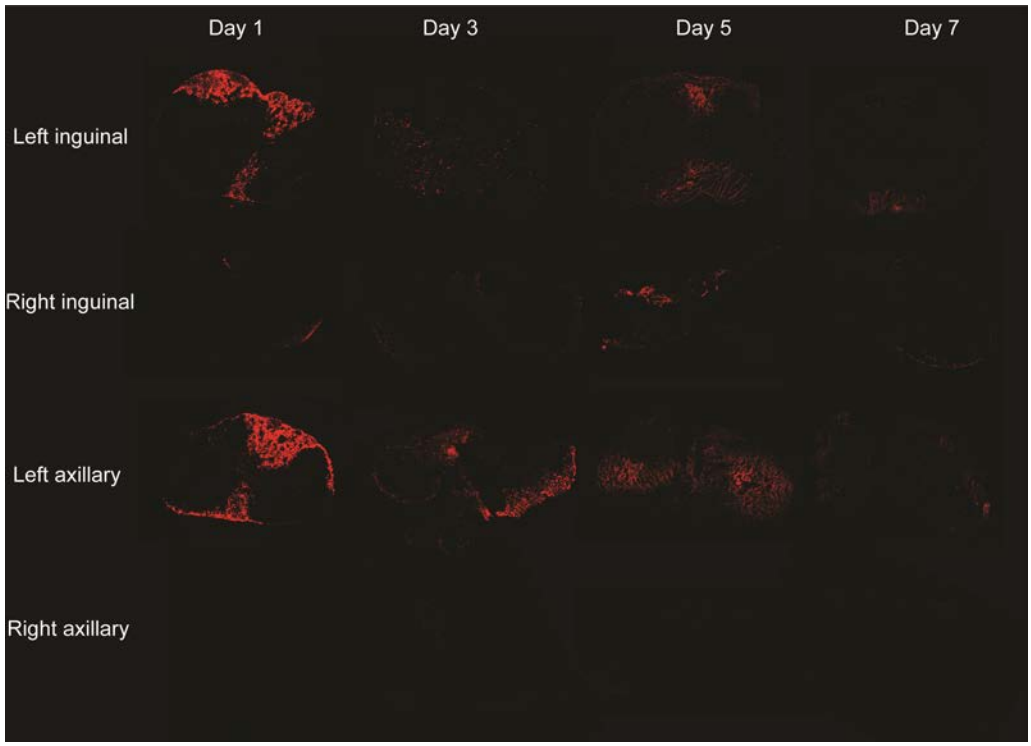

Figure 6.6: MOG-QD signal can be visualized in LN sections by fluorescent microscopy. LNs were removed at days 1, 3, 5, and 7 after MOG-QD injection, sectioned, and visualized by fluorescent microscopy.

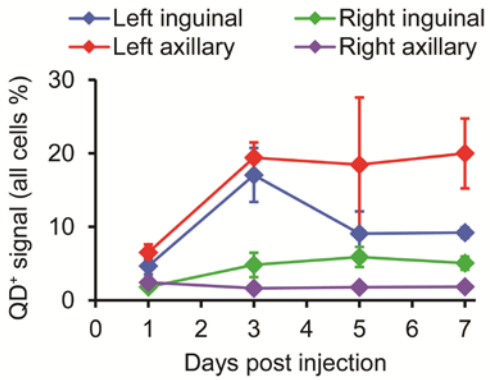

Figure 6.7: Biodistribution of MOG-QDs through the inguinal and axillary LNs of treated mice can be assessed over one week by flow cytometry. LNs were harvested days 1, 3, 5, and 7 *p.i.* and QD signal in all lymphocytes was quantified by flow cytometry.

6.3.3 MOG-QDs alter tissue composition of LNs they accumulate in

Of equal importance to understanding the biodistribution of particulate based immunotherapeutics, is the effect imparted on the tissues they accumulate in. As mentioned earlier, the autoreactive response characteristic of MS involves complex interactions of T cells, B cells, and innate immune cells (including APCs). The influx and efflux of cells to/from the LNs due to particle accumulation are therefore of great interest when designing immunotherapies for MS. Using the same experimental setup as before, we injected naïve mice with QDs displaying varying densities of MOG and examined the effect on frequency of T cells, B cells, macrophages, and dendritic cells in LNs. 24 hours after injection, there was little to no change in the percentage of any cell type compared to untreated mice in the left inguinal LNs (**Figure 6.8**). By day 3, there was a significant drop in T cell frequency (**Figure 6.8A**) that seemed to be mirrored by a large increase in B cell frequency (**Figure 6.8B**). Like with the QD uptake experiments, there were no significant differences between the treatment

groups. We hypothesize that this is due to the naïve state of the mice, but differences may be seen when mice are induced with EAE. These experiments will set up an important baseline for comparison to diseased mice. There was also a sharp peak in the frequency of macrophages at day 3 in the left inguinal. Interestingly, this directly correlates with the peak in overall QD signal seen by flow cytometry measurement. DCs followed a different frequency profile, with a peak after 5 days. There are many reasons cell frequency in LNs may change, including proliferation, inward migration of cells carrying antigen, or outward migration of effector cells.

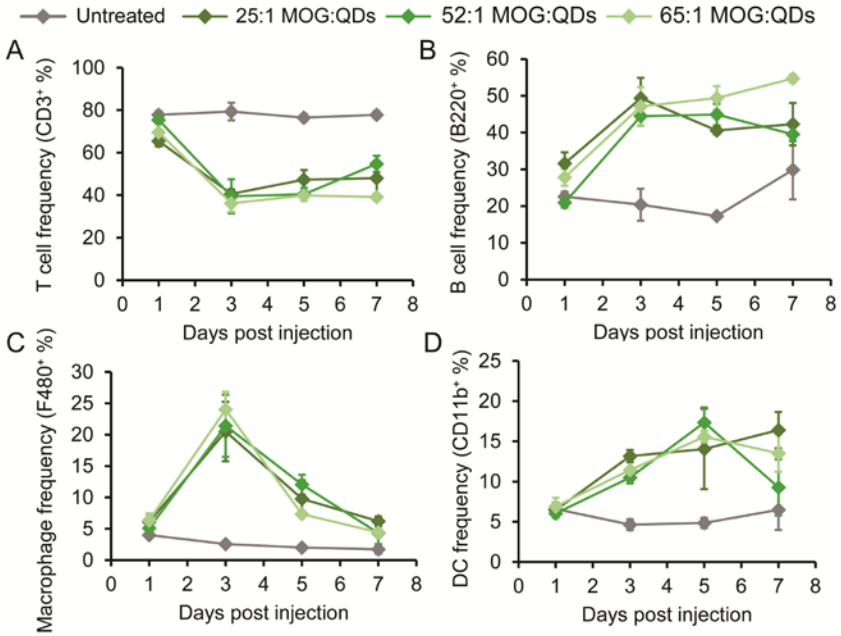

Figure 6.8: MOG-QDs alter the frequencies of specific immune cells in LNs. The left inguinal LNs of MOG-QD treated mice were harvested days 1, 3, 5, and 7 *p.i.* and the percentages of T cells ($CD3^+$, **A**), B cells ($B220^+$, **B**), macrophages ($F480^+$, **C**), and DCs ($CD11c^+$, **D**) were quantified by flow cytometry.

One method to further probe this question involves labelling cells of interest for tracking or monitoring proliferation. In one experiment we injected three treatments

groups: 25:1 MOG:QDs, 52:1 MOG:QDs, and 52:1 CTRL:QDs. The next day, $CD4^+$ T cells were isolated from transgenic 2D2 mice. These cells have receptors specific for MOG and will proliferate in response to MOG being presented by APCs. The T cells were then labelled with a dye that splits evenly between daughter cells during proliferation, and injected into the QD treated mice. After 72 hours, the LNs were harvested and analyzed by flow cytometry for the presence of labelled T cells. The LNs of mice that had been treated with MOG-QDs showed multiple generations of 2D2 T cell proliferation, indicating that they had interacted with MOG (Figure 6.9). The response was quantified, which revealed that in all LNs, except the left axillary, mice treated with 25:1 MOG:QDs showed a higher level of MOG-reactive T cell proliferation that 52:1 MOG:QDs (Figure 6.10). This is especially interesting because these groups received the same dose of MOG, but in the 25:1 treatment, the self-peptide was spread out over a larger number of QDs. This could indicate that T cell recognition of antigens is enhanced when more antigen-coated particles are available to be taken up by APCs. Importantly, the LNs of mice that had been treated with CTRL:QDs did not show any T cell proliferation, meaning that the recognized MOG was from particle treatment, rather than the myelin of the naïve mouse. It is important however, to determine the phenotype of the proliferated T cells to assess whether the response will skew towards inflammation or tolerance. As these studies were carried out in naïve mice, it will also be important to repeat the experiments in mice with EAE.

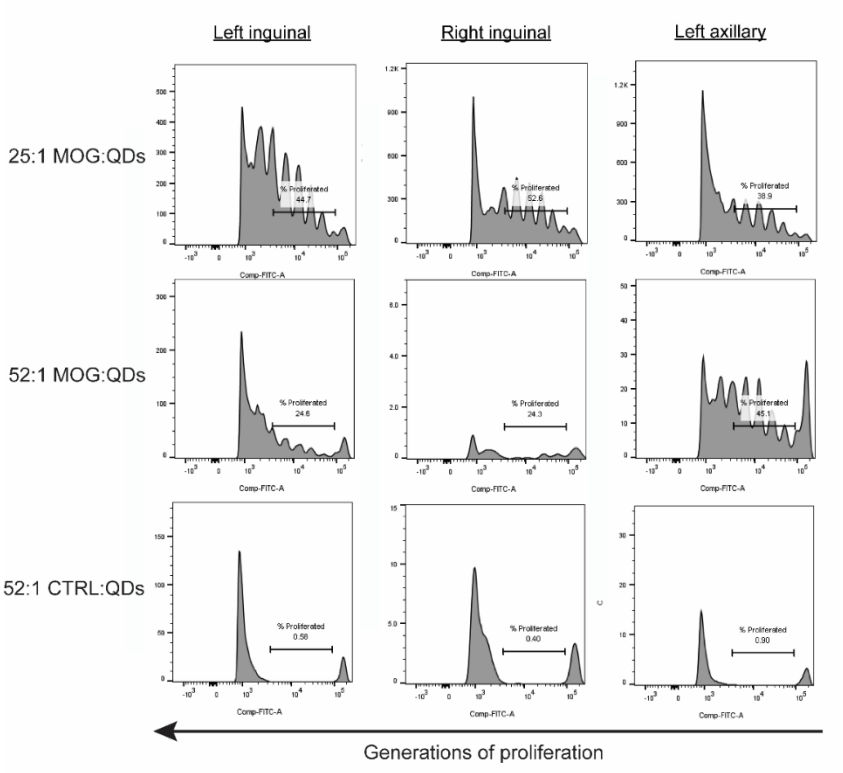

Figure 6.9: Multiple generations of T cells proliferate in LNs in response to MOG-QD treatment. Mice were injected with peptide-coated QDs and 24 hours later with 2D2 T cells containing a dye used to assess proliferation by dilution of the dye between daughter cells. After 3 days, LNs were harvested for analysis of proliferation dye signal by flow cytometry, with each peak indicated a generation of proliferation.

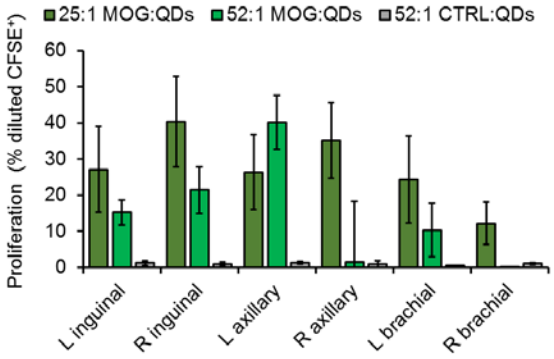

Figure 6.10: Increasing proliferation of MOG-specific T cells is correlated with decreasing self-peptide ligand density. Mice were injected with peptide-coated QDs and 2D2 T cells containing proliferation dye. After 3 days, T cell proliferation in LNs was quantified by flow cytometry.

6.4 Conclusions

Our studies provide fundamental new knowledge about the design of particulate carriers of immune signals. QDs allow the conjugation of a large and controllable amount of self-peptide, which proves advantageous for isolating the effects of dose and ligand density. Additionally, QDs are intrinsically fluorescent, allowing tracking of biodistribution. We have demonstrated that MOG-QDs rapidly drain to LNs on the injection side and can persist for up to one week. The particles are taken up by APCs, recruit additional APCs to the site, and even alter the frequencies of T and B cells in the LN. Many important studies still need to be carried out, including answering these same questions in a disease state, and analyzing the specific phenotypes of cells that develop. These future experiments are outlined in **Chapter 7**.

Chapter 7: Conclusions and Future Work

7.1 Outlook

The work completed in this dissertation describes two distinct platforms for inducing immunological tolerance. **Chapter 4** discussed the design of carrier-free polyplexes composed entirely of immune signals as a strategy to combat autoimmunity in EAE. This system allows the effects of the signals to be isolated without being impacted by a potentially immunogenic carrier. The platform is simple and modular, allowing for many different immune signals to be swapped in, meaning it can be applied to other autoimmune disease models or even to promote an inflammatory response. **Chapters 5 and 6** described QDs delivering self-antigen without any regulatory cue as a novel nanotechnology for tolerance induction. QDs are a well-defined tool that could be used to study fundamental questions about particle trafficking and the effects imparted on immune cells in LNs.

The two described strategies had the same goal of inducing antigen-specific tolerance, but the first delivered two immune signals (i.e. self-antigen, regulatory molecule) while the second approach delivered self-antigen alone. Both platforms successfully reduced disease severity in EAE, but the mechanisms of tolerance have yet to be fully characterized. With the QD platform, the proposed mechanism is that by displaying self-antigen in particulate form, which may loosely resemble apoptotic cells, we can stimulate draining to specialized microdomains of the LN and promote interactions with tolerogenic cell types. This is in contrast to how free self-antigen might be

processed and presented through more traditional pathways that drive inflammation. The proposed mechanism of the polyplexes requires that immune cells take up both signals simultaneously, with the goal of generating T_{REGs} that can control other autoreactive cells in the periphery. Cells that phagocytose the self-antigen alone may instead polarize inflammatory cells, which could exacerbate autoimmune disease. Immune cells encountering the regulatory molecule without self-antigen could promote non-specific suppression of inflammatory functions, leaving the immune system unable to fight infection. The stability of polyplexes *in vivo* must therefore be fully characterized and optimized. QDs, conversely, are a highly stable particle system, but concerns about clearance and toxicity exist in the clinic. For this reason, QDs were used solely as a tool to determine design parameters for inducing tolerance with particle-based delivery. It will therefore be necessary to determine if these parameters can be applied to types of particles that are more frequently used in clinical research and have demonstrated tolerability (i.e. polystyrene, PLGA). The mechanism of tolerance of this platform has also yet to be fully investigated. Due to the lack of inclusion of a regulatory signal, MOG-coated particles may promote T cell deletion or anergy, rather than only generating T_{REGs}. The mechanisms of action of both platforms are likely complex, involving multiple pathways. In summary, the polyplexes are most useful for isolating the effects of immune signals, providing a simple and modular platform for studying signal density and juxtaposition. The QDs are a desirable particle system for delivering self-antigen due to useful features enabling the study of advantageous design parameters for the delivery of immune signals in a particulate form. The findings

described thus far generated interesting areas for further exploration. Key ongoing and future work will be described in the sections below.

7.2 Future studies regarding mechanism of tolerance of immune polyplexes

As revealed in **Chapter 4**, complexes composed of a self-peptide recognized in EAE ($MOGR_2$) and a regulatory molecule that blunts TLR9 activation (GpG), produce a tolerogenic response *in vitro* and *in vivo*.[48] It was also demonstrated that the surface charge of these polyplexes could be controlled by altering the ratio that signals are mixed at. As discussed in **Chapter 3**, particle properties can impact cellular processes such as uptake and the subsequent immune response. We are therefore interested in systematically studying the effects of polyplex size and charge on DC uptake mechanism, intracellular trafficking, and tolerogenic response *in vitro*. Another important parameter specific to polyplexes is binding strength between the two components, which affects loading efficiency and cargo release.[268] Ongoing and future studies compare complexes formed by condensing GpG with $MOGR_2$ to those formed using $MOGR_9$ which is more cationic. Importantly, long arginine residues can act as cell-penetrating peptides that can cross the cell membrane without being actively endocytosed.[225]

We began by comparing the size and charge of complexes formed with either $MOGR_2$ or $MOGR_9$. The hydrodynamic diameter of either type of particle remained in the 100 – 200 nm range (**Figure 7.1A**). The change in surface charge as input ratio was systematically varied was similar regardless of the number of arginine residues (**Figure**

7.1B). The fact that size and charge remained similar at each ratio is important for isolating the effect of binding strength alone on cellular processes. Future characterization studies should include an EtBr assay to determine the relative binding strength of each peptide. Another question is whether $MOGR_9$ offers advantages in terms of cargo protection or polyplex stability. These experiments should be performed by incubating polyplexes in media with serum. In **Figure 3.2**, stability was assessed in serum by measuring particle size, but more stringent methods should involve spinning down polyplexes at various time points (e.g. 1 hour, 12 hours, 24 hours, 72 hours) and measuring absorbance of peptide and DNA in the supernatant. Signal presence in the supernatant will be one indication that the polyplexes have disassembled. Additionally, it is possible that the two immune signals can remain condensed even as one or both degrade due to their charged nature. In **Figure 3.1**, the ability of complexes to protect GpG from enzymatic degradation was assessed, but future studies should also measure the degradation of peptide. The stability and functionality of each immune signal is critical to the proposed mechanism of the polyplexes. The supernatants of polyplexes that have been incubated in serum and spun down should therefore also be analyzed by protein gel electrophoresis for the presence of peptide degradation products. In this assay, proteins travel across a charged gel and their migration is directly correlated to molecular weight. Samples containing multiple proteins or degradation products will have visual bands that can be compared to a molecular weight marker. If the polyplex supernatants reveal small molecular weight bands, it will provide an indication that the peptide has begun to degrade. The presence of degradation products in the polyplexes

can be determined by comparing the gel migration of freshly-made polyplexes to those that have been incubated in serum.

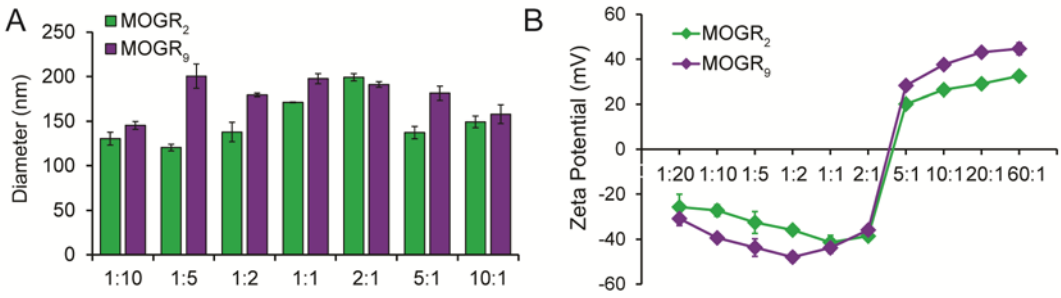

Figure 7.1: Size and charge of $MOGR_2$-GpG and $MOGR_9$-GpG polyplexes are comparable. DLS measurements performed in triplicate showed relatively small diameters regardless of signal ratio or number of arginine residues. (**B**) Zeta potential of complexes was measured in triplicate and indicated controllable surface charge.

Uptake mechanism of polyplexes formed with MOG tagged with different numbers of arginine was then compared. One way to determine the general method of polyplex internalization is to compare images at 37°C and 4°C. At the lower temperature, energy-dependent processes halt, inhibiting cellular endocytosis. At 37°C, $MOGR_2$-GpG polyplexes were readily taken up by DCs but at 4°C, no signal was detectable from the FITC-labelled MOG (**Figure 7.2**). By comparison, $MOGR_9$-GpG signal was visible at both temperatures, indicating that the polyplexes can enter cells without active phagocytosis. We hypothesize that this is due to the cell-penetrating nature of polyarginine tags. In order to further probe the uptake mechanism, a series of inhibitors should be used in future studies to target specific pathways. The following set of chemicals should be used: chlorpromazine (clathrin-mediated endocytosis), filipin (caveolae-mediated endocytosis), amiloride (cell adhesion molecule (CAM)-mediated endocytosis), wortmannin (micropinocytosis), and Caspase Inhibitor I (phagocytosis).[269] An example protocol would involve incubating primary DCs with

an inhibitor for 1 hour before treating with polyplexes for an additional hour. Flow cytometry or microscopy could then be used to analyze the extent of internalization.

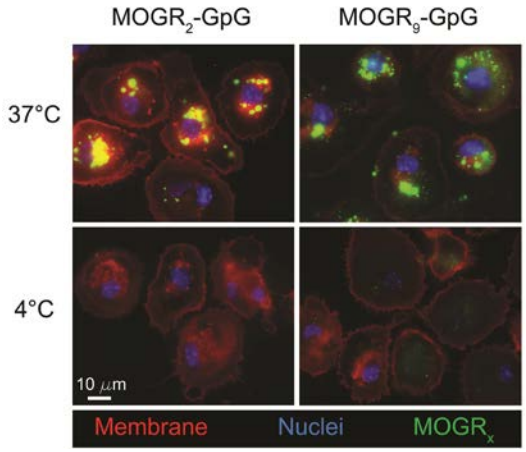

Figure 7.2: MOGR$_9$-GpG polyplexes can enter cells at 4°C, but those made with MOGR$_2$ cannot. CD11c$^+$ DCs were treated with polyplexes and incubated at 37°C or 4°C for 2 hours. The cells were then fixed, stained for the membrane (rhodamine wheat germ agglutinin) and nucleus (Hoechst), and uptake of FITC-labelled polyplexes was visualized by fluorescent microscopy.

The next experiments assessed how quickly polyplexes are internalized by DCs. Signal from either polyplex formulation was detectable by fluorescent microscopy (**Figure 7.3A**) or flow cytometry (**Figure 7.3B**) in just 10 minutes. At each time point (i.e. 10, 30, 60 minutes) the uptake of MOGR$_9$-GpG polyplexes was significantly higher than that of MOGR$_2$-GpG. We hypothesize that this is due to MOGR$_9$-GpG polyplexes entering cells by both endocytosis and by crossing the cell membrane. The inhibitor studies outlined above will test this hypothesis.

Due to the possible bimodal internalization mechanism, it is important to determine if MOGR$_9$-GpG polyplexes travel through the typical endosomal-lysosomal pathway. In one initial study, it was determined that FITC-labelled MOGR$_9$ was largely colocalized

with LysoTracker™ Red. Analyzing intracellular trafficking is important in determining whether the signals are taken up and processed together, which is important for the proposed mechanism of tolerance (**Figure 3.13)**. Future studies should further assess trafficking through endosomes by staining early endosomes (rab5), late endosomes (rab7), and recycling endosomes (rab11) and should label both immune signals in the polyplexes to determine if and when they disassemble.

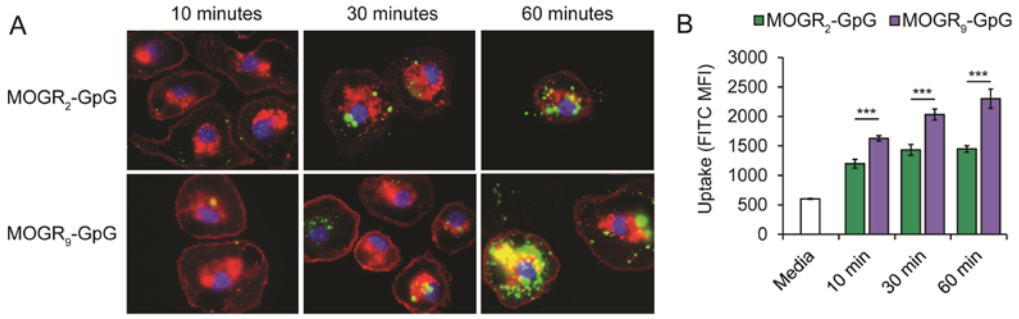

Figure 7.3: MOGR$_9$-GpG complexes are taken up more rapidly than MOGR$_2$-GpG complexes. CD11c$^+$ DCs were treated with polyplexes and incubated at 37°C for 10, 30, or 60 minutes. **A**) The cells were then fixed, stained for the membrane (rhodamine wheat germ agglutinin) and nucleus (Hoechst), and uptake of FITC-labelled polyplexes was visualized by fluorescent microscopy. **B**) Complex uptake was also quantified by flow cytometry. ***p < 0.001

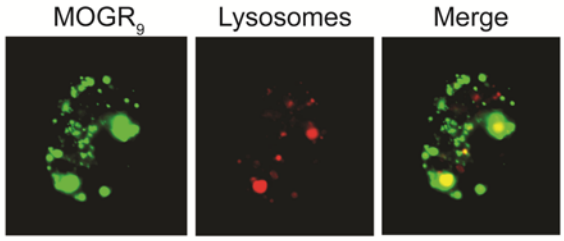

Figure 7.4: MOGR$_9$-GpG complexes are trafficked through lysosomes. CD11c$^+$ DCs were incubated with polyplexes and LysoTracker Red DND-99 for 2 hours at 37°C. Cells were then fixed and visualized by fluorescent microscopy.

Lastly, future studies should assess the impact of the number of arginine residues on *in vitro* regulatory response. First, a reporter cell line should be used to assess the impact

of the polyplexes on TLR9 signaling. In an example protocol, HEK-Blue™ mTLR9 cells will be incubated with the agonist CpG, prior to being treated with polyplexes. The level of signaling can be quantified by measuring SEAP levels using a spectrophotometer. Next, the ability of the complexes to "deactivate" DCs and polarize T cells towards regulatory phenotype should be analyzed. Similarly to the mTLR9 study, DCs would first be stimulated with CpG prior to incubation with complexes. Activation can then be measured by expression of CD40, CD80, and CD86 with a flow cytometer. Treated DCs should also be incubated with transgenic T cells that have receptors specific for MOG. After 72 hours, the phenotype of the T cells can be examined by staining for transcription factors (Tbet, RORγt, Foxp3) and analysis with a flow cytometer. An additional indicator of regulatory or inflammatory polarization is the secretion of cytokines. ELISA can be used to measure the levels of inflammatory (IL-6, IFN-γ) and regulatory (IL-10, TGF-β) cytokines produced by DC/T-cell cocultures.

The aforementioned experiments, studying cellular uptake, processing, activation, and phenotype, should also be conducted comparing other particle parameters. As mentioned, surface charge can be controlled, and we plan to adjust particle diameter by altering the initial concentration of polyplex mixing solutions. Future work should also test the modular ability of the platform by incorporating self-antigens from different disease models or immunomodulators that target different pathways. For example, the strategy could be tested in a relapsing-remitting model of MS by complexing GpG with a PLP. In a model of T1D, chromoagraninA, could be incorporated in place of MOG.

Importantly, TLR signaling has also recently been implicated in each of these autoimmune diseases.

7.3 Future studies utilizing quantum dots as a tool

Chapter 6 described initial studies carried out to assess the biodistribution of MOG-QDs. The impact of QD accumulation of the tissue composition of LNs was also assessed. Studies in **Chapter 5** also demonstrated that efficacy in EAE was inversely correlated with density of self-antigen display.[52] In studies in **Chapter 6**, however, there were no significant differences in the biodistribution or uptake of MOG-QDs with varying densities (**Figure 6.5**). Additionally, no differences were seen between densities when comparing the frequencies of different immune cell types in the LNs (**Figure 6.8**). It was demonstrated that self-peptide density did impact the response of MOG-specific T cells (**Figure 6.10)**. These experiments were carried out in healthy mice, which gives us a baseline for future studies that should be carried out in mice induced with EAE. We hypothesize that MOG-QDs will traffic differently in a disease state, when the self-antigen is being presented in LNs. Specifically, we expect MOG spread out over a larger number of QDs (i.e. 25:1) to be taken up more readily. To test this hypothesis, future studies should start by first inducing mice with EAE. Groups will then be treated with a matched dose of MOG but a varied number of QDs (25:1, 52:1, 65:1). A simple way to study biodistribution of the particles at a large number of time points (1 hour, 4 hours, 24 hours, 48 hours, 3 days, 7 days, and 14 days) is by live animal fluorescent imaging. This eliminates the need to euthanize animals and process LNs. To analyze specific cell types that take up MOG-QDs, the inguinal, axillary, and

brachial LNs should be harvested and stained for APC markers (e.g. F4/80, CD11c, CD11b) before analysis with a flow cytometer.

Future experiments should also study the specific phenotypes of cells that encounter MOG-QDs. As the goal of this platform is to induce tolerance, T cell polarization should be assessed. As with the previous experiment, cells will be analyzed with a flow cytometer but will be stained with phenotypic makers (i.e. Tbet, RORγt, Foxp3). It is important to note that the specific readouts should occur at time points before symptoms arise, when symptoms are worsening, and at peak disease. Reactivity of the harvested cells towards myelin should also be assessed. In an example protocol, cells isolated from the LNs and spleens of treated mice would be restimulated with MOG and cultured for 72 hours. The supernatants from cell culture would then be tested by ELISA for the presence of cytokines. Cells from untreated mice with EAE should produce inflammatory cytokines such as IL-6 and IFN-γ upon encountering MOG. If tolerance has been induced (i.e. in MOG-QD treated mice), the cells should secrete regulatory cytokines such as IL-10 or TGF-β. The studies described thus far were carried out with MOG-QDs being injected before disease symptoms arise. It would also be of interest to conduct the same set of experiments with other injection timelines including at initial disease onset, when symptoms are worsening, and at peak disease. These studies would be useful for determining not only how treatment time impacts tolerogenic outcome, but also how it changes biodistribution and impact on immune cells.

The impact of MOG peptide density on LN structure and remodeling should also be studied. As discussed in **Chapter 6**, LNs structure is directly related to the initiation of an inflammatory or tolerogenic immune response. Specifically, LNs from mice with EAE that have been treated with MOG-QDs (25:1, 52:1, 65:1) should be harvested at the previously specified time points, frozen, and sectioned. The immune cells analyzed by flow cytometry (i.e. T cells, B cells, and APCs) can then be stained and imaged to assess comingling of the T and B cell zones or colocalization of MOG-QDs with various cell types. Specific attention should also be paid to microdomains that the particles accumulate in. **Figure 5.11** shows MOG-QDs localized to an area containing $MARCO^{+}$ macrophages. These cells are thought to be involved in tolerance, so future studies should assess the impact of MOG display density on trafficking to these domains. The sectioned tissues mentioned above can also be stained for tolerogenic markers MARCO and SCARF1. LNs also feature differential expression of laminins α4 and α5 during states of immunity or tolerance. Imaging these markers is also of interest in the context of peptide ligand density. Taken together, the outlined experiments should reveal tolerance mechanisms of MOG-QDs, and define design rules specifically related to display of self-antigen. As with the previous section, it would be of interest to apply this platform to other disease models such as T1D and relapsing-remitting EAE.

Chapter 8: Contributions

My doctoral research has generated 4 peer-reviewed articles, with 3 additional articles in preparation or in review. I have published a first-author paper on each of the specific aims described in **Chapter 1**. One focuses on the development of a novel carrier-free system for delivery of immune signals to combat autoimmunity (*Biomaterials* 2017). The research with immune polyplexes is novel, based on a few ideas that are still new to the field including attempting to blunt TLR signaling as a mechanism of immunosuppression and the elimination of carriers to isolate the effects of immune signals. The other first-author manuscript, published as a cover article in *Advanced Function Materials* 2017, describes a QD-based platform for understanding fundamental questions involved in the promotion of immune tolerance. The work was also later featured on the cover of *Transplantation* 2018. The research was also featured in Multiple Sclerosis News Today and on the Sounds of Science podcast in GEN News. The platform was also filed in a US patent application. I am currently preparing a first author manuscript based on the work in **Chapter 6.** My work with QDs represents the first time that this material has been applied to autoimmunity. This research provides new insight at the interface of materials design and autoimmunity, targeting a key gap in the understanding of particle parameters necessary for tolerance induction.

Chapter 4 will be submitted as an invited review article, on which I am first author, to *Nano Today*. I was a supporting author on the additional mentioned publications, providing both technical assistance and support on experimental design. These papers also involve the synthesis of particles composed entirely of immune signals. I have also

presented my research at five national or international conferences, including Keystone Symposia, the World Biomaterials Congress, and annual meetings for the Biomedical Engineering Society and the American Association of Immunologists. Travel to these conferences has been supported by four awards from the University of Maryland. My doctoral work has been supported by the Department of Defense Science, Mathematics, And Research for Transformation (SMART) fellowship, which I was awarded in my second year of graduate study. As a part of this program, I completed a summer internship in which I did synthetic biology research.

As a DoD SMART Fellow, I also spoke on panels typically consisting of 20-50 undergraduate and graduate students interested in applying to graduate school and/or fellowships. I am able to share advice and perspective to hopefully increase their chance of successful applications. Through my sustained involvement in the NSF-funded Program to Enhance Participation in Research (PEPR), I have mentored a student from Wheaton High School for each of the past three years as they learn about a biomedical topic of their choosing. In monthly workshops, I assisted the student with reviewing research articles, writing a scholarly paper, and presenting a poster. I also organized a field trip for a group of 80 high school students to visit our research lab, where they got hands on experience with laboratory skills such as vaccine particle synthesis. These students would not typically get the opportunity to have such immersive biomedical research experiences; I hope these efforts encourage them to pursue STEM careers. I have also served at the department, college, and university levels through leadership positions and committee work. In my first year, I was elected

as BGSS president by my peers. Over two years, I led a board that plans 10-15 events per year focused on professional development, academic enrichment, volunteering, and social gathering. These events included panels on finding faculty positions, scientific writing workshops, canned food drives, and department barbecues. As president, I also acted as an ambassador for the department by planning events such as the Student Choice Seminar that brings a distinguished professor from another university to campus for a guest lecture attended by the bioengineering students and faculty. I was also asked by Dean Darryll Pines to serve on the chair search committee for the Bioengineering Department. I evaluated applications, interviewed candidates, and arranged lunches with undergraduate and graduate students for each of the 6 applicants invited for campus interviews. Last spring, I was elected to the University of Maryland Senate to serve as a senator representing full-time graduate students. I was also asked by the Senate Chair to serve as chair of the Student Affairs Committee, where I led a board of approximately 20 people to tackle issues such as public transportation and course evaluation procedures.

Appendix

First Author Publications:

1. **Krystina L. Hess**, Igor L. Medintz, Christopher M Jewell; "Developing inorganic nanomaterials for immunological applications," *Nano Today* **2018**. (*invited review in preparation*)

2. **Krystina L. Hess**, Eunkeu Oh, Lisa H. Tostanoski, James I. Andorko, Kimihiro Susumu, Jeffrey R. Deschamps, Igor L. Medintz, Christopher M Jewell; "Engineering immunological tolerance using quantum dots to tune the density of self-antigen display", *Advanced Functional Materials* **2017**. (*cover article*)
   featured in Genetic Engineering and Biotechnology News Sounds of Science Podcast
   featured on the cover of *Transplantation*, 2018

3. **Krystina L. Hess**, James I. Andorko, Lisa H. Tostanoski, Christopher M. Jewell; "Polyplexes assembled from self-peptides and regulatory nucleic acids blunt toll-like receptor signaling to combat autoimmunity", *Biomaterials* **2017**, 118: 51-62.

Co-Author Publications:

4. Michelle L. Bookstaver, **Krystina L. Hess**, Christopher M. Jewell; "Self-assembly of Immune Signals Improves Co-delivery to Antigen Presenting Cells and Accelerates Signal Internalization, Processing Kinetics, and Immune Activation" *Small* **2018**. (*in revision*)

5. James I. Andorko, **Krystina L. Hess**, Kevin G. Pineault, Christopher M. Jewell; "Intrinsic immunogenicity of rapidly-degradable polymers evolves during degradation", *Acta Biomaterialia* **2016**, 32: 24-34.

6. James I. Andorko, **Krystina L. Hess**, Christopher M. Jewell; "Harnessing Biomaterials to Engineer the Lymph Node Microenvironment for Immunity or Tolerance" *AAPS Journal* **2015**, 17 (2): 323-338.
   ****featured in special issue on immune engineering****

Patent Filings:

7. "Harnessing Quantum Dots to Study, Visualize, and Promote Immune Tolerance." Christopher M. Jewell, **Krystina L. Hess**, Igor Medintz, Kimihiro Susumu, Eunkeu Oh; PCT application number US17/28124. Filed April 18, **2017**.

References

[1] Riera Romo M, Pérez-Martínez D, Castillo Ferrer C. Innate immunity in vertebrates: an overview. Immunology. 2016;148:125-39.

[2] Ruddle N, Akirav E. Secondary lymphoid organs: responding to genetic and environmental cues in ontogeny and the immune response. Journal of Immunology. 2009;183:2205-12.

[3] Mueller S, Germain R. Stromal cell contributions to the homeostasis and functionality of the immune system. Nature Reviews Immunology. 2009;9:618-29.

[4] Reddy S, van der Vlies A, Simeoni E, Angeli V, Randolph G, O'Neil C, et al. Exploiting lymphatic transport and complement activation in nanoparticle vaccines. Nature biotechnology. 2007;25:1159-64.

[5] Swartz M, Hubbell J, Reddy S. Lymphatic drainage function and its immunological implications: From dendritic cell homing to vaccine design. Seminars in Immunology. 2008;20:147-56.

[6] Foged C, Brodin B, Frokjaer S, Sundblad A. Particle size and surface charge affect particle uptake by human dendritic cells in an in vitro model. International Journal of Pharmaceutics. 2005;298:315-22.

[7] Andorko J, Hess K, Jewell C. Harnessing Biomaterials to Engineer the Lymph Node Microenvironment for Immunity or Tolerance. AAPS Journal. 2014:1-16.

[8] Boehm T, Swann J. Origin and evolution of adaptive immunity. Annual review of animal biosciences. 2014;2:259-83.

[9] Kontos S, Grimm A, Hubbell J. Engineering antigen-specific immunological tolerance. Current opinion in immunology. 2015;35:80-8.

[10] National Institue of Environmental Health Sciences. Autoimmune Disease Fact Sheet. 2012.

[11] Nylander A, Hafler D. Multiple sclerosis. Journal of Clinical Investigation. 2012;122:1180-8.

[12] Lutterotti A, Martin R. Antigen-specific tolerization approaches in multiple sclerosis. Expert opinion on investigational drugs. 2014;23:9-20.

[13] Simons M, Lyons D. Axonal selection and myelin sheath generation in the central nervous system. Current Opinion in Cell Biology. 2013;25:512-9.

[14] Min Y, Kristiansen K, Boggs J, Husted C, Zasadzinski J, Israelachvili J. Interaction forces and adhesion of supported myelin lipid bilayers modulated by

myelin basic protein. Proceedings of the National Academy of Sciences of the United States of America. 2009;106:3154-9.

[15] Dendrou C, Fugger L, Friese M. Immunopathology of multiple sclerosis. Nature Reviews Immunology. 2015;15:545-58.

[16] Hemmer B, Archelos J, Hartung H-P. New concepts in the immunopathogenesis of multiple sclerosis. Nature Reviews Neuroscience. 2002;3:291.

[17] Comabella M, Khoury S. Immunopathogenesis of multiple sclerosis. Clinical immunology. 2012;142:2-8.

[18] McFarland H, Martin R. Multiple sclerosis: a complicated picture of autoimmunity. Nature immunology. 2007;8:913-9.

[19] Bailey S, Schreiner B, McMahon E, Miller S. CNS myeloid DCs presenting endogenous myelin peptides 'preferentially' polarize CD4+ T(H)-17 cells in relapsing EAE. Nature immunology. 2007;8:172-80.

[20] Centonze D, Muzio L, Rossi S, Cavasinni F, De Chiara V, Bergami A, et al. Inflammation Triggers Synaptic Alteration and Degeneration in Experimental Autoimmune Encephalomyelitis. Journal of Neuroscience. 2009;29:3442-52.

[21] Centonze D, Muzio L, Rossi S, Furlan R, Bernardi G, Martino G. The link between inflammation, synaptic transmission and neurodegeneration in multiple sclerosis. Cell Death And Differentiation. 2009;17:1083.

[22] Popescu B, Lucchinetti C. Pathology of Demyelinating Diseases. Annual Review of Pathology: Mechanisms of Disease. 2012;7:185-217.

[23] Piehl F. A changing treatment landscape for multiple sclerosis: challenges and opportunities. Journal of Internal Medicine. 2014;275:364-81.

[24] Gammon J, Dold N, Jewell C. Improving the clinical impact of biomaterials in cancer immunotherapy. Oncotarget. 2016;7:15421-43.

[25] Tostanoski L, Chiu Y-C, Gammon J, Simon T, Andorko J, Bromberg J, et al. Reprogramming the Local Lymph Node Microenvironment Promotes Tolerance that Is Systemic and Antigen Specific. Cell Reports. 2016;16:2940-52.

[26] Ankur S, A. P. Hydrogels and Scaffolds for Immunomodulation. Advanced Materials. 2014;26:6530-41.

[27] Domachuk P, Tsioris K, Omenetto F, Kaplan D. Bio-microfluidics: Biomaterials and Biomimetic Designs. Advanced Materials. 2010;22:249-60.

[28] Andorko J, Hess K, Pineault K, Jewell C. Intrinsic immunogenicity of rapidly-degradable polymers evolves during degradation. Acta Biomaterialia. 2016;32:24-34.

[29] Irvine D, Jewell C. Vaccine and Immunotherapy Delivery. In: Ducheyne P, editor. Comprehensive Biomaterials: Elsevier Ltd; 2011. p. 315-32.

[30] Hubbell J, Thomas S, Swartz M. Materials engineering for immunomodulation. Nature. 2009;462:449-60.

[31] Kwon Y, James E, Shastri N, Fréchet J. In vivo targeting of dendritic cells for activation of cellular immunity using vaccine carriers based on pH-responsive microparticles. Proceedings of the National Academy of Sciences of the United States of America. 2005;102:18264-8.

[32] Zhao X, Jain S, Benjamin Larman H, Gonzalez S, Irvine D. Directed cell migration via chemoattractants released from degradable microspheres. Biomaterials. 2005;26:5048-63.

[33] Cohen J, Beaudette T, Tseng W, Bachelder E, Mende I, Engleman E, et al. T-cell activation by antigen-loaded pH-sensitive hydrogel particles in vivo: the effect of particle size. Bioconjugate Chemistry. 2009;20:111-9.

[34] Heffernan M, Kasturi S, Yang S, Pulendran B, Murthy N. The stimulation of CD8+ T cells by dendritic cells pulsed with polyketal microparticles containing ion-paired protein antigen and poly(inosinic acid)-poly(cytidylic acid). Biomaterials. 2009;30:910-8.

[35] Cerritelli S, Velluto D, Hubbell J. PEG-SS-PPS: Reduction-Sensitive Disulfide Block Copolymer Vesicles for Intracellular Drug Delivery. Biomacromolecules. 2007;8:1966-72.

[36] Napoli A, Valentini M, Tirelli N, Muller M, Hubbell J. Oxidation-responsive polymeric vesicles. Nature Materials. 2004;3:183-9.

[37] Bachmann M, Jennings G. Vaccine delivery: a matter of size, geometry, kinetics and molecular patterns. Nature Reviews Immunology. 2010;10:787-96.

[38] Demento S, Eisenbarth S, Foellmer H, Platt C, Caplan M, Mark Saltzman W, et al. Inflammasome-activating nanoparticles as modular systems for optimizing vaccine efficacy. Vaccine. 2009;27:3013-21.

[39] Sharp F, Ruane D, Claass B, Creagh E, Harris J, Malyala P, et al. Uptake of particulate vaccine adjuvants by dendritic cells activates the NALP3 inflammasome. Proceedings of the National Academy of Sciences of the United States of America. 2009;106:870-5.

[40] Termeer C, Benedix F, Sleeman J, Fieber C, Voith U, Ahrens T, et al. Oligosaccharides of Hyaluronan activate dendritic cells via toll-like receptor 4. Journal of Experimental Medicine. 2002;195:99-111.

[41] Termeer C, Hennies J, Voith U, Ahrens T, Weiss J, Prehm P, et al. Oligosaccharides of hyaluronan are potent activators of dendritic cells. Journal of Immunology. 2000;165:1863-70.

[42] Schanen B, Das S, Reilly C, Warren W, Self W, Seal S, et al. Immunomodulation and T Helper TH1/TH2 Response Polarization by CeO2 and TiO2 Nanoparticles. PLOS ONE. 2013;8:e62816.

[43] Pescatori M, Bedognetti D, Venturelli E, Ménard-Moyon C, Bernardini C, Muresu E, et al. Functionalized carbon nanotubes as immunomodulator systems. Biomaterials. 2013;34:4395-403.

[44] Tomić S, Janjetović K, Mihajlović D, Milenković M, Kravić-Stevović T, Marković Z, et al. Graphene quantum dots suppress proinflammatory T cell responses via autophagy-dependent induction of tolerogenic dendritic cells. Biomaterials. 2017;146:13-28.

[45] Stankiewicz J, Kolb H, Karni A, Weiner H. Role of immunosuppressive therapy for the treatment of multiple sclerosis. Neurotherapeutics : the journal of the American Society for Experimental NeuroTherapeutics. 2013;10:77-88.

[46] Yeste A, Nadeau M, Burns E, Weiner H, Quintana F. Nanoparticle-mediated codelivery of myelin antigen and a tolerogenic small molecule suppresses experimental autoimmune encephalomyelitis. Proceedings of the National Academy of Sciences of the United States of America. 2012;109:11270-5.

[47] Maldonado R, LaMothe R, Ferrari J, Zhang A, Rossi R, Kolte P, et al. Polymeric synthetic nanoparticles for the induction of antigen-specific immunological tolerance. Proceedings of the National Academy of Sciences of the United States of America. 2015;112:E156-65.

[48] Hess K, Andorko J, Tostanoski L, Jewell C. Polyplexes assembled from self-peptides and regulatory nucleic acids blunt toll-like receptor signaling to combat autoimmunity. Biomaterials. 2017;118:51-62.

[49] Tostanoski L, Chiu Y-C, Andorko J, Guo M, Zeng X, Zhang P, et al. Design of Polyelectrolyte Multilayers to Promote Immunological Tolerance. ACS Nano. 2016;10:9334-45.

[50] Hunter Z, McCarthy D, Yap W, Harp C, Getts D, Shea L, et al. A biodegradable nanoparticle platform for the induction of antigen-specific immune tolerance for treatment of autoimmune disease. ACS Nano. 2014;8:2148-60.

[51] Pishesha N, Bilate A, Wibowo M, Huang N-J, Li Z, Deshycka R, et al. Engineered erythrocytes covalently linked to antigenic peptides can protect against autoimmune disease. Proceedings of the National Academy of Sciences of the United States of America. 2017;114:3157-62.

[52] Hess K, Oh E, Tostanoski L, Andorko J, Susumu K, Deschamps J, et al. Engineering Immunological Tolerance Using Quantum Dots to Tune the Density of Self-Antigen Display. Advanced Functional Materials. 2017:1700290-n/a.

[53] Getts D, Martin A, McCarthy D, Terry R, Hunter Z, Yap W, et al. Microparticles bearing encephalitogenic peptides induce T-cell tolerance and ameliorate experimental autoimmune encephalomyelitis. Nature biotechnology. 2012;30:1217-24.

[54] Kontos S, Kourtis I, Dane K, Hubbell J. Engineering antigens for in situ erythrocyte binding induces T-cell deletion. Proceedings of the National Academy of Sciences of the United States of America. 2013;110:E60-8.

[55] Moon J, Huang B, Irvine D. Engineering nano- and microparticles to tune immunity. Advanced Materials. 2012;24:3724-46.

[56] Getts D, Shea L, Miller S, King N. Harnessing nanoparticles for immune modulation. Trends in immunology. 2015;36:419-27.

[57] Irvine D, Hanson M, Rakhra K, Tokatlian T. Synthetic Nanoparticles for Vaccines and Immunotherapy. Chemical reviews. 2015;115:11109-46.

[58] Da Silva C Chalouni C, Williams A, Hartl D, Lee C, Elias J. Chitin is a size-dependent regulator of macrophage TNF and IL-10 production. Journal of Immunology. 2009;182:3573-82.

[59] Sunshine J, Perica K, Schneck J, Green J. Particle shape dependence of CD8+ T cell activation by artificial antigen presenting cells. Biomaterials. 2014;35:269-77.

[60] Andorko J, Pineault K, Jewell C. Impact of molecular weight on the intrinsic immunogenic activity of poly(beta amino esters). Journal of Biomedical Materials Research Part A. 2017;105:1219-29.

[61] Irvine D, Swartz M, Szeto G. Engineering synthetic vaccines using cues from natural immunity. Nature Materials. 2013;12:978.

[62] Tostanoski L, Gosselin E, Jewell C. Engineering tolerance using biomaterials to target and control antigen presenting cells. Discovery medicine. 2016;21:403-10.

[63] Andorko J, Jewell C. Designing biomaterials with immunomodulatory properties for tissue engineering and regenerative medicine. Bioengineering & Translational Medicine. 2017;2:139-55.

[64] Bookstaver M, Tsai S, Bromberg J, Jewell C. Improving Vaccine and Immunotherapy Design Using Biomaterials. Trends in Immunology. 2017.

[65] Dowling J, Mansell A. Toll-like receptors: the swiss army knife of immunity and vaccine development. Clinical & Translational Immunology. 2016;5:e85.

[66] Sapsford K, Algar W, Berti L, Gemmill K, Casey B, Oh E, et al. Functionalizing Nanoparticles with Biological Molecules: Developing Chemistries that Facilitate Nanotechnology. Chemical Reviews. 2013;113:1904-2074.

[67] Boverhof D, Bramante C, Butala J, Clancy S, Lafranconi M, West J, et al. Comparative assessment of nanomaterial definitions and safety evaluation considerations. Regulatory Toxicology and Pharmacology. 2015;73:137-50.

[68] Pfeiffer C, Rehbock C, Hühn D, Carrillo-Carrion C, de Aberasturi DJ, Merk V, et al. Interaction of colloidal nanoparticles with their local environment: the (ionic) nanoenvironment around nanoparticles is different from bulk and determines the physico-chemical properties of the nanoparticles. Journal of The Royal Society Interface. 2014;11.

[69] Oh E, Delehanty J, Klug C, Susumu K, Russ Algar W, Goswami R, et al. Utility of PEGylated dithiolane ligands for direct synthesis of water-soluble Au, Ag, Pt, Pd, Cu and AuPt nanoparticles. Chemical Communications. 2018.

[70] Brust M, Walker M, Bethell D, Schiffrin D, Whyman R. Synthesis of thiol-derivatised gold nanoparticles in a two-phase Liquid-Liquid system. Journal of the Chemical Society, Chemical Communications. 1994:801-2.

[71] Palui G, Aldeek F, Wang W, Mattoussi H. Strategies for interfacing inorganic nanocrystals with biological systems based on polymer-coating. Chemical Society Reviews. 2015;44:193-227.

[72] Wenrong Y, Pall T, Gooding J, Simon P, Filip B. Carbon nanotubes for biological and biomedical applications. Nanotechnology. 2007;18:412001.

[73] Algar W, Prasuhn D, Stewart M, Jennings T, Blanco-Canosa J, Dawson P, et al. The Controlled Display of Biomolecules on Nanoparticles: A Challenge Suited to Bioorthogonal Chemistry. Bioconjugate Chemistry. 2011;22:825-58.

[74] Blanco-Canosa J, Wu M, Susumu K, Petryayeva E, Jennings T, Dawson P, et al. Recent progress in the bioconjugation of quantum dots. Coordination Chemistry Reviews. 2014;263-264:101-37.

[75] Medintz I. Universal tools for biomolecular attachment to surfaces. Nature Materials. 2006;5:842.

[76] Front Matter. Chemoselective and Bioorthogonal Ligation Reactions: Wiley-VCH Verlag GmbH & Co. KGaA; 2017. p. i-xxii.

[77] Zobel M, Neder R, Kimber S. Universal solvent restructuring induced by colloidal nanoparticles. Science. 2015;347:292-4.

[78] Vranish J, Ancona M, Walper S, Medintz I. Pursuing the Promise of Enzymatic Enhancement with Nanoparticle Assemblies. Langmuir. 2017.

[79] Ding S, Cargill A, Medintz I, Claussen J. Increasing the activity of immobilized enzymes with nanoparticle conjugation. Current Opinion in Biotechnology. 2015;34:242-50.

[80] Docter D, Westmeier D, Markiewicz M, Stolte S, Knauer SK, Stauber RH. The nanoparticle biomolecule corona: lessons learned - challenge accepted? Chemical Society Reviews. 2015;44:6094-121.

[81] Lundqvist M, Augustsson C, Lilja M, Lundkvist K, Dahlbäck B, Linse S, et al. The nanoparticle protein corona formed in human blood or human blood fractions. PLOS ONE. 2017;12:e0175871.

[82] Sapsford K, Tyner KM Dair B, Deschamps J, Medintz I. Analyzing Nanomaterial Bioconjugates: A Review of Current and Emerging Purification and Characterization Techniques. Analytical Chemistry. 2011;83:4453-88.

[83] Oh E, Liu R, Nel A, Gemill K, Bilal M, Cohen Y, et al. Meta-analysis of cellular toxicity for cadmium-containing quantum dots. Nature Nanotechnology. 2016;11:479.

[84] Khlebtsov N, Dykman L. Biodistribution and toxicity of engineered gold nanoparticles: a review of in vitro and in vivo studies. Chemical Society Reviews. 2011;40:1647-71.

[85] Elsaesser A, Howard C. Toxicology of nanoparticles. Advanced Drug Delivery Reviews. 2012;64:129-37.

[86] Giovanni M, Yue J, Zhang L, Xie J, Ong C, Leong D. Pro-inflammatory responses of RAW264.7 macrophages when treated with ultralow concentrations of silver, titanium dioxide, and zinc oxide nanoparticles. Journal of Hazardous Materials. 2015;297:146-52.

[87] Chao Y, Karmali P, Mukthavaram R, Kesari S, Kouznetsova V, Tsigelny I, et al. Direct Recognition of Superparamagnetic Nanocrystals by Macrophage Scavenger Receptor SR-AI. ACS Nano. 2013;7:4289-98.

[88] Cobaleda-Siles M, Henriksen-Lacey M, Ruiz de Angulo A, Bernecker A, Gomez Vallejo V, Szczupak B, et al. An iron oxide nanocarrier for dsRNA to target lymph nodes and strongly activate cells of the immune system. Small (Weinheim an der Bergstrasse, Germany). 2014;10:5054-67.

[89] Pricker S. Medical uses of gold compounds: Past, present and future. Gold Bulletin. 1996;29:53-60.

[90] Sumbayev V, Yasinska I, Garcia C, Gilliland D, Lall G, Gibbs B, et al. Gold Nanoparticles Downregulate Interleukin-1β-Induced Pro-Inflammatory Responses. Small (Weinheim an der Bergstrasse, Germany). 2013;9:472-7.

[91] Franca A, Aggarwal P, Barsov E, Kozlov S, Dobrovolskaia M, Gonzalez-Fernandez A. Macrophage scavenger receptor A mediates the uptake of gold colloids by macrophages in vitro. Nanomedicine : nanotechnology, biology, and medicine. 2011;6:1175-88.

[92] Tsai C-Y, Lu S-L, Hu C-W, Yeh C-S, Lee G-B, Lei H-Y. Size-Dependent Attenuation of TLR9 Signaling by Gold Nanoparticles in Macrophages. Journal of Immunology. 2012;188:68-76.

[93] Moyano D, Goldsmith M, Solfiell D, Landesman-Milo D, Miranda O, Peer D, et al. Nanoparticle Hydrophobicity Dictates Immune Response. Journal of the American Chemical Society. 2012;134:3965-7.

[94] Bajwa N, Mehra N, Jain K, Jain N. Pharmaceutical and biomedical applications of quantum dots. Artificial Cells, Nanomedicine, and Biotechnology. 2016;44:758-68.

[95] Banerjee A, Pons T, Lequeux N, Dubertret B. Quantum dots–DNA bioconjugates: synthesis to applications. Interface Focus. 2016;6:20160064.

[96] Mo D, Hu L, Zeng G, Chen G, Wan J, Yu Z, et al. Cadmium-containing quantum dots: properties, applications, and toxicity. Applied Microbiology and Biotechnology. 2017;101:2713-33.

[97] Kosaka N, Mitsunaga M, Choyke P, Kobayashi H. In vivo real-time lymphatic draining using quantum-dot optical imaging in mice. Contrast Media & Molecular Imaging. 2013;8:96-100.

[98] Romoser A, Chen P, Berg J, Seabury C, Ivanov I, Criscitiello M, et al. Quantum dots trigger immunomodulation of the NFκB pathway in human skin cells. Molecular Immunology. 2011;48:1349-59.

[99] Fadel T, Fahmy T. Immunotherapy applications of carbon nanotubes: from design to safe applications. Trends in Biotechnology. 2014;32:198-209.

[100] Dumortier H. When carbon nanotubes encounter the immune system: Desirable and undesirable effects. Advanced Drug Delivery Reviews. 2013;65:2120-6.

[101] Li H, Tan X-Q, Yan L, Zeng B, Meng J, Xu H-Y, et al. Multi-walled carbon nanotubes act as a chemokine and recruit macrophages by activating the PLC/IP3/CRAC channel signaling pathway. Scientific Reports. 2017;7:226.

[102] Izquierdo J, Bonilla-Abadia F, Canas C, Tobon G. Calcium, channels, intracellular signaling and autoimmunity. Reumatologia clinica. 2014;10:43-7.

[103] Hassan H, Smyth L, Rubio N, Ratnasothy K, Wang J, Bansal SS, et al. Carbon nanotubes' surface chemistry determines their potency as vaccine nanocarriers in vitro and in vivo. Journal of Controlled Release. 2016;225:205-16.

[104] Qin Y, Zhou Z-W, Pan S-T, He Z-X, Zhang X, Qiu J-X, et al. Graphene quantum dots induce apoptosis, autophagy, and inflammatory response via p38 mitogen-activated protein kinase and nuclear factor-κB mediated signaling pathways in activated THP-1 macrophages. Toxicology. 2015;327:62-76.

[105] Haensch C, Hoeppener S, Schubert U. Chemical modification of self-assembled silane based monolayers by surface reactions. Chemical Society Reviews. 2010;39:2323-34.

[106] Kakizawa Y, Seok Lee J, Bell B, Fahmy T. Precise manipulation of biophysical particle parameters enables control of proinflammatory cytokine production in presence of TLR 3 and 4 ligands. Acta Biomaterialia. 2017;57:136-45.

[107] Mahony D, Cavallaro A, Stahr F, Mahony T, Qiao S, Mitter N. Mesoporous Silica Nanoparticles Act as a Self-Adjuvant for Ovalbumin Model Antigen in Mice. Small (Weinheim an der Bergstrasse, Germany). 2013;9:3138-46.

[108] Morishige T, Yoshioka Y, Inakura H, Tanabe A, Narimatsu S, Yao X, et al. Suppression of nanosilica particle-induced inflammation by surface modification of the particles. Archives of Toxicology. 2012;86:1297-307.

[109] Marzaioli V, Aguilar-Pimentel J, Weichenmeier I, Luxenhofer G, Wiemann M, Landsiedel R, et al. Surface modifications of silica nanoparticles are crucial for their inert versus proinflammatory and immunomodulatory properties. International Journal of Nanomedicine. 2014;9:2815-32.

[110] Oh W-K, Kim S, Choi M, Kim C, Jeong Y, Cho B-R, et al. Cellular Uptake, Cytotoxicity, and Innate Immune Response of Silica−Titania Hollow Nanoparticles Based on Size and Surface Functionality. ACS Nano. 2010;4:5301-13.

[111] Nishijima N, Hirai T, Misato K, Aoyama M, Kuroda E, Ishii K, et al. Human Scavenger Receptor A1-Mediated Inflammatory Response to Silica Particle Exposure Is Size Specific. Frontiers in Immunology. 2017;8:379.

[112] Versiani A, Astigarraga R, Rocha E, Barboza A, Kroon E, Rachid M, et al. Multi-walled carbon nanotubes functionalized with recombinant Dengue virus 3 envelope proteins induce significant and specific immune responses in mice. Journal of Nanobiotechnology. 2017;15:26.

[113] Pradhan B, Guha D, Murmu K, Sur A, Ray P, Das D, et al. Comparative efficacy analysis of anti-microbial peptides, LL-37 and indolicidin upon conjugation with CNT, in human monocytes. Journal of Nanobiotechnology. 2017;15:44.

[114] Volarevic V, Paunovic V, Markovic Z, Simovic Markovic B, Misirkic-Marjanovic M, Todorovic-Markovic B, et al. Large Graphene Quantum Dots Alleviate Immune-Mediated Liver Damage. ACS Nano. 2014;8:12098-109.

[115] Pusic K, Aguilar Z, McLoughlin J, Kobuch S, Xu H, Tsang M, et al. Iron oxide nanoparticles as a clinically acceptable delivery platform for a recombinant blood-stage human malaria vaccine. The FASEB Journal. 2013;27:1153-66.

[116] Xu L, Liu Y, Chen Z, Li W, Liu Y, Wang L, et al. Surface-Engineered Gold Nanorods: Promising DNA Vaccine Adjuvant for HIV-1 Treatment. Nano Letters. 2012;12:2003-12.

[117] Gianvincenzo P, Calvo J, Perez S, Alvarez A, Bedoya L, Alcami J, et al. Negatively charged glyconanoparticles modulate and stabilize the secondary structures of a gp120 V3 loop peptide: toward fully synthetic HIV vaccine candidates. Bioconjugate Chemistry. 2015;26:755-65.

[118] Calderon-Gonzalez R, Frande-Cabanes E, Teran-Navarro H, Marimon J, Freire J, Salcines-Cuevas D, et al. GNP-GAPDH1-22 nanovaccines prevent neonatal listeriosis by blocking microglial apoptosis and bacterial dissemination. Oncotarget. 2017;8:53916-34.

[119] Kaba S, Brando C, Guo Q, Mittelholzer C, Raman S, Tropel D, et al. A nonadjuvanted polypeptide nanoparticle vaccine confers long-lasting protection against rodent malaria. Journal of Immunology 2009;183:7268-77.

[120] Chen Y, Hung Y, Lin W, Huang G. Assessment of gold nanoparticles as a size-dependent vaccine carrier for enhancing the antibody response against synthetic foot-and-mouth disease virus peptide. Nanotechnology. 2010;21:195101.

[121] Zhou Q, Zhang Y, Du J, Li Y, Zhou Y, Fu Q, et al. Different-Sized Gold Nanoparticle Activator/Antigen Increases Dendritic Cells Accumulation in Liver-Draining Lymph Nodes and CD8+ T Cell Responses. ACS Nano. 2016;10:2678-92.

[122] Tao W, Ziemer K, Gill H. Gold nanoparticle-M2e conjugate coformulated with CpG induces protective immunity against influenza A virus. Nanomedicine : nanotechnology, biology, and medicine. 2014;9:237-51.

[123] Tao W, Hurst B, Shakya A, Uddin M, Ingrole R, Hernandez-Sanabria M, et al. Consensus M2e peptide conjugated to gold nanoparticles confers protection against H1N1, H3N2 and H5N1 influenza A viruses. Antiviral research. 2017;141:62-72.

[124] Gregory A, Judy B, Qazi O, Blumentritt C, Brown K, Shaw A, et al. A gold nanoparticle-linked glycoconjugate vaccine against Burkholderia mallei. Nanomedicine: Nanotechnology, Biology, and Medicine. 2015;11:447-56.

[125] Ngugi S, Ventura V, Qazi O, Harding S, Kitto G, Estes D, et al. Lipopolysaccharide from Burkholderia thailandensis E264 provides protection in a murine model of melioidosis. Vaccine. 2010;28:7551-5.

[126] Torres A, Gregory A, Hatcher C, Vinet-Oliphant H, Morici L, Titball R, et al. Protection of non-human primates against glanders with a gold nanoparticle glycoconjugate vaccine. Vaccine. 2015;33:686-92.

[127] Muruato L, Tapia D, Hatcher C, Kalita M, Brett P, Gregory A, et al. The Use of Reverse Vaccinology in the Design and Construction of Nano-glycoconjugate Vaccines against Burkholderia pseudomallei. Clinical and Vaccine Immunology. 2017.

[128] Marques Neto L, Kipnis A, Junqueira-Kipnis A. Role of Metallic Nanoparticles in Vaccinology: Implications for Infectious Disease Vaccine Development. Frontiers in Immunology. 2017;8:239.

[129] Niikura K, Matsunaga T, Suzuki T, Kobayashi S, Yamaguchi H, Orba Y, et al. Gold Nanoparticles as a Vaccine Platform: Influence of Size and Shape on Immunological Responses in Vitro and in Vivo. ACS Nano. 2013;7:3926-38.

[130] Skrastina D, Petrovskis I, Lieknina I, Bogans J, Renhofa R, Ose V, et al. Silica Nanoparticles as the Adjuvant for the Immunisation of Mice Using Hepatitis B Core Virus-Like Particles. PLOS ONE. 2014;9:e114006.

[131] Virginio V, Bandeira N, Leal F, Lancellotti M, Zaha A, Ferreira H. Assessment of the adjuvant activity of mesoporous silica nanoparticles in recombinant Mycoplasma hyopneumoniae antigen vaccines. Heliyon. 2017;3:e00225.

[132] Zhao K, Rong G, Guo C, Luo X, Kang H, Sun Y, et al. Synthesis, characterization, and immune efficacy of layered double hydroxide@SiO2 nanoparticles with shell-core structure as a delivery carrier for Newcastle disease virus DNA vaccine. International Journal of Nanomedicine. 2015;10:2895-911.

[133] Mody K, Mahony D, Cavallaro A, Zhang J, Zhang B, Mahony T, et al. Silica Vesicle Nanovaccine Formulations Stimulate Long-Term Immune Responses to the Bovine Viral Diarrhoea Virus E2 Protein. PLOS ONE. 2015;10:e0143507.

[134] Mahony D, Cavallaro A, Mody K, Xiong L, Mahony T, Qiao S, et al. In vivo delivery of bovine viral diahorrea virus, E2 protein using hollow mesoporous silica nanoparticles. Nanoscale. 2014;6:6617-26.

[135] Mahony D, Mody K, Cavallaro A, Hu Q, Mahony T, Qiao S, et al. Immunisation of Sheep with Bovine Viral Diarrhoea Virus, E2 Protein Using a Freeze-Dried Hollow Silica Mesoporous Nanoparticle Formulation. PLOS ONE. 2015;10:e0141870.

[136] Hu Z, Song B, Xu L, Zhong Y, Peng F, Ji X, et al. Aqueous synthesized quantum dots interfere with the NF-κB pathway and confer anti-tumor, anti-viral and anti-inflammatory effects. Biomaterials. 2016;108:187-96.

[137] Dewitte H, Verbeke R, Breckpot K, De Smedt S, Lentacker I. Nanoparticle design to induce tumor immunity and challenge the suppressive tumor microenvironment. Nano Today. 2014;9:743-58.

[138] Cheung A, Mooney D. Engineered materials for cancer immunotherapy. Nano Today. 2015;10:511-31.

[139] Brinãs RP, Sundgren A, Sahoo P, Morey S, Rittenhouse-Olson K, Wilding G, et al. Design and Synthesis of Multifunctional Gold Nanoparticles Bearing Tumor-Associated Glycopeptide Antigens as Potential Cancer Vaccines. Bioconjugate Chemistry. 2012;23:1513-23.

[140] Lin A, Mattos Almeida J, Bear A, Liu N, Luo L, Foster A, et al. Gold Nanoparticle Delivery of Modified CpG Stimulates Macrophages and Inhibits Tumor Growth for Enhanced Immunotherapy. PLOS ONE. 2013;8:e63550.

[141] Lee I-H, Kwon H-K, An S, Kim D, Kim S, Yu M, et al. Imageable Antigen-Presenting Gold Nanoparticle Vaccines for Effective Cancer Immunotherapy In Vivo. Angewandte Chemie. 2012;51:8800-5.

[142] Almeida J, Figueroa E, Drezek R. Gold nanoparticle mediated cancer immunotherapy. Nanomedicine: Nanotechnology, Biology and Medicine. 2014;10:503-14.

[143] Almeida J, Lin A, Figueroa R, Foster A, Drezek R. In vivo Gold Nanoparticle Delivery of Peptide Vaccine Induces Anti-Tumor Immune Response in Prophylactic and Therapeutic Tumor Models. Small (Weinheim an der Bergstrasse, Germany). 2015;11:1453-9.

[144] de Titta A, Ballester M, Julier Z, Nembrini C, Jeanbart L, van der Vlies A, et al. Nanoparticle conjugation of CpG enhances adjuvancy for cellular immunity and memory recall at low dose. Proceedings of the National Academy of Sciences of the United States of America. 2013;110:19902-7.

[145] Ahn S, Lee I-H, Kang S, Kim D, Choi M, Saw P, et al. Gold Nanoparticles Displaying Tumor-Associated Self-Antigens as a Potential Vaccine for Cancer Immunotherapy. Advanced Healthcare Materials. 2014;3:1194-9.

[146] Kang S, Ahn S, Lee J, Kim J, Choi M, Gujrati V, et al. Effects of gold nanoparticle-based vaccine size on lymph node delivery and cytotoxic T-lymphocyte responses. Journal of Controlled Release 2017;256:56-67.

[147] Huijbers EJ, Ringvall M, Femel J, Kalamajski S, Lukinius A, Abrink M, et al. Vaccination against the extra domain-B of fibronectin as a novel tumor therapy. The FASEB Journal. 2010;24:4535-44.

[148] Zhang P, Chiu Y-C, Tostanoski L, Jewell C. Polyelectrolyte Multilayers Assembled Entirely from Immune Signals on Gold Nanoparticle Templates Promote Antigen-Specific T Cell Response. ACS Nano. 2015;9:6465-77.

[149] Zhang P, Andorko J, Jewell C. Impact of dose, route, and composition on the immunogenicity of immune polyelectrolyte multilayers delivered on gold templates. Biotechnology and Bioengineering. 2017;114:423-31.

[150] Sacchetti C, Rapini N, Magrini A, Cirelli E, Bellucci S, Mattei M, et al. In Vivo Targeting of Intratumor Regulatory T Cells Using PEG-Modified Single-Walled Carbon Nanotubes. Bioconjugate Chemistry. 2013;24:852-8.

[151] Smith B, Ghosn E, Rallapalli H, Prescher J, Larson T, Herzenberg L, et al. Selective uptake of single-walled carbon nanotubes by circulating monocytes for enhanced tumour delivery. Nature Nanotechnology. 2014;9:481-7.

[152] Smith B, Zavaleta C, Rosenberg J, Tong R, Ramunas J, Liu Z, et al. High-resolution, serial intravital microscopic imaging of nanoparticle delivery and targeting in a small animal tumor model. Nano Today. 2013;8.

[153] Meng J, Meng J, Duan J, Kong H, Li L, Wang C, et al. Carbon Nanotubes Conjugated to Tumor Lysate Protein Enhance the Efficacy of an Antitumor Immunotherapy. Small (Weinheim an der Bergstrasse, Germany). 2008;4:1364-70.

[154] Villa C, Dao T, Ahearn I, Fehrenbacher N, Casey E, Rey D, et al. Single-Walled Carbon Nanotubes Deliver Peptide Antigen into Dendritic Cells and Enhance IgG Responses to Tumor-Associated Antigens. ACS Nano. 2011;5:5300-11.

[155] Zhao D, Alizadeh D, Zhang L, Liu W, Farrukh O, Manuel E, et al. Carbon Nanotubes Enhance CpG Uptake and Potentiate Anti-Glioma Immunity. Clinical Cancer Research. 2011;17:771-82.

[156] Keisari Y, Hochman I, Confino H, Korenstein R, Kelson I. Activation of local and systemic anti-tumor immune responses by ablation of solid tumors with intratumoral electrochemical or alpha radiation treatments. Cancer Immunology, Immunotherapy. 2014;63:1-9.

[157] Mehta A, Oklu R, Sheth R. Thermal Ablative Therapies and Immune Checkpoint Modulation: Can Locoregional Approaches Effect a Systemic Response? Gastroenterology Research and Practice. 2016;2016:9251375.

[158] Zhou F, Wu S, Song S, Chen W, Resasco D, Xing D. Antitumor immunologically modified carbon nanotubes for photothermal therapy. Biomaterials. 2012;33:3235-42.

[159] Chen Q, Xu L, Liang C, Wang C, Peng R, Liu Z. Photothermal therapy with immune-adjuvant nanoparticles together with checkpoint blockade for effective cancer immunotherapy. Nature Communications. 2016;7:13193.

[160] Mejías R, Pérez-Yagüe S, Gutiérrez L, Cabrera L, Spada R, Acedo P, et al. Dimercaptosuccinic acid-coated magnetite nanoparticles for magnetically guided in vivo delivery of interferon gamma for cancer immunotherapy. Biomaterials. 2011;32:2938-52.

[161] Moore A, Grimm J, Han B, Santamaria P. Tracking the Recruitment of Diabetogenic CD8+ T-Cells to the Pancreas in Real Time. Diabetes. 2004;53:1459-66.

[162] Shevtsov M, Nikolaev B, Yakovleva L, Parr M, Marchenko Y, Eliseev I, et al. 70-kDa heat shock protein coated magnetic nanocarriers as a nanovaccine for induction of anti-tumor immune response in experimental glioma. Journal of Controlled Release. 2015;220:329-40.

[163] Shevtsov M, Pozdnyakov A, Mikhrina A, Yakovleva L, Nikolaev B, Dobrodumov A, et al. Effective immunotherapy of rat glioblastoma with prolonged intratumoral delivery of exogenous heat shock protein Hsp70. International journal of cancer. 2014;135:2118-28.

[164] Cho N-H, Cheong T-C, Min J, Wu J, Lee S, Kim D, et al. A multifunctional core–shell nanoparticle for dendritic cell-based cancer immunotherapy. Nature Nanotechnology. 2011;6:675-82.

[165] Heckman K, DeCoteau W, Estevez A, Reed K, Costanzo W, Sanford D, et al. Custom Cerium Oxide Nanoparticles Protect against a Free Radical Mediated Autoimmune Degenerative Disease in the Brain. ACS Nano. 2013;7:10582-96.

[166] Moraes A, Paula R, Pradella F, Santos M, Oliveira E, von Glehn F, et al. The Suppressive Effect of IL-27 on Encephalitogenic Th17 Cells Induced by Multiwalled Carbon Nanotubes Reduces the Severity of Experimental Autoimmune Encephalomyelitis. CNS Neuroscience & Therapeutics. 2013;19:682-7.

[167] Clemente-Casares X, Santamaria P. Nanomedicine in autoimmunity. Immunology Letters. 2014;158:167-74.

[168] Serra P, Santamaria P. Nanoparticle-based autoimmune disease therapy. Clinical Immunology. 2015;160:3-13.

[169] Northrup L, Sestak J, Sullivan B, Thati S, Hartwell B, Siahaan T, et al. Co-delivery of autoantigen and b7 pathway modulators suppresses experimental autoimmune encephalomyelitis. AAPS Journal. 2014;16:1204-13.

[170] Northrup L, Christopher M, Sullivan B, Berkland C. Combining antigen and immunomodulators: Emerging trends in antigen-specific immunotherapy for autoimmunity. Advanced drug delivery reviews. 2016;98:86-98.

[171] Quintana F, Murugaiyan G, Farez M, Mitsdoerffer M, Tukpah A-M, Burns E, et al. An endogenous aryl hydrocarbon receptor ligand acts on dendritic cells and T cells to suppress experimental autoimmune encephalomyelitis. Proceedings of the National Academy of Sciences of the United States of America. 2010;107:20768-73.

[172] Nguyen N, Kimura A, Nakahama T, Chinen I, Masuda K, Nohara K, et al. Aryl hydrocarbon receptor negatively regulates dendritic cell immunogenicity via a kynurenine-dependent mechanism. Proceedings of the National Academy of Sciences of the United States of America. 2010;107:19961-6.

[173] Mezrich J, Fechner J, Zhang X, Johnson B, Burlingham W, Bradfield C. An interaction between kynurenine and the aryl hydrocarbon receptor can generate regulatory T cells. Journal of Immunology. 2010;185:3190-8.

[174] Yeste A, Takenaka M, Mascanfroni I, Nadeau M, Kenison J, Patel B, et al. Tolerogenic nanoparticles inhibit T cell–mediated autoimmunity through SOCS2. Science Signaling. 2016;9:ra61-ra.

[175] Sloane J, Batt C, Ma Y, Harris Z, Trapp B, Vartanian T. Hyaluronan blocks oligodendrocyte progenitor maturation and remyelination through TLR2. Proceedings of the National Academy of Sciences of the United States of America. 2010;107:11555-60.

[176] Reynolds JM, Martinez G, Chung Y, Dong C. Toll-like receptor 4 signaling in T cells promotes autoimmune inflammation. Proceedings of the National Academy of Sciences of the United States of America. 2012;109:13064-9.

[177] Santoni M, Andrikou K, Sotte V, Bittoni A, Lanese A, Pellei C, et al. Toll like receptors and pancreatic diseases: From a pathogenetic mechanism to a therapeutic target. Cancer Treatment Reviews. 2015;41:569-76.

[178] Celhar T, Magalhães R, Fairhurst A-M. TLR7 and TLR9 in SLE: when sensing self goes wrong. Immunologic Research. 2012;53:58-77.

[179] Prinz M, Garbe F, Schmidt H, Mildner A, Gutcher I, Wolter K, et al. Innate immunity mediated by TLR9 modulates pathogenicity in an animal model of multiple sclerosis. Journal of Clinical Investigation. 2006;116:456-64.

[180] Opal SM, Laterre P, Francois B, et al. Effect of eritoran, an antagonist of md2-tlr4, on mortality in patients with severe sepsis: The access randomized trial. Journal of the American Medical Association. 2013;309:1154-62.

[181] Yang H, Kozicky L, Saferali A, Fung S-Y, Afacan N, Cai B, et al. Endosomal pH modulation by peptide-gold nanoparticle hybrids enables potent anti-inflammatory activity in phagocytic immune cells. Biomaterials. 2016;111:90-102.

[182] Tsai S, Shameli A, Yamanouchi J, Clemente-Casares X, Wang J, Serra P, et al. Reversal of Autoimmunity by Boosting Memory-like Autoregulatory T Cells. Immunity. 2010;32:568-80.

[183] Clemente-Casares X, Blanco J, Ambalavanan P, Yamanouchi J, Singha S, Fandos C, et al. Expanding antigen-specific regulatory networks to treat autoimmunity. Nature. 2016;530:434-40.

[184] Singha S, Shao K, Yang Y, Clemente-Casares X, Sole P, Clemente A, et al. Peptide-MHC-based nanomedicines for autoimmunity function as T-cell receptor microclustering devices. Nature nanotechnology. 2017;12:701-10.

[185] Park EJ, Kim H, Kim Y, Yi J, Choi K, Park K. Inflammatory responses may be induced by a single intratracheal instillation of iron nanoparticles in mice. Toxicology. 2010;275:65-71.

[186] Chen B-A, Jin N, Wang J, Ding J, Gao C, Cheng J, et al. The effect of magnetic nanoparticles of Fe(3)O(4) on immune function in normal ICR mice. International Journal of Nanomedicine. 2010;5:593-9.

[187] Shen C-C, Liang H-J, Wang C-C, Liao M-H, Jan T-R. A role of cellular glutathione in the differential effects of iron oxide nanoparticles on antigen-specific T cell cytokine expression. International Journal of Nanomedicine. 2011;6:2791-8.

[188] Shen C-C, Wang C-C, Liao M-H, Jan T-R. A single exposure to iron oxide nanoparticles attenuates antigen-specific antibody production and T-cell reactivity in ovalbumin-sensitized BALB/c mice. International Journal of Nanomedicine. 2011;6:1229-35.

[189] Shen C-C, Liang H-J, Wang C-C, Liao M-H, Jan T-R. Iron oxide nanoparticles suppressed T helper 1 cell-mediated immunity in a murine model of delayed-type hypersensitivity. International Journal of Nanomedicine. 2012;7:2729-37.

[190] Liu H, Tang W, Li C, Lv P, Wang Z, Liu Y, et al. CdSe/ZnS Quantum Dots-Labeled Mesenchymal Stem Cells for Targeted Fluorescence Imaging of Pancreas Tissues and Therapy of Type 1 Diabetic Rats. Nanoscale research letters. 2015;10:959.

[191] Mannucci S, Calderan L, Quaranta P, Antonini S, Mosca F, Longoni B, et al. Quantum dots labelling allows detection of the homing of mesenchymal stem cells administered as immunomodulatory therapy in an experimental model of pancreatic islets transplantation. Journal of Anatomy. 2017;230:381-8.

[192] Getts D, Terry R, Getts M, Deffrasnes C, Muller M, van Vreden C, et al. Therapeutic inflammatory monocyte modulation using immune-modifying microparticles. Science translational medicine. 2014;6:219ra7.

[193] Lutterotti A, Yousef S, Sputtek A, Sturner K, Stellmann J, Breiden P, et al. Antigen-specific tolerance by autologous myelin peptide-coupled cells: a phase 1 trial in multiple sclerosis. Science translational medicine. 2013;5:188ra75.

[194] Kennedy M, Tan L, Dal Canto M, Tuohy V, Lu Z, Trotter J, et al. Inhibition of murine relapsing experimental autoimmune encephalomyelitis by immune tolerance to proteolipid protein and its encephalitogenic peptides. Journal of Immunology. 1990;144:909-15.

[195] Smith C, Miller S. Multi-Peptide Coupled-Cell Tolerance Ameliorates Ongoing Relapsing EAE Associated with Multiple Pathogenic Autoreactivities. Journal of autoimmunity. 2006;27:218-31.

[196] Kostarelos K, Bianco A, Prato M. Promises, facts and challenges for carbon nanotubes in imaging and therapeutics. Nature Nanotechnology. 2009;4:627.

[197] Zhao L, Seth A, Wibowo N, Zhao C-X, Mitter N, Yu C, et al. Nanoparticle vaccines. Vaccine. 2014;32:327-37.

[198] Hayter S, Cook M. Updated assessment of the prevalence, spectrum and case definition of autoimmune disease. Autoimmunity Reviews. 2012;11:754-65.

[199] Kochi Y. Genetics of autoimmune diseases: perspectives from genome-wide association studies. International Immunology. 2016;28:155-61.

[200] Swartz M, Hirosue S, Hubbell J. Engineering approaches to immunotherapy. Science translational medicine. 2012;4:148rv9.

[201] Gammon J, Tostanoski L, Adapa A, Chiu Y-C, Jewell C. Controlled delivery of a metabolic modulator promotes regulatory T cells and restrains autoimmunity. Journal of Controlled Release. 2015;210:169-78.

[202] Hernandez-Pedro N, Espinosa-Ramirez G, de la Cruz V, Pineda B, Sotelo J. Initial immunopathogenesis of multiple sclerosis: innate immune response. Clinical and Developmental Immunology. 2013;2013:413465.

[203] Santoni M, Andrikou K, Sotte V, Bittoni A, Lanese A, Pellei C, et al. Toll like receptors and pancreatic diseases: From a pathogenetic mechanism to a therapeutic target. Cancer treatment reviews. 2015;41:569-76.

[204] Krieg A, Yi A, Matson S, Waldschmidt T, Bishop G, Teasdale R, et al. CpG motifs in bacterial DNA trigger direct B-cell activation. Nature. 1995;374:546-9.

[205] Shirota H, Klinman D. Recent progress concerning CpG DNA and its use as a vaccine adjuvant. Expert review of vaccines. 2014;13:299-312.

[206] Klinman DM, Yi AK, Beaucage SL, Conover J, Krieg AM. CpG motifs present in bacteria DNA rapidly induce lymphocytes to secrete interleukin 6, interleukin 12, and interferon gamma. Proceedings of the National Academy of Sciences of the United States of America. 1996;93:2879-83.

[207] Ho P, Fontoura P, Ruiz P, Steinman L, Garren H. An immunomodulatory GpG oligonucleotide for the treatment of autoimmunity via the innate and adaptive immune systems. Journal of Immunology. 2003;171:4920-6.

[208] Ho P, Fontoura P, Platten M, Sobel R, DeVoss J, Lee L, et al. A suppressive oligodeoxynucleotide enhances the efficacy of myelin cocktail/IL-4-tolerizing DNA vaccination and treats autoimmune disease. Journal of Immunology. 2005;175:6226-34.

[209] Jewell C, Lynn D. Surface-Mediated Delivery of DNA: Cationic Polymers Take Charge. Current Opinion in Colloid and Interface Science. 2008;13:395-402.

[210] Lachelt U, Wagner E. Nucleic Acid Therapeutics Using Polyplexes: A Journey of 50 Years (and Beyond). Chemical reviews. 2015;115:11043-78.

[211] Kozielski K, Rui Y, Green J. Non-viral nucleic acid containing nanoparticles as cancer therapeutics. Expert opinion on drug delivery. 2016:1-13.

[212] Joo W, Jeong J, Nam K, Blevins K, Salama M, Kim S. Polymeric delivery of therapeutic RAE-1 plasmid to the pancreatic islets for the prevention of type 1 diabetes. Journal of Controlled Release. 2012;162:606-11.

[213] Mandke R, Singh J. Cationic nanomicelles for delivery of plasmids encoding interleukin-4 and interleukin-10 for prevention of autoimmune diabetes in mice. Pharmaceutical research. 2012;29:883-97.

[214] Huang L, Lemos H, Li L, Li M, Chandler P, Baban B, et al. Engineering DNA nanoparticles as immunomodulatory reagents that activate regulatory T cells. Journal of Immunology. 2012;188:4913-20.

[215] Huang L, Li L, Lemos H, Chandler P, Pacholczyk G, Baban B, et al. Cutting edge: DNA sensing via the STING adaptor in myeloid dendritic cells induces potent tolerogenic responses. Journal of Immunology. 2013;191:3509-13.

[216] Lemos H, Huang L, Chandler P, Mohamed E, Souza G, Li L, et al. Activation of the STING adaptor attenuates experimental autoimmune encephalitis. Journal of Immunology. 2014;192:5571-8.

[217] Özhalıcı-Ünal H, Armitage B. Fluorescent DNA Nanotags Based on a Self-Assembled DNA Tetrahedron. ACS Nano. 2009;3:425-33.

[218] Chen H, Ho Y-P, Jiang X, Mao H-Q, Wang T-H, Leong KW. Simultaneous Non-invasive Analysis of DNA Condensation and Stability by Two-step QD-FRET. Nano today. 2009;4:125-34.

[219] Vardevanyan P, Antonyan A, Parsadanyan M, Davtyan H, Karapetyan A. The binding of ethidium bromide with DNA: interaction with single- and double-stranded structures. Experimental & Molecular Medicine. 2003;35:527-33.

[220] Vardevanyan P, Arakelyan V, Parsadanyan M, Antonyan A, Hovhannisyan G, Shahinyan M. Analysis of experimental binding curves of EtBr with single- and double-stranded DNA at small fillings. Modern Physics Letters B. 2014;28:1450178.

[221] Brubaker S, Bonham K, Zanoni I, Kagan J. Innate immune pattern recognition: a cell biological perspective. Annual review of immunology. 2015;33:257-90.

[222] Yuan B, Zhao L, Fu F, Liu Y, Lin C, Wu X, et al. A novel nanoparticle containing MOG peptide with BTLA induces T cell tolerance and prevents multiple sclerosis. Molecular immunology. 2014;57:93-9.

[223] Deshayes S, Morris MC, Divita G, Heitz F. Cell-penetrating peptides: tools for intracellular delivery of therapeutics. Cellular and Molecular Life Sciences. 2005;62:1839-49.

[224] Walrant A, Correia I, Jiao C, Lequin O, Bent E, Goasdoue N, et al. Different membrane behaviour and cellular uptake of three basic arginine-rich peptides. Biochimica et biophysica acta. 2011;1808:382-93.

[225] Copolovici D, Langel K, Eriste E, Langel U. Cell-Penetrating Peptides: Design, Synthesis, and Applications. Acs Nano. 2014;8:1972-94.

[226] Haensler J, Szoka F. Polyamidoamine cascade polymers mediate efficient transfection of cells in culture. Bioconjugate Chemistry. 1993;4:372-9.

[227] Boussif O, Lezoualc'h F, Zanta M, Mergny M, Scherman D, Demeneix B, et al. A versatile vector for gene and oligonucleotide transfer into cells in culture and in vivo: polyethylenimine. Proceedings of the National Academy of Sciences of the United States of America. 1995;92:7297-301.

[228] Gebhart C, Kabanov A. Evaluation of polyplexes as gene transfer agents. Journal of Controlled Release. 2001;73:401-16.

[229] Fromen C, Rahhal T, Robbins G, Kai M, Shen T, Luft J, et al. Nanoparticle surface charge impacts distribution, uptake and lymph node trafficking by pulmonary antigen-presenting cells. Nanomedicine. 2016;12:677-87.

[230] Procaccini C, De Rosa V, Pucino V, Formisano L, Matarese G. Animal models of Multiple Sclerosis. European journal of pharmacology. 2015;759:182-91.

[231] Chiu Y-C, Gammon J, Andorko J, Tostanoski L, Jewell C. Modular Vaccine Design Using Carrier-Free Capsules Assembled from Polyionic Immune Signals. ACS biomaterials science & engineering. 2015;1:1200-5.

[232] Chiu Y-C, Gammon J, Andorko J, Tostanoski L, Jewell C. Assembly and Immunological Processing of Polyelectrolyte Multilayers Composed of Antigens and Adjuvants. ACS applied materials & interfaces. 2016;8:18722-31.

[233] Bluestone J, Bour-Jordan H, Cheng M, Anderson M. T cells in the control of organ-specific autoimmunity. Journal of Clinical Investigation. 2015;125:2250-60.

[234] Gratz I, Rosenblum M, Maurano M, Paw J, Truong H, Marshak-Rothstein A, et al. Cutting edge: Self-antigen controls the balance between effector and regulatory T cells in peripheral tissues. Journal of Immunology. 2014;192:1351-5.

[235] Louveau A, Smirnov I, Keyes T, Eccles J, Rouhani S, Peske J, et al. Structural and functional features of central nervous system lymphatic vessels. Nature. 2015;523:337-41.

[236] Aspelund A, Antila S, Proulx S, Karlsen T, Karaman S, Detmar M, et al. A dural lymphatic vascular system that drains brain interstitial fluid and macromolecules. Journal of Experimental Medicine. 2015;212:991-9.

[237] Probst C, Zrazhevskiy P, Bagalkot V, Gao X. Quantum dots as a platform for nanoparticle drug delivery vehicle design. Advanced drug delivery reviews. 2013;65:703-18.

[238] Algar W, Susumu K, Delehanty J, Medintz I. Semiconductor Quantum Dots in Bioanalysis: Crossing the Valley of Death. Analytical Chemistry. 2011;83:8826-37.

[239] Rosenthal S, Chang J, Kovtun O, McBride J, Tomlinson I. Biocompatible Quantum Dots for Biological Applications. Chem Biol. 2011;18:10-24.

[240] Andrasfalvy B, Galinanes G, Huber D, Barbic M, Macklin J, Susumu K, et al. Quantum dot-based multiphoton fluorescent pipettes for targeted neuronal electrophysiology. Nat Methods. 2014;11:1237-+.

[241] Boeneman K, Delehanty J, Blanco-Canosa J, Susumu K, Stewart M, Oh E, et al. Selecting Improved Peptidyl Motifs for Cytosolic Delivery of Disparate Protein and Nanoparticle Materials. Acs Nano. 2013;7:3778-96.

[242] Agarwal R, Domowicz M, Schwartz N, Henry J, Medintz I, Delehanty J, et al. Delivery and Tracking of Quantum Dot Peptide Bioconjugates in an Intact Developing Avian Brain. Acs Chem Neurosci. 2015;6:494-504.

[243] Hauck T, Anderson R, Fischer H, Newbigging S, Chan W. In vivo quantum-dot toxicity assessment. Small (Weinheim an der Bergstrasse, Germany). 2010;6:138-44.

[244] Ye L, Yong K, Liu L, Roy I, Hu R, Zhu J, et al. A pilot study in non-human primates shows no adverse response to intravenous injection of quantum dots. Nature nanotechnology. 2012;7:453-8.

[245] Kim S, Lim Y, Soltesz EG, De Grand A, Lee J, Nakayama A, et al. Near-infrared fluorescent type II quantum dots for sentinel lymph node mapping. Nature biotechnology. 2004;22:93-7.

[246] Susumu K, Oh E, Delehanty J, Blanco-Canosa J, Johnson B, Jain V, et al. Multifunctional Compact Zwitterionic Ligands for Preparing Robust Biocompatible Semiconductor Quantum Dots and Gold Nanoparticles. Journal of the American Chemical Society. 2011;133:9480-96.

[247] Sapsford K, Farrell D, Sun S, Rasooly A, Mattoussi H, Medintz I. Monitoring of enzymatic proteolysis on a electroluminescent-CCD microchip platform using quantum dot-peptide substrates. Sensors and Actuators B: Chemical. 2009;139:13-21.

[248] Medintz I, Clapp A, Mattoussi H, Goldman E, Fisher B, Mauro J. Self-assembled nanoscale biosensors based on quantum dot FRET donors. Nature Materials. 2003;2:630.

[249] Prasuhn D, Deschamps J, Susumu K, Stewart M, Boeneman K, Blanco-Canosa J, et al. Polyvalent display and packing of peptides and proteins on semiconductor quantum dots: predicted versus experimental results. Small (Weinheim an der Bergstrasse, Germany). 2010;6:555-64.

[250] Medintz I, Clapp A, Brunel F, Tiefenbrunn T, Tetsuo Uyeda H, Chang E, et al. Proteolytic activity monitored by fluorescence resonance energy transfer through quantum-dot-peptide conjugates. Nature Materials. 2006;5:581-9.

[251] Boeneman K, Deschamps J, Buckhout-White S, Prasuhn D, Blanco-Canosa J, Dawson P, et al. Quantum Dot DNA Bioconjugates: Attachment Chemistry Strongly Influences the Resulting Composite Architecture. ACS Nano. 2010;4:7253-66.

[252] Medintz I, Pons T, Susumu K, Boeneman K, Dennis A, Farrell D, et al. Resonance Energy Transfer Between Luminescent Quantum Dots and Diverse Fluorescent Protein Acceptors. Journal of Physical Chemistry C: Nanomaterials and Interfaces. 2009;113:18552-61.

[253] Medintz I, Sapsford K, Clapp A, Pons T, Higashiya S, Welch J, et al. Designer variable repeat length polypeptides as scaffolds for surface immobilization of quantum dots. The journal of physical chemistry B. 2006;110:10683-90.

[254] Breithaupt C, Schubart A, Zander H, Skerra A, Huber R, Linington C, et al. Structural insights into the antigenicity of myelin oligodendrocyte glycoprotein. Proceedings of the National Academy of Sciences of the United States of America. 2003;100:9446-51.

[255] Pons T, Medintz I, Wang X, English D, Mattoussi H. Solution-Phase Single Quantum Dot Fluorescence Resonance Energy Transfer. Journal of the American Chemical Society. 2006;128:15324-31.

[256] Medintz I, Konnert J, Clapp A, Stanish I, Twigg M, Mattoussi H, et al. A fluorescence resonance energy transfer-derived structure of a quantum dot-protein bioconjugate nanoassembly. Proceedings of the National Academy of Sciences of the United States of America. 2004;101:9612-7.

[257] Algar WR, Malonoski A, Deschamps JR, Blanco-Canosa JB, Susumu K, Stewart MH, et al. Proteolytic Activity at Quantum Dot-Conjugates: Kinetic Analysis Reveals Enhanced Enzyme Activity and Localized Interfacial “Hopping”. Nano Letters. 2012;12:3793-802.

[258] Algar W, Ancona M, Malanoski A, Susumu K, Medintz I. Assembly of a Concentric Förster Resonance Energy Transfer Relay on a Quantum Dot Scaffold: Characterization and Application to Multiplexed Protease Sensing. ACS Nano. 2012;6:11044-58.

[259] Warren K, Iwami D, Harris D, Bromberg J, Burrell B. Laminins affect T cell trafficking and allograft fate. Journal of Clinical Investigation. 2014;124:2204-18.

[260] Arredouani M, Franco F, Imrich A, Fedulov A, Lu X, Perkins D, et al. Scavenger Receptors SR-AI/II and MARCO limit pulmonary dendritic cell migration and allergic airway inflammation. Journal of Immunology. 2007;178:5912-20.

[261] Korn T, Reddy J, Gao W, Bettelli E, Awasthi A, Petersen T, et al. Myelin-specific regulatory T cells accumulate in the CNS but fail to control autoimmune inflammation. Nature medicine. 2007;13:423-31.

[262] Tostanoski L, Jewell C. Engineering self-assembled materials to study and direct immune function. Advanced Drug Delivery Reviews. 2017;114:60-78.

[263] Zinkernagel R, Stephan E, Peter A, Stephan O, Thomas K, Hans H. Antigen localisation regulates immune responses in a dose- and time-dependent fashion: a geographical view of immune reactivity. Immunological Reviews. 1997;156:199-209.

[264] Burrell B, Nakayama Y, Xu J, Brinkman C, Bromberg J. Regulatory T Cell Induction, Migration, and Function in Transplantation. Journal of Immunology. 2012;189:4705-11.

[265] Burrell B, Bromberg J. Fates of CD4(+) T Cells in a Tolerant Environment Depend on Timing and Place of Antigen Exposure. American Journal of Transplantation. 2012;12:576-89.

[266] Katakai T, Hara T, Sugai M, Gonda H, Shimizu A. Lymph Node Fibroblastic Reticular Cells Construct the Stromal Reticulum via Contact with Lymphocytes. Journal of Experimental Medicine. 2004;200:783-95.

[267] Santhakumar M, Bali P. Dendritic cell control of tolerogenic responses. Immunological Reviews. 2011;241:206-27.

[268] Vasiliu T, Cojocaru C, Rotaru A, Pricope G, Pinteala M, Clima L. Optimization of Polyplex Formation between DNA Oligonucleotide and Poly(l-Lysine): Experimental Study and Modeling Approach. International Journal of Molecular Sciences. 2017;18:1291.

[269] Muro S. A DNA Device that Mediates Selective Endosomal Escape and Intracellular Delivery of Drugs and Biologicals. Advanced Functional Materials. 2014;24:2899-906.